Slave-side Devices for Micromanipulation in a Haptic Teleoperation Scenario

Pablo Estevez Castillo

Propositions belonging to the thesis

Slave-side devices for micromanipulation in a haptic teleoperation scenario

Pablo Estevez

1. Haptic teleoperation systems can only become a viable option against competing technologies when the abilities and limitations of the operator are acknowledged and included in the design-optimization process. Only then the resulting systems can exploit the operator intelligence and the precision of the robots in the system at their maximum, without incurring in unnecessary costs (this thesis).
2. Using haptic micromanipulation systems in structured, repetitive tasks would constitute a fundamentally inefficient use both of the operators, who would not be using their reasoning abilities, and of the manipulator-technology available in the market, by not exploiting the speed and level of automation that can be currently reached (this thesis).
3. Positioners with both low stiffness actuators and low stiffness controllers provide a safe and stable manipulation of delicate microcomponents, but the associated positioning errors constrain their usability in automatic systems. Such a limitation is not relevant when teleoperation is used, thus creating a niche of application for such systems and control principles in teleoperated micromanipulation (this thesis).
4. Defining the specifications of a system can be as much of a contribution, as designing the system that fulfills such requirements.
5. Giving to the PhD students some level of freedom in choosing their research goals generates in them a level of motivation difficult to achieve otherwise, regardless of whether such goals may seem unrealistic at the beginning. After all, a man's reach should exceed his grasp, or what's a heaven for? [Robert Browning].
6. Supervision of master and bachelor students should be promoted during the PhD studies. The efforts involved on the part of the PhD student are generally surpassed by the benefits of an enriching exchange between the supervisor and supervised student. Moreover, the difficulties found on the way constitute a training in project management, otherwise absent in most PhD programs.
7. Solid governmental institutions constitute a damper for sociopolitical processes. In that sense, they may slow-down the progress of societies, and reduce their efficiency and performance by wasting energy . On the other hand, as in the case of mechatronic systems, they are often the only way to guarantee the stability of the society.
8. English proficiency of Dutch people provides an excellent social bridge for foreigners at their arrival, but develops into a communication brick-wall as time passes as the latter are not enforced to learn the Dutch language.
9. Many theses by foreign students in The Netherlands include propositions about their adaptation problems regarding Dutch cuisine. Such tendency should be taken into account by the TU Delft as an indication of the need for a wider variety in the menu of an institution with an international focus.
10. According to data from Section 4.3 of this thesis, operators without the letter O in their names (as declared at the start of the test) have larger average errors in haptic-guided line-following tasks, with a significance value p = 1.2 %. This results may serve as a guideline for staffing precision assembly facilities, or just as a reminder that statistical results with good significance value are still subjected to a not-zero probability of been wrong.

These propositions are regarded as opposable and defendable, and have been approved as such by the supervisor, Prof.ir. R.H. Munnig Schmidt.

Stellingen behorende bij het proefschrift

Slave-side devices for micromanipulation in a haptic teleoperation scenario

Pablo Estevez

1. Haptische bediening op afstand kan alleen een acceptabele optie zijn ten opzichte van concurrerende technieken als de mogelijkheden en beperkingen van de gebruiker erkend en meegenomen worden in het ontwerp-optimalisatie proces. Alleen dan kan het resulterende systeem de intelligentie van de gebruiker en de precisie van het systeem maximaal benutten, zonder onnodige kosten te veroorzaken (dit proefschrift)
2. Het gebruik van haptische micro-manipulatiesystemen bij gestructureerde, zich herhalende taken impliceert een fundamenteel inefficiënt gebruik van zowel de gebruikers, die in dat geval hun redeneervermogen niet zouden benutten, en van de manipulatortechnologie die beschikbaar is in de markt, vanwege het niet benutten van de snelheid en automatiseringsgraad die momenteel gehaald kan worden (dit proefschrift).
3. Positioneersystemen die tegelijkertijd gebruik maken van actuatoren met lage stijfheid en besturingssystemen met lage stijfheid bieden een veilige en stabiele manier voor het hanteren van kwetsbare micro-componenten, maar de inherente positioneerfouten beperken hun gebruik in geautomatiseerde systemen. Een dergelijke beperking is niet relevant wanneer tele-manipulatie wordt gebruikt, en daarmee wordt een toepassingsniche ontsloten voor dergelijke systemen en besturingsprincipes binnen op afstand bestuurde micromanipulatie (dit proefschrift).
4. Het definiëren van de systeem specificaties kan een even grote bijdrage opleveren als het ontwerp van het systeem zelf dat aan die eisen voldoet.
5. De PhD student een bepaald niveau van vrijheid geven in het kiezen van onderzoeksdoelen genereert een innerlijke motivatie die moeilijk op een andere manier is te behalen, ongeacht of die doelen aan het begin onrealistisch lijken. Tenslotte geldt: a man's reach should exceed his grasp, or what's a heaven for? [Robert Browning].
6. Het begeleiden van master en bachelor studenten zou bevorderd moeten worden tijdens het PhD traject. De inspanningen van de kant van de PhD student worden in het algemeen overtroffen door de voordelen van een verrijkende uitwisseling tussen de begeleider en de student. Bovendien, de moeilijkheden die onderweg ervaren worden vormen een training in project management, die anderszins afwezig is in de meeste PhD programma's.
7. Solide overheidsinstellingen zijn een demper voor socio-politieke processen. Ze kunnen de vooruitgang in de maatschappij afremmen, en hun efficiëntie en prestaties worden gereduceerd door het verlies van energie. Aan de andere kant, net als bij mechatronische systemen, zijn ze de enige manier om stabiliteit in de maatschappij te garanderen.
8. De Engelse taalvaardigheid van Nederlanders is een excellente sociale brug voor buitenlanders bij hun aankomst, maar het wordt een communicatie-muur na verloop van tijd omdat de laatsten niet gedwongen zijn om de Nederlandse taal te leren.
9. Veel van de proefschriften van buitenlandse promovendi in Nederland bevatten stellingen over hun aanpassingsproblemen met betrekking tot de Nederlandse keuken . Met dit verschijnsel moet rekening worden gehouden door de TU Delft als een indicatie voor de behoefte van een breder gevarieerd menu van een instituut met een internationale focus.
10. In overeenstemming met gegevens uit Paragraaf 4.3 van dit proefschrift blijken gebruikers zonder de letter O in hun naam (als opgegeven bij het begin van de test) een grotere gemiddelde fout te maken in haptisch-geleide lijn-volg taken, met een significantie waarde p=1.2%. Dit resultaat kan dienen als een richtlijn voor het aannemen van personeel voor precisie assemblage faciliteiten, of als een herinnering aan het feit dat statistische resultaten met hoge significantie nog steeds fout kunnen zijn met een kans ongelijk aan nul.

Deze stellingen worden opponeerbaar en verdedigbaar geacht en zijn als zodanig goedgekeurd door de promotor, Prof.ir. R.H. Munnig Schmidt.

Slave-side devices for micromanipulation in a haptic teleoperation scenario.

Proefschrift

ter verkrijging van de graad van doctor
aan de Technische Universiteit Delft,
op gezag van de Rector Magnificus prof.ir. K.C.A.M. Luyben,
voorzitter van het College voor Promoties,
in het openbaar te verdedigen
op dinsdag 12 juni 2012 om 10:00 uur
door

Pablo ESTEVEZ CASTILLO

Magister en Ingeniería Electrónica
Universidad Simón Bolívar
geboren te Mérida, Venezuela

Dit proefschrift is goedgekeurd door de promotor:
Prof.ir. R.H. Munnig Schmidt

Copromotor Dr.ir. M. Tichem

Samenstelling promotiecommissie:

Rector Magnificus	Voorzitter
Prof.ir. R.H. Munnig Schmidt	Technische Universiteit Delft, promotor
Dr.ir. M. Tichem	Technische Universiteit Delft, co-promotor
Prof. P. Lutz	University of Franche-Comté, Femto-ST Institute
Prof.dr.ir. M. Steinbuch	Technische Universiteit Eindhoven
Prof.dr. P.J. French	Technische Universiteit Delft
Prof.dr. F.C.T. van der Helm	Technische Universiteit Delft
Prof.dr.ir. A. van Keulen	Technische Universiteit Delft
Prof.dr. U. Staufer	Technische Universiteit Delft, reservelid

This research has been carried out with the support of the Microned program.

ISBN 978-94-91104-08-4

Contents

Summary

Haptic teleoperation is a promising approach for dealing with the manipulation of micro-objects, fabricated in small series or as prototypes, and in processes which are novel or uncertain. Human operators provide their ability to plan, understand and react when faced with unexpected situations during the manipulation process, while robotic devices ensure the levels of precision required by the tasks.

In order to improve the state of this field, this thesis intends to understand how to better support a human operator performing micromanipulation tasks, and based on that understanding develop a system for teloperated micromanipulation, focusing on the slave-side devices. The first stage of this research is an in-depth analysis of the requirements coming from the kind of tasks which the system must deal with, from the support that is possible and useful to give to the human operator, and from the abilities and limitations of that user. Following those requirements, a system-concept is developed, consisting of the integration of commercially available products with custom developed components. In particular, a 6 DOF magnetic levitation stage is developed as a fine positioning stage for the slave robot, achieving a movement range of 200 x 200 x 200 μm and rotations of 18 to 42 mrad, with Minimum Incremental Motion of 50 nm and 3.5 to 7 μrad. A silicon based force sensor is also developed to explore possibilities for force and torque sensing during micromanipulation. This force sensor measure loads in 6 DOF, within a range of 4 to 30 mN in forces and 4 to 50 μNm in torques, and with noise levels up to 13 to 27 $\mu N/\sqrt{Hz}$ and 11 to 43 $nNm/\sqrt{Hz}$. The system is integrated and characterized, and its usefulness is demonstrated through the performance of micromanipulation tasks by human operators.

A general conclusion drawn from this research is that in order to make haptic teleoperated micromanipulation systems a viable and competitive option, it is vital to identify the kind of tasks for which haptic teleoperated micromanipulation systems can be a solution, and to optimize such systems and its components for these applications and for the haptic teleoperation scenario. In order to do so, one must understand

both the advantages and limitations that this approach offers compared to its main competitors: automatic manipulation, self assembly, unaided manipulation by hand, among others. In particular, the highest potential of teloperated systems is on dealing with uncertain situations, thanks to the reasoning abilities of the human operators. Therefore, the use of these systems in structured and repetitive tasks does not constitute a fair demonstration of their advantages. Likewise, the use of components meant for automatic manipulation which often over-perform some of the motor abilities of the user, results in systems which are more complex and expensive than required, thus undermining some of the main advantages of using teleoperated systems.

Following that reasoning, this work places particular attention to the definition of the requirements. By carefully studying the consequences of including a human operator in the system, and the special needs arising from the tasks and support modes, it is possible to optimize system components for this particular niche. Thus, the resulting system can deal with the situations normally encountered in teleoperated micromanipulation, without incurring in significant costs or complexities often found in systems intended for automatic manipulation, and without having to compromise properties useful for this application.

Samenvatting

Haptische bediening op afstand waarin de mogelijkheden van de menselijke gebruiker en robot technologie worden gecombineerd, is een veelbelovende benadering voor het manipuleren van zeer kleine voorwerpen die in kleine series of als prototype vervaardigd worden en waarbij vaak nieuwe en onbekende processen worden toegepast. De menselijke gebruiker verleent het proces zijn vaardigheid in het plannen, het begrip van het systeem en zijn reactievermogen op onverwachte situaties. Het gerobotiseerde deel van het systeem stelt het niveau van precisie zeker dat voor de taak vereist is.

Als verbetering in dit veld beoogt deze thesis het begrip te vergroten over de manier waarop de gebruiker het best geholpen kan worden bij dergelijke micromanipuleer taken en, gebaseerd op dat begrip, een systeem voor afstandsbediende micromanipulatie te ontwikkelen met de nadruk op de apparatuur aan de "slaaf" zijde van het systeem waar de bewerking plaatsvindt. De eerste stap in dit onderzoek is een grondige analyse van de vereisten op basis van het soort taken dat het systeem moet afhandelen en de nuttige ondersteuning die het systeem zou kunnen leveren aan de gebruiker, rekening houdend met zijn mogelijkheden en beperkingen. Uit deze vereisten is een systeemconcept ontwikkeld dat gebaseerd is op de optimale integratie van enerzijds zorgvuldig geselecteerde commercieel verkrijgbare componenten als ook specifiek ontwikkelde deelsystemen. In het bijzonder is een in zes richtingen (6 DOF) magnetisch gelagerde stage ontworpen als positioneersysteem voor de slaaf-robot, met een bewegingsbereik van 200 x 200 x 200 μm en een rotatiebereik van 18 tot 42mrad, met een verplaatsingsresolutie van 50 nm en 3,5 tot 7 μrad. Ook is een Silicium technologie gebaseerde krachtsensor ontwikkeld om de mogelijkheden van het meten van krachten en momenten tijdens manipulatiehandelingen te onderzoeken. Deze krachtsensor meet krachten in 6 DOF, met een bereik van 4 tot 30 mN voor de krachten en 4 tot 50 μNm voor de momenten, met een ruisniveau van 13 tot 27 $\mu N/\sqrt{Hz}$ en 11 tot 43 $nNm/\sqrt{Hz}$. Het systeem is gentegreerd en getest en het nuttig gebruik is aangetoond met behulp van het verrichten van specifieke micromanipuleer taken door testpersonen.

Een algemene conclusie van dit werk is dat, door de bestudering van de gevolgen van de invloed van de menselijke gebruiker op de besturing van het systeem en de speciale behoeften die voortkomen uit de taken en ondersteuningswijzen, het mogelijk is de onderdelen van het systeem te optimaliseren voor dit bijzondere toepassingsgebied. Om dit te bereiken moeten zowel de voordelen en beperkingen van deze benadering begrepen worden in vergelijking met de belangrijkste andere technieken, waaronder automatische manipulatie, zelf-assemblage en pure handmatige assemblage. De grootste potentie van op afstand bediende systemen is het kunnen omgaan met onzekere situaties, dankzij het vermogen van de menselijke gebruiker. Het gebruik van dergelijke system in taken die vaak herhaald worden maakt om die reden niet gebruik van de grootste voordelen. Evenzo, het gebruik van componenten die bedoeld zijn voor automatische manipulatie, die vaak over-presteren binnen dit concept, resulteert in systemen die complexer en duurder zijn dan vereist, wat ook sommige van de hoofdvoordelen van op afstand bediende systemen ondermijnt.

Deze redenering volgend vraagt dit werk bijzondere aandacht bij de definitie van de eisen. Door het zorgvuldig definiren van de gevolgen van het inbrengen van een menselijke gebruiker in het systeem, en de speciale behoeften die voortkomen uit de taken en ondersteuningswijzen is het mogelijk de onderdelen van het systeem te optimaliseren voor dit bijzondere toepassingsgebied. Op deze wijze is het voor het systeem mogelijk om effectief om te gaan met de typische situaties die zich voordoen bij afstandsbediende micromanipulatie, zonder de significante toename van de kosten en de complexiteit die vaak in volledig geautomatiseerde systemen gevonden worden en die het nuttig gebruik in deze toepassing in de weg kunnen staan.

Chapter 1

Introduction

In today's emerging technologies, where the size of components is reaching the lower micrometer range, traditional macro-manipulation processes are being challenged to their limits. This is due to the requirements of high precision motion and small tolerances, usually less than a few micrometers and currently reaching the sub-micrometer level, and to physical phenomena which are difficult to model and to monitor. Furthermore, the handled parts are often delicate and fragile, requiring a control of forces in the micro-Newton range or below.

When dealing with microproducts that are produced in low-to-medium quantities with many variants or with novel and uncertain processes, the automation of their manipulation process may not be economically profitable, because of the limited flexibility of the available assembly devices, the complexity and variability of the manipulation sequences, and the need to continuously adapt and react to the phenomena occurring at the micro-scale. For that reason the manual approach with the aid of a microscope is often the method used in these cases. However, the pure manual approach is often not sufficient to fulfill the requirements, due to the difficulty of human operators to control the small forces allowed and observe the precision aspects during the manipulation.

Teleoperated systems are an interesting alternative to the unassisted manual assembly. The use of a robotic device in charge of the direct manipulation of the micro-objects allows for levels of precision impossible to achieve by the human hand. At the same time, the presence of the human operator, compared with the more rigid approach of automatic microassembly, improves the flexibility of the system thanks to the capability of the operator to plan, adapt, understand and react to unexpected situations during the manipulation process. The use of 3D teleoperation-interfaces provides a natural interface for the operators to command the manipulation tools,

and the presence of force-feedback in those interfaces can reduce the risk of damaging handled parts, while improving the understanding that the operators achieve of the remote environment and lowering their workload.

This thesis deals with the design of a micromanipulation system specially tailored to teleoperation. This first chapter intends to introduce the reader both to the topics of haptic teleoperation and of micromanipulation, which are touched in Sections 1.1 and 1.2, respectively. Section 1.3 gives an overview of the work by groups currently working on the area of teleoperated micromanipulation. With this basis, Section 1.4 presents the definition of the problem to be tackled by this thesis, and Section 1.5 explains the methodology to be followed in order to do so. Finally, Section 1.6 provides a short reading guide for this thesis, indicating the content of the different parts and chapters.

1.1 The haptic teleoperation scenario

When an operation cannot be carried out by an operator directly holding a tool, a teleoperation system becomes necessary. In a teleoperation scenario, the operator is separated from the operation, and the tool is divided in two parts: one part with which the operator interacts, called the *master device*, and one part which interacts with the remote environment and performs the operation, called the *slave device*. These devices are connected by a control system (either electrical or mechanical) in charge of ensuring that the slave-side of the tool follows the commands issued by the operator in the master-side. Teleoperation is a powerful concept in situations where an operation has to be carried out remotely from the operator, due to inherent risk or the inaccessibility of the operation environment, or to differences in scale. Many situations have been identified where teleoperation could be an interesting option, including handling of hazardous materials [77], surgery [81], space missions [10], assembly and micromanipulation [31].

The separation between the operator and the operation can nevertheless have adverse effects. The feedback that the operator can receive from the interactions of the tool with the environment is reduced in a teleoperation scenario, and the introduction of graphical user interfaces (GUI), dials or buttons may turn out to be unnatural for an operator used to handle the tools directly. Three-dimensional teleoperation-interfaces with force-feedback can then be a promising approach to solve this issue. These devices allow the communication of position and force commands to the slave device directly through position and force actions on the master device, and provide force and position feedback through the same device. In doing so, such devices generate a sense of telepresence [7], generate new communication channels, and reduce the required information processing for the user, thus augmenting the operator performance [70]. This teleoperation scheme is called *haptic teleoperation*, in reference to the Greek

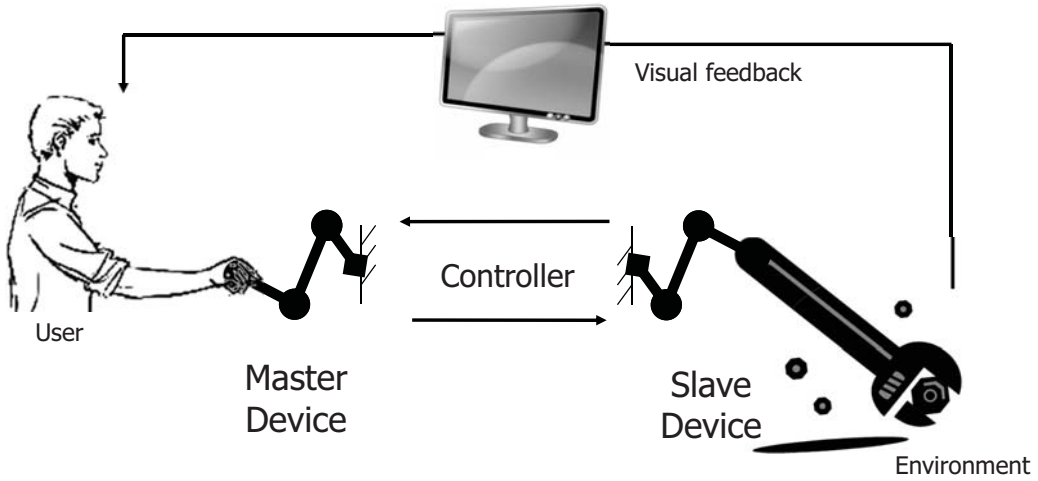

Figure 1.1: *Basic components of a haptic teleoperation system: a master device, a slave device, a controller to interconnect both devices, and, often, visual feedback.*

word for the sense of touch. A haptic teleoperation system is composed in its most basic configuration of a master device, a slave device, and a controller interconnecting both devices, as can be seen in Figure 1.1. In addition, most systems include a vision sensor.

Haptic teleoperation controllers

As described by Goran Christiansson in [23], the controller of a haptic teleoperation system is of the multiple-input-multiple-output (MIMO) type, since it must at the same time control both the master and slave devices, based on force and position information collected from those two devices. Several controller architectures can be used by this controller, each one being a particular case of the general MIMO architecture.

The most commonly implemented controllers divide the controller in two separate channels, one taking references from the master device and controlling the slave device, and one operating likewise in the opposite direction. The first of these 2-channel controllers is called *position error control* or *position-position control*, and consists of one loop measuring the master position and using it as a reference for a local position-loop in the slave side, and one loop measuring the slave position and controlling the master position based on it. The second 2-channel controller is called *position-force controller*, and is composed of a position-loop in the slave robot following the position of the master device, and a force-loop in the master device, using as a reference the

forces resulting from the interaction of the slave device with the environment.

In both of the aforementioned 2-channel controller architectures, not all the information which can be measured is being used for control purposes, thus unnecessarily reducing the search space for optimal controllers. As a solution to this problem, 4-channel controllers have been developed, which use all the measurements available in the system (force and position, in the master and in the slave devices) to control the master and slave device. In some cases, additional channels are included when other sources of information are present, as is the case when internal deformations of the master and slave devices are also considered.

Stability problems are common in haptic teleoperation, with instability often been reported as a consequence of communication time delays, sampling time delays, high control gains or sharp impedance transitions in the environment with which the slave and master devices interact. These instabilities are a topic of extensive research in the control engineering community. In existent system, the instabilities are often treated by adding physical or virtual dampers, lowering the system mechanical stiffness, or lowering the controller gains. All these techniques have negative effects on the system performance, and therefore their parameters must be carefully tuned to ensure robustness in realistic situations, while keeping performance as high as possible.

1.2 Application niche: micromanipulation for prototyping and small series

Automation is desirable for most micromanipulation cases: it is fast, repeatable and requires no supervision. Nevertheless, in some cases it is not possible to apply this strategy. Small series of products or prototypes may not be worth the cost and efforts of automating the operation. In other cases, scenarios unknown in advance, dynamic situations or lack of knowledge of the properties of the objects require the judgment of a human operator to dynamically analyze the situation and adapt the action plan accordingly. It is in these cases where a haptic teleoperation scheme becomes interesting. It is therefore important to understand that the value of haptic teleoperation systems is in their ability to tackle a variety of tasks and situations. Even if benchmarks are used as study cases and for assessment, the resulting system should not be limited or optimized solely to deal with such benchmarks, and should instead keep its properties sufficiently broad as to be applicable to a variety of problems.

Several examples can be found in literature of prototypes and processes for which micromanipulation is required. Whether in the specific case an automated or teleoperated manipulation routine is applied, depends on the focus of the research work which is often the manipulated object and not its manipulation, on the expected or

required yield, and on the equipment available. What is important for this thesis is that these products and processes are being developed and used, and that a system for haptic teleoperated micromanipulation could become an important aid in their development. In the field of MEMS and MOEMS, micromanipulation is used to assemble components fabricated independently and possibly through different technologies, into complex functional systems. That is for instance the case in [87], where a planetary gear system is assembled out of gears fabricated with LIGA technology, in a housings fabricated separately by precision engineering methods. The work of Yantao et al. in [74] is another example of MEMS manipulation, where micro-mirrors are lifted from the wafer where they are fabricated into an upright position. In the case of MOEMS, [71] reports on the assembly of a miniature electron beam steering column composed of several patterned-silicon electron-lenses, while Bargiel et al. have developed a free-space micro-optical bench and demonstrated the assembly of elements fabricated by different technologies into complex optical systems [13]. In life science, micromanipulation is also used when studying or acting on cells, microorganisms, and their organs. A common application within that field is the injection of cells, as presented in [75] and [88]. Another example is reported by [28], where silicate micro-particles are released in the vicinity of E-Coli bacterias to study their reaction. Minimally invasive surgeries are another field where haptic teleoperated micromanipulation finds itself useful, as shown in [39, 57, 15, 80].

In several of the aforementioned applications objects have typical dimensions in the micrometer range (up to a few hundreds of micrometers), and due to their fragility the force and torque to be controlled are respectively in the mN and μNm range with μN and nNm resolution. Moreover, they all deal with the fabrication of experimental prototypes, the execution of novel procedures, and the presence of uncertain conditions, a perfect environment to profit from the combination of the intelligence of a human-operator and the precision of robotic-devices.

1.3 Systems for haptic teleoperated micromanipulation

Teleoperation systems have been utilized in micromanipulation applications by many groups, specially from 1990. Some of them have been developed specifically for teleoperation, while in others teleoperation is just a step toward the automation of their functioning. A list of some interesting and recent systems is given in Tables 1.1 and 1.2, and the following subsections give a short summary of characteristics commonly found in this kind of systems.

Table 1.1: *Properties of systems for teleoperated micromanipulation developed by groups working currently in the field (Continued in Table 1.2).*

Reference	Group / Institute	DOFs	Movement resolution	Movement range	Vision system
[84]	CATS, RPI / NIST	3 translations per probe x 2 probes, and 3 DOF in the base (x,y,and θ_z)	∼2µm and 1mdeg in each axis	∼5mm in each translation axis	Top and side cameras
[68]	IWB, TUMunich / HFI, UBMunich	2 DOF in the base (x,y), 1 DOF in the tool/camera (z)	1µm		2 cameras
[67]	IRIS - Zurich	4 DOF in the base (x, y, z, θ_z) and 2 DOF gripper (rotations)	∼2mdeg, 25nm	12.5mm (x, y, z), > ±50 degrees	2 cameras with special lighting system
[83]	Texas Tech University / University of Maryland	1 DOF in the base (x) and 2 DOF in the tool (y,z)	∼0.4µm	∼11mm	Microscopes
[73]	Michigan State University / Chinese University of Hong Kong	3 DOF in the base and 3 DOF in the manipulator			Zenithal view microscope
[22]	Laboratoire de Production Microtechnique, EPFL	4 DOF in the base (x, y, z, θ_z), and 3 DOF in tool	0.5 µm	150mm in each axis	Zenithal camera
[30]	IPCR, Karlsruhe	3 DOF mobile robot (x, y, θ_z) and 3 rotations of the tool	10nm	unlimited	Several cameras and vision systems for supervision and positioning
[75]	ARC Seibersdorf Research, Austria / CRIM Lab and ARTS Lab, Scuola Superiore SantAnna	3 DOF in the tool	Sub-nanometer resolution		
[11]	Nagoya University / Tokai Rika Co., JAPAN	3 DOF in the tool	Fast stage 40nm - coarse stage 26nm	Fine stage 100µm - coarse stage 25mm	
[13]	FEMTO-ST, Besançon	4 DOF in the tool (θ_y, and coarse x, y, z) and 4 DOF in the base (θ_z, and fine x, y, z)	Nanometer resolution (fine stage) and 1.1 µdegrees	25 mm (coarse stage)	3 cameras

Table 1.2: *Properties of systems for teleoperated micromanipulation developed by groups working currently in the field (Continued from Table 1.1).*

Reference	Force sensing	End Effector	Master device	Teleoperation	Demonstrator
[84]	Estimated through the vision system from deformations	2 independent probes, used as a gripper	GUI	Some components are autimatically placed, other through teleoperation	Tripod structure out of 4 plates of 500μm length
[68]	1 DOF force sensor in the base	Mechanical and vacuum gripper	2 DOF force feedback joystick	Teleoperated in velocity or position	Pick and place $1 \times 1 \times 0.5\text{mm}^3$ chip
[67]	Force sensing gripper, force estimations from virtual reality simulation	Mechanical, capacitive and vacuum grippers	3D mouse and a Phantom master device	The user interacts with a virtual reality simulation, updated through image recognition	Assemble of 3D structure of $\tilde{1}\text{mm}^3$ out of 2 plates
[83]	Force sensing gripper	Femtotools gripper	Falcon master device	Teleoperation with force feedback from gripping	Pick and place 45 spheres
[73]	2 DOF PVDF force sensor (5μN range)	Single probe	Force feedback joystick, across Internet	Switching between automated and teleoperated with force feedback in 2 DOF	Lift micro-mirrors from wafer
[22]		Interchangeable grippers and a glue dispenser	GUI	The user configures and triggers preprogramed sequences (pick, place, dispense glue)	Watch plate assembly
[30]	Force sensing gripper (2mN resolution)	Mechanical gripper with glued strain gauges	6D mouse	Teleoperated through the 6D-Mouse and GUI. Acoustic signal to indicate range limits, and visual indication of force	Lens assembly
[75]	3 DOF microforce sensor, 03N for normal and ±50mN for tangential forces with a resolution of 11 bits	Single probe	Phantom master device	Haptic teleoperation, with the user interacting with a model of the compliance of the environment	Cell palpation and cell injection
[11]	Custom 3 DOF force sensor		Custom 3 DOF master device	The user interacts with a virtual reality simulation, updated through image recognition	Cells manipulation
[13]	No force sensing (but mentions the need for it)	Piezo-actuated gripper, 2 DOF per finger	Joystick	Teleoperation through software-commands, joystick, and automation of subtasks	Re-configurable MOEMS

1.3.1 Positioning

For the positioning of the tools and the components in the slave side, different schemes can be observed. All the reported systems present at least the 3 translational DOFs between the tools and the work-table, up to 6DOF in some systems, and even more when redundancy is required or additional tools must be used [22, 84]. These DOFs are normally divided between the work-table and the manipulator(s). In that way, most systems provide the work-table with the planar DOFs (translations along x and y axis, and rotation around the vertical axis), and use the remaining DOFs to drive the tool. In particular, the use of coaxial rotation stages for the tool permits a fixed location of the tool tip, thus making this a preferred option [67].

Additionally, it is a common technique to use combinations of fast stages with long range and low resolution for coarse positioning, and fine stages for the more delicate operations. Ranges larger than 10 mm and 90 degrees are common, with movement resolutions in the micrometer and millidegree level, or even in the nanometer level when using piezoelectric actuators. A particular case are systems with mobile manipulators, as in [30]. Mobile manipulators can position themselves across large workspaces, thus only being limited by the size of the plate on top of which they maneuver.

1.3.2 Sensing

The sensing capabilities of the systems are commonly limited to position feedback in the positioning stages, visual feedback from microscopes and cameras, and force feedback from sensors in the work-table or the manipulation tools.

The feedback from the positioning stages is not always a requisite, with some systems operating in open-loop and others using image recognition algorithms as end-point position feedback for the whole positioning system [84].

Visual feedback is achieved by means of cameras and microscopes monitoring the manipulation. The use of two cameras is often necessary in order to reconstruct 3D information [68, 67]. It is also useful to count with a global view of the whole workspace in addition to the local vision feedback. For instance [22] presents a system where an initial *global scene* is acquired and is latter used as a reference for the position of the different components to be manipulated, while a detailed view guides precise manipulation operations.

Force sensing can be achieved in different ways, either indirectly by the reaction forces in the system or directly at the point of operation. Indirect measurements can be done with force sensors in the work-table or between the manipulator of the tool and the tool-tip, while direct force measurement can be achieved with sensors placed in the tool-tip. Many of the systems limit themselves to sensing the grasping force with sensors implanted in the gripper fingers in order to ensure a solid but delicate

grasp of the manipulated objects, like is the case when using the grippers developed by Femtotools in [67, 83], or with custom developed sensorized grippers using glued strain gauges [30]. For the measurement of interaction forces between the tools and the manipulated objects, some groups have developed force sensors which are used in the position of a wrist, that is, between the base and the tip of the tool. In that way [73] describes 1 DOF and 2 DOF sensors based on the piezoelectric effect in PVDF, and [75] uses a 3DOF sensor fabricated in silicon using the piezoresistive principle. Given the difficulty of integrating tools with sensors measuring forces in several DOFs, these systems use mostly probes as the end effector mounted on the sensor. Other groups have placed force sensors in the work-plate instead of in the tool, like is the case of the 1 DOF vertical force sensor used in [68], or of the system suggested in [56] for measuring forces in multiple DOFs with an array of 1DOF force sensors holding the work-plate. Wason et al. report on the option of using visual information to estimate the forces in the microenvironment in [84].

1.3.3 Teleoperation interfaces and haptic feedback

The range of teleoperation interfaces depicted in Tables 1.1 and 1.2 starts with systems using only a GUI, in which the user inputs positioning or force application commands for the system to follow, as is the case in [84]. In some cases, the GUI allows the user to configure and trigger more complex pre-programed routines, for instance to pick, place or transport a component [22].

The next step in teleoperation interfaces is the introduction of 3D input devices. These devices range from 2 DOF to 6 DOF joysticks [68, 73] and 3D or 6D mice [30, 67], to haptic input devices like the 6 DOF Phantom from Sensable [67, 75] and the 3 DOF Falcon from Novint [83]. When a mismatch exists between the DOFs of the input device and the DOFs to be controlled in the slave device, the device mapping is changed depending on the needs of the step to be executed [83, 68].

When force measurements are available, that information can be presented to the user through the master device, thus achieving haptic teleoperation. In order to do so, most systems use the position-force control scheme explained in Section 1.1. Many systems count with measurements of the gripping force, but not with a force reflecting gripper in their master device, thus requiring graphical indicators or transformations of the gripping movements and forces of the slave device into, for instance, pushing motions in the master device [83]. Force-feedback of the interaction forces in multiple DOFs is usually not available, due at least in part to the lack of suitable force sensors. When the characteristics of the setup make it impossible to render the measured forces at the slave side in the master device, other methods are used to estimate and render such forces for the user. One example is the work of [75], where the bandwidth of

the sensor is too low for providing direct force-feedback from the slave interactions to the user, but is enough to create a model of the compliance of the environment which can then be used in the master side for rendering purposes. Probs et al. in [67] and Arai et al. in [11] extend this concept and create a virtual-reality (VR) model of the remote environment, which is constantly updated thanks to visual information coming from the real work-environment. In that way, the user can interact with this VR model, access views which would not be possible to obtain from the real system and, if direct force measurements are not available, obtain force feedback from the simulated interactions. In spite of the large amount of reported research on micro-manipulation, haptic tele-operation is nevertheless only seldom applied in this field, and only to a limited extent. This is probably caused by the problems with stability of haptic controllers often reported in the literature, and by the absence of appropriate force sensors and sensorized tools.

1.4 Open challenges in the slave-side and problem definition

Using haptic technology for micro-manipulation has shown promising results. Many challenges remain nevertheless which need to to be overcome, with regard to design and control of multiple-DOF haptic teleoperated systems for performing dexterous tasks. Among them, within the devices in the slave side of the teleoperation system it is possible to identify the following:

1. The existing haptic environments present grasping force feedback, but no or little feedback in terms of interaction force (i.e. the force exerted on grasped microparts by other elements present in the assembly environment).

2. Existing slave devices are not optimized for the presence of a human operator in the loop, resulting either in systems over-performing the user (and therefore unnecessarily expensive) or in non-transparent operations.

3. No or little attention is given to psychophysic parameters (those accounting for the limitations and abilities of human operators) during the design of devices intended for haptic teleoperated micromanipulation. When assessing the designed system, the human operator is again often disregarded and characterizations are based solely on the performance of the devices, and not on their interaction with the user and the capability of the user to perform tasks aided by the system.

These challenges yield to the following problem definition for this thesis.

Problem definition

The intention of this thesis is to understand how a user can be better supported in order to accomplish micromanipulation tasks by using haptic teleoperation. This thesis makes use of that understanding as a basis for the design of slave-side devices specifically intended for this application, and for the integration of a full haptic teleoperation system. In particular, this thesis focuses on the study of two slave-side devices: the positioning system and the force sensor.

1.5 Methodology

Figure 1.2 shows a diagram of the methodology used in this thesis, which can be described as follows:

1. The analysis starts by defining an application niche, which in this case is that of micromanipulation for prototyping and small series, within a haptic teleoperation scenario.

2. System requirements are defined for that application niche. Several aspects are analyzed to arrive to those requirements:

   - This work focuses in haptic teleoperation systems. In such systems the users interact, sense and control mainly displacements and forces. Consequently, they interact with the environment through its impedance. Therefore, a classification and decomposition of tasks in their simplest primitives is performed, in terms of the positioning goal or force-application goal of the user and in terms of the environment-impedance in which such operation is performed.
   - In parallel, the haptic teleoperation scenario is analyzed, and the different modes in which such a system can operate are identified. Then, specific suggestions are made on what operation modes could improve operator performance, considering the micromanipulation primitives previously described, and on the implementations specific to this problem.
   - The fact that a human operator will be part of the system makes it necessary to consider also psychophysic aspects of that operator.

3. Based on the system requirements, a system is designed, implemented and integrated. The final system is composed of commercially available components, as well as of components developed for this application. In particular, a magnetic levitation stage and a silicon based force and torque sensor are developed in this thesis.

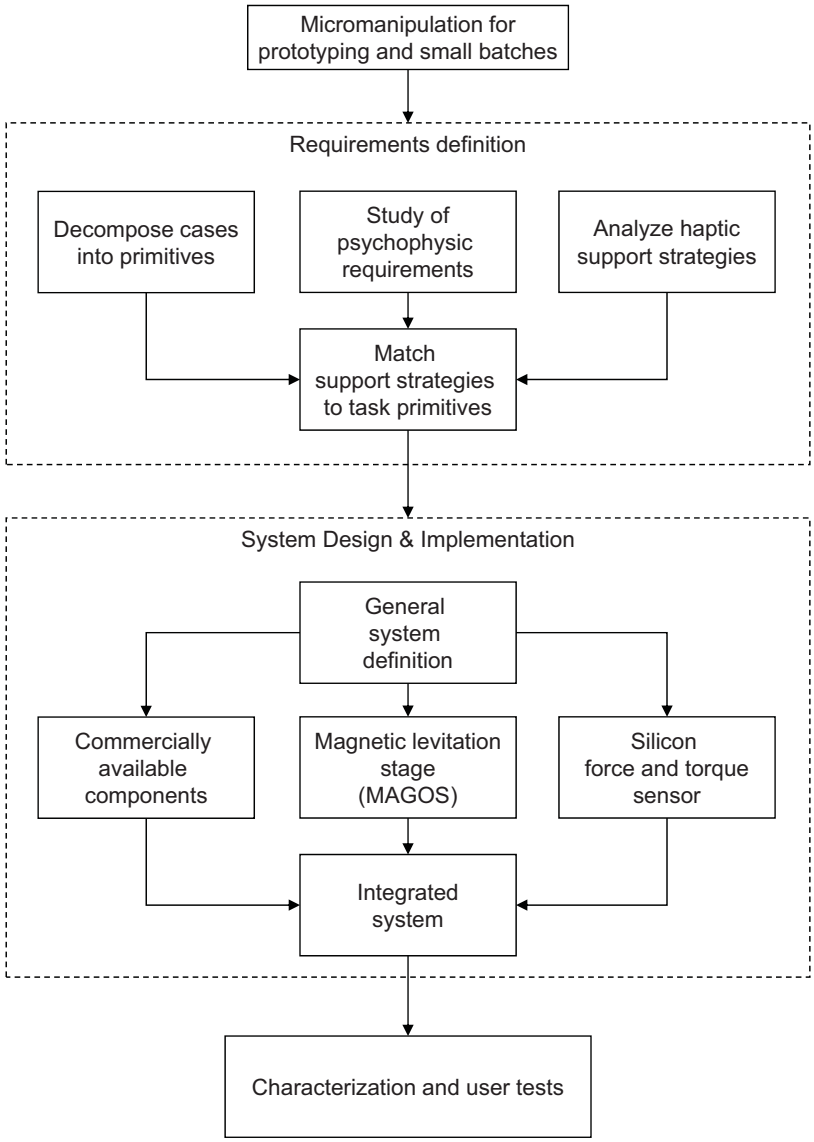

Figure 1.2: *Methodology Diagram*

4. The integrated system is characterized and user tests are performed to validate its usefulness for teleoperated micromanipulation tasks.

1.6 Reading guide

The work described in this thesis followed a classic Systems Engineering V-model design process: it started with the definition of the top-down requirements and the matching bottom-up specifications, followed by a general system design, and then by the design and implementation of the system components. After components were produced they were tested independently, integrated, and tested as an integrated system. Consequently, this book is divided in 3 main parts: Part I is devoted to the definition of the system requirements, Part II deals with the design and integration of the system, and Part 3, focuses on the characterization, validation and discussion of the system.

Eight chapters can be found within these 3 parts. A short introduction to these chapters is given in the following list, in order to guide the readers to and through the sections that can be more interesting for them.

- Chapter 2 deals with the description and decomposition of micromanipulation tasks. It gives a structured view into the situations encountered in micromanipulation, and which could be targeted by haptic teleoperation systems.

- Chapter 3 focuses on the applicability of haptic teleoperation to the micromanipulation problem. In order to do so, the chapter starts by classifying the different modes in which a system for haptic teleopearation can support a user, a classification which can also be useful for other fields of application.

- Chapter 4 identifies several parameters and design rules that arise from the presence of a human operator in the system. This chapter is partly based on a literature review of known facts about the acting and sensing capabilities of humans, and partly on psychophysic studies conducted during this research. These test analyze the requirement of the operators regarding the accuracy of the system, and the ability of the operators to adapt to different configurations of the positioning stages.

- Chapter 5 uses the previous chapters as a basis to describe the requirements for the haptic teleoperation system, such that it satisfies both the needs arising from the tasks and from the presence of the human operator.

- Chapter 6 moves into the conceptual design of the system. The system components realized in this work are briefly described, as is the integration between them and with commercial products. The details on the developed components are dealt with in separate chapters (7 and 8).

- Chapter 7 describes in detail the design, development and characterization of a 6 DOF magnetic levitation stage, intended as a slave device for the haptic teleoperation system. Encompassing aspects of mechanics, electronics, instrumentation, control and real-time software, this chapter will be of particular interest for mechatronic, mechanic, electronic and control engineers.

- Chapter 8 describes in detail the design, development and characterization of a silicon based 6 DOF force and torque sensor. This chapter deals mostly with aspects of silicon fabrication, piezoresistive sensing, signal acquisition and signal processing, and is therefore of special interest for experts in micro-engineering, mechatronics and electronics.

- Chapter 9 gives an overview of the properties achieved by the final system and its components. Moreover, this chapter demonstrates the ability of the developed system to support an operator on micromanipulation tasks, by describing the execution of 2 tasks by an operator using this system. In particular, a psychophysic test demonstrates the advantages arising from the presence of haptic feedback in the system.

- Chapter 10 gives a summary of the conclusions derived after this work, and finalizes with recommendations for future work in the field. It must be noted nevertheless, that within each chapter conclusions are given on the topics of the chapter.

Part I

From the haptic micromanipulation problem to system requirements

A complete understanding of the requirements arising from the targeted tasks, from the usage scenario, from the presence of the human operator and from the kind of support that is useful to provide to that user, allows for the optimization of the haptic teleoperation system designed in this thesis. The first 3 chapters of this part explore the aforementioned sources of requirements by discussing the requirements coming from the micromanipulation tasks (Chapter 2), the use of haptic teleoperation (Chapter 3) and the presence of the human operator (Chapter 4). The last chapter of this part takes that discussion as a basis to arrive to the system requirements.

Chapter 2

The micro-manipulation field

Micromanipulation is a wide field, involving many types of physical manipulation of parts with sizes, features or clearances in the sub-millimeter range. For each product or task a different set of operations must be carried out. Automatic micromanipulation systems are therefore designed and optimized for such a set of operations, augmenting the yield and repeatability for a certain task but often sacrificing the flexibility of the system.

Teleoperated systems, on the other hand, value flexibility as one of their main assets, thanks to the planning ability, learning ability and adaptability of the human operators. Thus, such systems should be designed to provide functionalities useful to many tasks. It is not realistic to optimize a system for performing each possible micromanipulation task, but it is possible to generate a set of elementary *task-primitives*[1], design systems to perform such primitives, and exploit the system capabilities when performing more complex tasks (as mentioned by Morrow in [60]).

This Chapter presents a novel classifications system to describe the spectrum of tasks that can be encountered in micromanipulation, focusing on the force-application or positioning goal of the operator, and of the impedance of the environment in which the tasks must be performed. The description is focused on tasks often encountered in micromanipulation, but many of its concepts could be easily extrapolated to other situations. This chapter starts by describing, in section 2.2, a representative set of elementary *task-primitives* which constitute the building blocks of a *task*. Primitives and combinations of primitives from this list will often be used in this thesis to describe relevant tests and usage scenarios for the developed system. The second part of this

[1] In the sense of basic functions from which more complex functions can be constructed.

chapter (section 2.3) studies the particular characteristics of relevant tasks in micromanipulation (compared to macromanipulation). Within this section, the operations are further grouped into three categories that represent a useful set of comparable tasks in the analysis of micromanipulation systems, and are used to define the requirements for the devices studied in this thesis.

2.1 Introduction

Many research groups define task classifications, categories, or simple lists, mostly as a framework to describe complex micromanipulation operations. Therefore, the categories are defined either based on the function of the operation, or on chronological order in the manipulation process. For instance [84] breaks the assembly sequence of a complex structure into 2 *tasks* (assembly sequences), and further into sequential *steps*: x-y positioning, z positioning, grasping, lifting, rotation, insertion and release. Similarly, [47] decomposes surgical *tasks* into *steps* (e.g. move, orient, insert, puncture, hold, retract), that are used both to understand user intent and to define the system behavior (assistance mode) during their execution. [78] uses also sequential steps to describe a micromanipulation operation, and [33] mentions feeding, positioning, releasing, alignment and fixing phases, among many other similar classifications in the literature. Hansen et al. [36] take a different approach and creates a set of clearly specified and measurable parameters to describe and compare different assembly techniques, such as the materials to which they can be applied or the possibility to revert the step, but most parameters are function-related and have a different interpretation for different assembly steps.

In contrast with the previous cases, where tasks are decomposed based on sequential order or functionality, other work focuses on the force and position profiles of each operation. Positioning and control of forces between tools and the environment is a common parameter during most micromanipulation tasks, while other operations (such as glue application, UV activation, heating or gripping) are step- or field-specific. Therefore, such classifications provide a way to relate operations between different fields (microsurgery and microassembly for instance), and within the same field or task, between different steps that share similar characteristics. These classifications are also of particular interest for this thesis, since force and position carry the main information that is exchanged between operators and the system through haptic teleoperation interfaces. An example of this approach is the one used in [60], where manipulation tasks are classified by the relative motions between two rigid parts (considering only free-moving and stiff-contact relations). The set of all possible kinematic constrains between the two parts is defined, the resulting motion spaces described, and it is suggested to design re-usable algorithms for these primitive operations. Some

classifications (for instance [9]), focusing mostly on 1DOF problems, use a simplified version that only considers the constrained or unconstrained cases (or hard contact and free air, respectively), optionally including contact transitions and force constrained tasks.

2.2 Decomposition of manipulation processes in force and position primitives

The approach taken in this thesis is to decompose manipulation processes into primitives, based on the nature of the intended force/position interaction between the tool and the environment, and the impedance with which the environment reacts. It is important to notice that impedance is understood here as describing in a general sense the relation between forces applied on the environment and the resulting displacements. In that sense, impedance includes stiffness, damping and inertial terms among other. In such way, it is possible to create the following classification of task-primitives (with some example operations). A diagram can be found for reference in Figure 2.1.

- Zero Impedance: Tasks realized in free air, with full movement freedom, and no interaction forces. This is the case for instance when transporting an object between locations, aligning it to the environment or visually inspecting it.
- Impedance transitions: Tasks where during the execution the stiffness of the environment presents a sudden change. This includes cases like:
  - Zero impedance → Infinite or Fixed Stiffness, e.g. when establishing contact with the environment.
  - Fixed Stiffness → Zero impedance, e.g. when breaking silicon components from substrates, using snap fixtures, piercing membranes [75], or detaching objects from glue, tape, and even from the substrate due to capillary, van der Waals or electrostatic forces.
- Non-extreme impedance: Cases where constant contact is maintained and impedance of the environment has a non-extreme value. May also represent certain force fields (magnetic, electrostatic). Depending on the kind of impedance, the interaction can be for instance one or a combination of friction (e.g. while sliding against a surface), damping (e.g. when moving in liquids or applying them to a surface), and stiffness (e.g. by the use of flexible tools). Other impedance descriptions are possible, some of them non-linear or time variant, like is for instance the case when performing a press-fit insertion or interacting with magnetic fields.

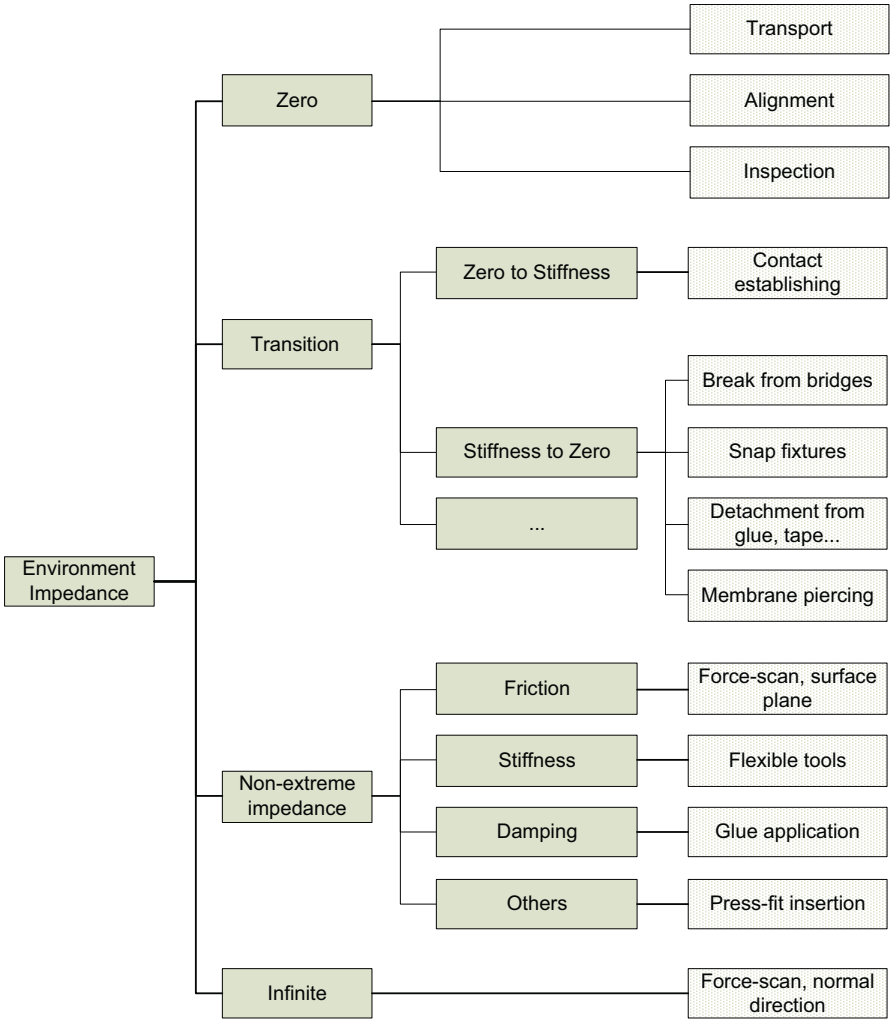

Figure 2.1: *Taxonomy of tasks execution primitives. Some examples are presented at the end of each branch, with white background.*

- Infinite Impedance: Tasks realized in constant contact with a fixed solid object. There are no appreciable displacements, and any inputs generate changes in the interaction force. This situation occurs when parts must be held in contact, for instance while curing glue. Also, when scanning a surface (for painting or scratching it, or placing an object), the normal direction presents an infinite impedance situation. It must be noted that even if a certain level of compliance is always present, for *infinite impedance* tasks the normal displacements while in contact with an object are neither important not useful for the completion of

the task.

2.3 Characteristics specific to micromanipulation tasks

Micromanipulated objects range in sizes between a few micrometers and a few millimeters. Even though there is not a sharp difference betweens these objects and other objects outside of that range, for objects below a few micrometers different physical phenomena become dominant. Therefore, specialized tools are required for their observation and manipulation, and those tools are not always compatible with the tools used in the microworld. Objects measuring several millimeters on the other side, can be directly manipulated by hand, and are therefore not a main target of this work.

Features within the microcomponents and the tolerance of such features, can have much smaller sizes. These features often guide the manipulation operation, where such features must be aligned, engaged or targeted by the tools. Parts clearance and size of object features may differ widely, but for the cases targeted in this work values between 200nm and 2µm may be reasonably expected, given current microfabrication techniques. Even though the parts and features are in the micrometer level, the whole micromanipulation operation may take place in a much larger area. The objects considered in this work are expected to be placed by hand or by low-precision equipment in trays in the range of several millimeters.

In the rotational degrees of freedom, objects can present arbitrary initial rotations, requiring up to $\pm 180^\circ$ to become aligned between themselves or with environment features. From the 3 rotation axes, 2 are nevertheless much less used in micromanipulation tasks, since many of these occur in what is called a 2.5D environment. Micro objects are often manufactured via planar fabrication technologies, and exhibit forms resulting from a 2D profile and a constant (or at most stepped) elevation. Therefore, the rotation around the axis normal to the work-table plane (the *vertical* axis) may present arbitrary values, while the rotations around the remaining axis tend to be relatively small. Even though there are as well situations in which full 3D tasks may be necessary, this thesis focuses in the 2.5D case, where the vertical misalignments (rotation around the axes parallel to the surface) are assumed negligible.

2.3.1 The three groups of micromanipulation operations

As can be seen from the previous paragraphs, the whole micromanipulation operation is performed within an area of a few millimeters, while some steps must reach features with a motion resolution below the micrometer level. Nevertheless, the resulting requirements on workspace and motion resolution do not need to be covered at the same time. It is convenient to differentiate between 3 groups of operations and ana-

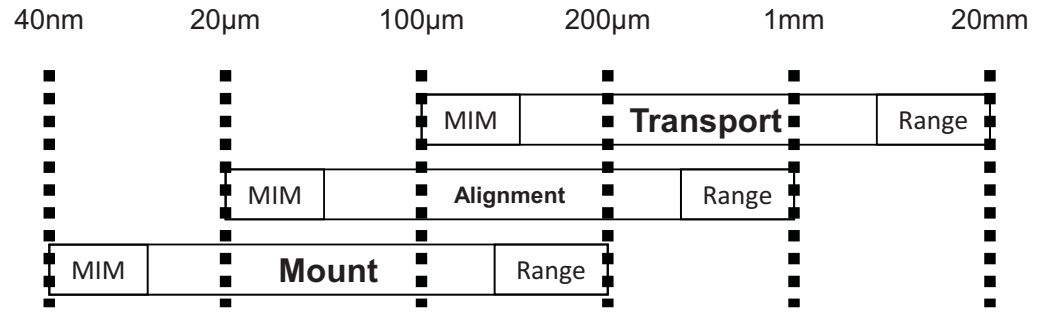

Figure 2.2: *Operation groups on micromanipulation, and their corresponding ranges and minimum incremental motions (MIMs).*

lyze their requirements separately: a group of coarse transport operations, a group of alignment operations, and a last group of fine mounting operations[2]. Each group of operations requires to cover a different range, with a different minimum incremental motion (MIM)[3], as indicated in figure 2.2, and extended in the following paragraphs[4].

Transport operations

This category groups operations where free air displacements are required over the whole workspace of several millimeters. This is the case when the tools must reach for or transport an object, or reach for a position within the workspace. Since the operations are executed in free air, only position control of the slave robot is necessary. Even though the workspace required in these operations must be larger than the common tray sizes (several millimeters), the required MIM must be just enough to ensure a positioning within the size of the manipulated objects and subassemblies. Repeatability in the range of the parts size may also be useful in order to perform semi-automatic operations.

Typically in micromanipulation-tasks and due to the 2.5D characteristics of the parts, the focus is on the 2 planar translational degrees of freedom. Course rotational alignment can be also obtained in this step. In the contact direction overshoot must be prevented, and therefore clearance in this direction is left high. When considering teleoperation, the system must be able to follow the scaled human speed, accelerations and frequencies. Nevertheless, the user is not expected to perform complex trajectories, and therefore only end-point-following is necessary for the highest frequencies.

[2]Similar classifications can be found in the literature, for instance in [76].

[3]Minimum Incremental Motion (MIM) is the smallest increment of motion a device is capable of consistently and reliably delivering [3].

[4]This section is based on and extended in previous work from the author, appearing in [61].

That is, the system must reach the desired final location, but there is no requirement for the slave trajectory to follow closely the trajectory commanded by the operator.

Alignment operations

When the tool is within the manipulation location, a more careful operation of positioning and alignment is carried out. The focus is still on position control in free air, even though some interaction and contact between the tool and the environment could occur or be part of the operation. For this purpose, force measurement and control is required, with enough resolution to not damage the parts. This operation occurs within the parts size, up to visual verification and in the vicinity of obstacles. The positioning range should thus be enough to cover the subassembly area, while the MIM must be at least half of the range of the following, finer group.

Mount operations

In this group, contact occurs between the tool (or gripped parts) and the environment, in order to scan the surface, probe or push objects, grip, place, align, insert parts, etc. A mixture of force and visual feedback can be used. Force monitoring provides information from the interaction to the user or control system, and force control should ensure no-damage to the parts and low contact forces in order to minimize friction and improve position resolution. The highest MIM must allow scanning within the clearance of assemblies, features size or the resolution of the operation, also on the rotation around the vertical axis, and compliance or alignment may be necessary in the remaining tilting angles. In the case of teleoperation, the minimum range must scale the ratio between motion-resolution and range of the user (around 1:100, see section 4.2), but a bigger range may improve the operability.

Some of the most commonly encountered primitives and operations in micromanipulation that correspond to this category are listed below:

- Contact establishing or probing: The tool and the substrate are brought into contact. The main direction of movement is the approach. Movements are typically slow and cautious, since a big overshoot can be destructive. The movement continues until proximity or contact is detected by for instance force sensors, position sensors and a model of the system, or visual information. In micromanipulation, complex surface interactions may appear due to Van der Waals force, magnetic and electrostatic attraction or capillarity. They generate an area of negative stiffness which augments the risk of a destructive collision.

- Fixed-position/force tasks: Processes such as application and curing of glue [49], welding or electric characterization, require for the tool to maintain a position or contact force constant for a short period of time.

- Constrained motion: Mechanical constrains may limit the displacements of the tool in some DOFs, while in other DOFs the body remains free to move. Even though it is often necessary to load the constrains in order to guide the motion of the tool, overloading such constrains must be avoided to protect the parts, tools and substrate. This is typically achieved by a tuned and directed compliance, which allows the interaction forces to guide the constrained DOFs (without overloading the force-guides). Typical cases of constrained motion are insertion or peg-in-hole tasks (where the peg is constrained by the walls of the hole), surface scanning (constrained by the surface in its normal direction) and rotation of objects by using a contact point as a support and rotation axis.

Chapter 3

Application of a haptic teleoperation scheme to micromanipulation

This chapter explores the concept of haptic teleoperation, the possiblities it offers, and the way micromanipulation can profit from it. Analyzing various examples of haptic teleoperation reveals that there are major differences in the way in which commands are transferred from the operator to the slave, how control is shared with automation modules and how measurements in the remote domain and information derived from those measurements are presented to the user. It is also apparent that similar implementations are often presented under different names and descriptions, even though they share common underlying principles. It is therefore useful to have a complete and organized inventory of the possibilities offered by haptic teleoperation. Such an inventory would facilitate assessing the applicability of haptic teleoperation to a certain problem, and, within the problem, to identify the most useful implementation for the given tasks. Moreover, the use of a standard nomenclature would facilitate the comparison and cross-fertilization between different implementations of haptic teleoperation. Abbott et al. [7] point out the importance of generalizing the research in the field "so that knowledge gained in individual research efforts can advance the field as a whole".

Some classifications of haptic teleoperation modalities already exist. Abbott et al. [7], for instance, work on virtual fixtures (VF), and defines several options for their application, presenting two possible implementations (*guidance* and *forbidden region*

VF), and further dividing them into *passive* or *active*, *impedance* or *admittance* type, *hard* or *soft* effect and depending on whether the fixtures are applied to the slave or master robot. Abbink et al. [6] interpret the haptic teleoperation situation as a shared control between the operator and the computer, and thereafter identifies the options of *input-mixing shared control* and *haptic shared control*. The aforementioned modalities-analyses are valid and have proven successful in exploring options within their fields. Nevertheless, these classifications are often created ad-hoc, and are limited to the scope of a particular research. Other work suggest a continuum of possibilities between *full automation* and *manual teleoperation*, including in-between options like *supervisory* and *Director / Agent* control (e.g. [58]). Such descriptions are very general and therefore manage to cover a wide range of operation modalities. On the other hand, they fail to provide clear clues on the specific implementations of haptic teleoperation available for a given task.

A different approach is taken in this chapter to present an overview of the so-called operator support strategies. The proposed inventory reaches a wide set of options by describing the operations modalities through a common factor in most of the reported work: the sources and targets of the information transferred by the haptic teleoperation controller. Such an approach allows to identify and relate support modes across different fields or implementations of haptic teleoperated systems, classify the existing work and promote cross-fertilization. On the other hand, this inventory manages to identify specific implementations of haptic teleoperation within the aforementioned general description.

Section 3.1 of this chapter identifies several components of a haptic teleoperation system, and the channels though which information flows between them. Based on that description, section 3.2 introduces the proposed classification of support strategies. This taxonomy aims to identify the complete range of options available in haptic teleoperation, and is then used in section 3.3 (together with the micromanipulation primitives of section 2.2) to explore the value that each of them could have for micromanipulation.

3.1 Information channels in a haptic-teleoperation system

When an operator interacts with an environment, information flows in the form of actions of the user on the environment, and in the form of feedback from the interactions with the environment to the user. Figure 3.1a represents the case of a human operator performing a task directly, interacting with his limbs (and possibly through a tool) with a passive environment. The human user compares his goals with the information he gets from the interaction forces with the environment, and from visual and proprioceptive position information. Trying to achieve his goal, and unconsciously

using a model of his limb system and of the environment, the operator commands his limbs forces and impedance. The limb interacts then with the impedance of the environment, and such interactions define the displacements of the limb. In this situation, commands flow from the operator to his limbs, and information flows back to the operator representing the interaction of the limbs with the environment.

In a haptic teleoperation scenario, the operator interacts with the master device, while the environment interacts with the slave robot, as can be seen in Figure 3.1b. In the middle appears the Haptic Teleoperation Controller (*HT-Controller*), that commands both the master and the slave devices, while monitoring a whole range of forces and positions. Force and position information comes from the slave and master robots, the interfaces between master and limb and between slave and environment, together with other information available via additional sensors or models. It is important to notice that in general the HT-Controller can independently control the master and slave devices.

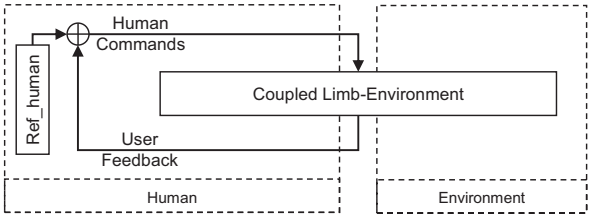

(a) *User-Environment Interaction.*

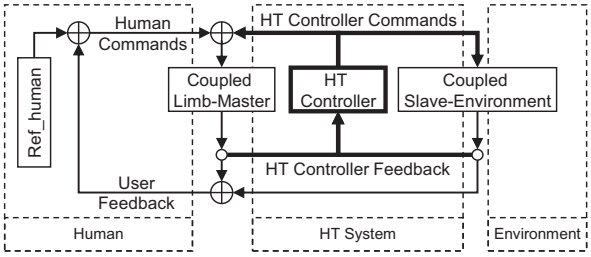

(b) *User to Environment Interaction through the master device, HT-Controller and slave device.*

Figure 3.1: *a) User-Environment Interaction. The intentions of the human are compared with sensory information, and correcting commands are sent to the limb. The interaction with the coupled limb and environment impedances defines the displacements of the limb. b) User to Environment Interaction through the master device, HT-Controller and slave device. The HT-Controller commands both the master and the slave devices, and monitors the forces and positions in different points of the diagram. The user receives visual feedback from the environment, plus force and position feedback from the master device.*

Figure 3.1b helps identifying different modes in which a teleoperation system may operate, depending on the flow of information. These modes are further explained in the following section.

First, the channels through which the HT-Controller can act, can be identified, namely by issuing commands to the slave device or to the master device.

Such commands may represent the force and position interactions at the other side of the HT-Controller, or can be deliberately issued by the HT-Controller based on other information or internal models and task execution plans. Therefore 3 sources can be identified from which the Force/Position commands are generated. One possible source are the signals indicating the commands sent by the user through the displacements of his limbs and the forces developed between the limb and the master device. In the second source, the signals come from the slave side (the remote environment), informing about the displacements of the slave robot, the reaction forces from the environment and even any forces coming from a possibly active environment. In general, not all of these channels need to be measured by sensors, and the information can in some cases come from environment models, be deduced from indirect measurements or even come from a virtual environment. What is important is whether this information represents the force or position phenomena at the other side of the teleoperation system. The third source is the HT-Controller itself, which can generate deliberate commands, not intended to represent the interactions on the other side of the teleoperation system but for instance based on knowledge of expected events or safety risks.

3.2 The Source-Target classification

By connecting the aforementioned command-sources to the acting channels it is possible to identify the main operation modes of the haptic teleoperation system and organize them on the classification categories shown in Figure 3.2. The following headers expand each source-action case, explaining some possibilities within them. References are made to their effect on task development and performance, and to their use in current literature. This information is summarized in Figure 3.3.

3.2.1 From Master-Human Interactions to Slave Commands: teleoperation

In teleoperation the user operates a distant device. In a transparent case, the commands to the slave copy those issued by the operator. Nevertheless, the disconnection between master and slave allows the HT-Controller to modify the signal with linear and non-linear transfer functions. Teleoperation requires, next to the HT-Controller,

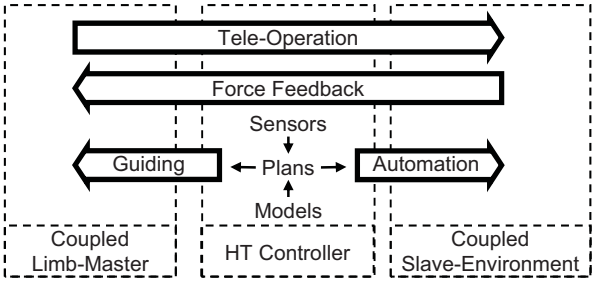

Figure 3.2: *Operation modes of the haptic teleoperation system, based on sources and targets of information. Tele-Operation occurs when information is transmitted from the master environment to the slave environment, force-feedback when the information flows from the slave environment to the master environment. The HT-Controller can also issue deliberate commands based on sensor information and models, resulting in either automation or guidance routines.*

a master device able to measure the user commands (e.g. a joystick) in the ranges, resolutions and bandwidths in which the user operates, and a slave device (e.g. a positioner robot) able to follow them with specifications matching the task. Some interesting cases are described here.

Signal scaling:

The forces or displacements commanded by the user can be scaled in order to cover bigger ranges at lower resolutions (by upscaling) or achieve higher resolutions in smaller ranges (by downscaling). The scale factor can be dynamically adjusted during the operation, achieving then a range-to-resolution ratio bigger than what is comfortably achievable by the operator limb. Both micro and macro teleoperation cases are developed in [68], while control issues are studied in [63].

Filtering:

Different filters may be implemented to reduce the transmission of involuntary or dangerous signals, like limb tremor, or any signals above the human controllable bandwidth (between 2 and 10 Hz according to [18]).

Modify the dynamics:

The zero-order dynamics of position commands can be changed, for instance, to velocity or acceleration commands, as shown in [68] where position and velocity control are compared. [56] shows an implementation with seamless transitions between two dynamic conditions.

Teleoperation mode		→	Resulting advantage	Requirements
Teleoperation	Pure	→	Separates operator from environment	Separation of the system in a master and a slave devices, communicated by the haptic teleoperation controller
	Signal Scaling	→	Higher movement ranges or resolutions	
			Dynamic range-to-resolution ratio	
	Filtering of unwanted frequencies	→	Commands out of the voluntary movements frequencies	
			Dangerous high frequency movements	
			Instable frequencies of manipulation system or teleoperation controller	
	Other	→	Bigger ranges through velocity control	
	Non-linear transformation	→	Limit movements under dangerous conditions of force, velocity, position.	
Force Feedback	Pure	→	The user interacts with the forces between the tool and the environment	Measurement or estimation of forces in the slave device, and force feedback capability on the master device.
	Signal Scaling	→	Higher force sensitivity or range	
			Dynamic range-to-resolution ratio	
			Adjustment to the stiffness and fragility of the environment	
	Filtering	→	Focus operator in certain frequencies	
			Limit high frequency force changes	
			Avoid system instable frequencies	
			Minimize noise transmited to the user	
	Non-linear transformation	→	Limit forces outside of safety values	
			Frequency-shift to bring interaction signals to the user sensitive bandwidth	
Guiding	Passive Guiding	→	Limit DOF's with virtual fixtures	Models and/or sensorized monitoring of the remote environment, and force feedback capability on the master device.
			Guide with virtual fixtures	
			Limit speeds and frequencies by adding damping, friction or inertia	
			HT-controller/user shared control	
			Inform the user about transformations being applied to his commands	
	Active Guiding	→	Inform about automatic processes	
			HT-controller/user shared control	
			Training and correcting	
Automation		→	Tools sub-operations	Models and/or sensorized monitoring of the remote environment.
			Free air navigation	

Figure 3.3: *Summary of the operator support modes in haptic teleoperation, their possible effect on the operation performance, and the requirements imposed by them to the system.*

Non-Linear transformations:

Nonlinear transformations of the signal are also possible, as is the case when limiting user commands. In this way the system can limit unsafe speeds, forces or displacements outside of the actuators safety range. These relations may be made dependent on position, time, or other environment conditions.

3.2.2 From Slave-Environment Interactions to Master Commands: Force feedback

By controlling the impedance of the master device to represent the reactions of a passive environment, force feedback is achieved. Equivalently, active forces from an active environment can be rendered as master device commands. This support strategy has at least two positive effects. On one side, it is a fast and natural way to inform the user about such interactions, as is the case in [30] where force sensing indicates the user that a handled object has slipped away. But force feedback also accomplishes a second objective by guiding the movements of the hand by pure physical interaction, in the same way in which a ruler guides the user to make a straight line by imposing an impedance barrier.

These signals, as in the previous case, can be transparently transferred to the user to faithfully represent the remote environment, but they can also be scaled to augment the effective sensitivity of the user to forces, while sacrificing the range, or vice versa. An application can be seen in [68], while related control issues are discussed in [63]. Filtering, limiting and in general linear and nonlinear transformations of the signals are likewise possible, and allow a reshaping of the perceived impedance of the environment.

For force feedback to be achieved, it is necessary to measure the forces between the tool and the environment. Moreover, the master device must not only be able to measure user commands, but also to render forces to the user. Finally, the requirements on the HT-Controller become more stringent in order to avoid instabilities in the resulting bilateral controller.

3.2.3 From HT-Controller to Master Commands: Guiding

The controller can use models and measurements of the environment, the goals of the user, task execution plans or pre-programmed settings to generate guiding forces on the master side. These forces do not represent interactions at the slave side, but will still affect the displacements of the master device and the way the user interacts with it. The HT-Controller requires a good model of the environment and its interactions in order to derive useful guiding forces. This category can be further divided depending on whether the guiding is passive or active.

Passive guiding:

This case represents the so called *virtual fixtures*. They are rendered to the user as impedances, feeding back position dependent forces that do not add energy to the system, like in the case of force feedback. Nevertheless, contrary to force feedback, they do not represent components of the distant environment and instead "overlay abstract sensory information on top of a workspace" [70].

In most of the literature, virtual fixtures only represent stiffness barriers which can be used to guide the movements along certain axis or planes (again, as in the case of a ruler), or to prevent the access to a forbidden region (hardware limits, collision regions, etc.). Nevertheless, other impedances can also be represented. Damping or friction can for instance diminish vibrations and limit speeds and movements bandwidth, either generally or in specific regions.

As in the case of force feedback, virtual fixtures can be used both to inform the user and to serve as a guide for user movements, not necessarily at the same time. On one hand, the use of high impedances or the combination with commands limiting (like those mentioned in section 3.2.1) generate a system that simply forbids the slave to overcome certain constraints. In such cases it may seem unnecessary to limit the user movements since his commands can anyway be limited, but the fixture acts as an information channel, creates a sense of telepresence [7] and reduces the required information processing for the user, notably augmenting its performance [70].

On the other hand, soft impedances in the absence of command limiters allow for a negotiation between the HT-Controller and the user: the HT-Controller can suggest a certain barrier by creating an impedance, and the user can decide to what degree to follow it by tuning its commanding force and limb impedance (as shown in [6]).

Active guiding:

The HT-Controller can also send deliberate force commands to the master device in order to actively guide its movements, contrary to the passive case of the virtual fixtures (even though this case is considered by some authors a *dynamic virtual fixture* [6] [8]). Lee et al. [52] show an application to mobile robots, where forces at the master device guide the operator away from collision situations, and a similar study is done for automotive steering applications in [6]. Basdogan et al. [14] uses haptic guidance to suggest optimal trajectories to users in steering microparticles.

Similar to the case of the virtual fixtures, this guidance serves two purposes depending on its strength and on whether the user commands are being ignored, or faithfully transmitted to the slave device. In the first case, a strong non-overridable guidance is used to inform the user of an automatic process: the HT-Controller is performing an automatic operation with the slave device, and the master device is

guided to follow such operation with no chance for the user to change it. Since the user actions do not influence the slave behavior, the guidance fulfills only an informational purpose, and creates a sense of telepresence for the user [7]. This mode can also be used for demonstrating operations to the user in training systems. In the second case, an overridable guidance is used, and the user commands are transmitted to the slave device (in teleoperation mode). In this way, the user can negotiate with the HT-Controller, through the application of forces in the master device, the commands sent to the slave. The control of the slave device is haptically shared between them, as explained in [6].

3.2.4 From HT-Controller and Slave-Environment Interactions to Slave Commands: Automation

The HT-Controller can use information from the sensors in the environment, models and discrete user-commands to generate a plan, and directly command the slave to perform it, disregarding user force/position commands at the master device. This case corresponds to automation, and can be useful for certain sub-tasks within a more complex non-automated task, reducing the workload of the operator who can focus on other parts of the operation. It also can be used to take over the control of parts of the operation, in order to execute them in a safer or optimal way. [30], for instance, uses a sequence of manual and automated control steps in their assembly process. Nevertheless, as in guiding, this support mode is only possible when a good model of the environment and taks-goals is available, and when sensor information can be used by the HT-Controller to generate and follow its automation routines.

3.2.5 Additional channels

Different additional channels can be used by the HT-Controller to provide feedback to the user. Vibrations have been used to indicate distances [21], visual indicators can show applied forces [30], and sounds can be triggered at workspace limits (also in [30]), among many other options.

3.2.6 Mixing modes

Even though in this classification the operation modes are explained separately, the reader must keep in mind that they are in general co-existing. Most research in the literature present a combination of operation modes acting at the same time, and even changing dynamically through the task execution.

3.3 Applicability of haptic teleoperation to micromanipulation

By revisiting the characteristics of micromanipulation tasks described in chapter 2 and referring to figure 3.3, it is possible to identify how a system for micromanipulation could benefit from different support strategies of haptic teleoperation, in order to improve the performance of an operator, as well as the necessary hardware and software components to be developed in order to implement such strategies. The middle column of Figure 3.3 shows an inventory of the advantages resulting from each support strategy. It is then possible to relate these advantages to the issues of the case in study, and asses the support mode against the capabilities and limitations of the available equipments. It is easy to observe the potential benefits of applying most of the modes present in such table. This section will emphasize issues specific to micromanipulation tasks and typical micromanipulation equipment. Figure 3.4 further summarizes these relations by crossing the task-primitives of micromanipulation explained in section 2.2, with the teleoperation operation modes of section 3.2. For an easier reading, the modes are commented in the following paragraphs in the same order they appear in Figures 3.3 and 3.4.

First of all, the scaling issues in micromanipulation are obvious. The positioning precision and force sensing resolution of humans seldom match those required for microassembly. This situation can easily be improved by downscaling the user displacements and upscaling the measured forces. Changing scales dynamically, allows to adapt to different working conditions, and permits working with much larger range to motion-resolution ratios that what is normally achievable by human operators. Positioning stages are available with motion-resolutions below the micrometer, and relatively large motion ranges, and could easily follow the resulting trajectories. These stages are nevertheless often not designed for human teleoperation, and additional optimization of their properties could be achieved when considering this specific scenario.

Force feedback of the interactions of the tool with the environment is also useful during micromanipulation operations. Indeed, in micromanipulation visual feedback is often obstructed by instruments much bigger than the target features, and limited in resolution, depth of focus and in general clarity. In this situation, force sensors and force feedback could provide an alternative and natural channel to identify contacts and understand the interactions with the environment. Another problem that is usually encountered in micromanipulation is the disturbance of vibrations coming from the floor and from the instruments themselves, which can easily be in the range of the tasks displacements. Even though dealing with such vibrations is largely a local issue of the slave device, their effect on the haptic teleoperation loop could be

<table>
<tr><th colspan="2">Task primitive / Support mode</th><th>Zero Stiffness</th><th colspan="2">Transitions</th><th>Intermediate stiffness</th><th>Infinite Stiffness</th></tr>
<tr><td></td><td></td><td></td><td>Stiff-->zero</td><td>Zero-->stiff</td><td></td><td></td></tr>
<tr><td rowspan="5">Tele-operation</td><td>General</td><td colspan="5">The separation of operator and environment augments the flexibility of the system</td></tr>
<tr><td>(Down) Scaling</td><td colspan="5">Improve resolution and precision of the actions, while reducing the workload on the operator</td></tr>
<tr><td>Limit</td><td>Reduce collisions, avoid actuator overload and overshoots</td><td colspan="2">Limit positioning overshoots</td><td colspan="2">Limit force overloads in actuators and tools</td></tr>
<tr><td>Filter</td><td colspan="5" rowspan="2">Achieves larger positioning ranges (through dynamic scaling or velocity feedback), and can filter out involuntary or dangerous movements, but may result confusing for the operators</td></tr>
<tr><td>Change Dynamics</td></tr>
<tr><td rowspan="4">Force Feedback</td><td>General</td><td rowspan="4">Does not apply</td><td colspan="2">Permits goal identification (e.g. contact, breakage), and control of the interactions</td><td>Allow for characterization, and for controlling the nature and magnitude of interactions</td><td>Provide kinematic information and guiding</td></tr>
<tr><td>(Up) Scaling</td><td colspan="4">Improve resolution and precision on the application of forces, reducing the workload and protecting the handled objects</td></tr>
<tr><td>Limit</td><td colspan="4">Ensures user safety, and improves system stability, though it may confuse the user.</td></tr>
<tr><td>Filter</td><td colspan="4">Attenuates or amplifies certain effects, though it may confuse the user</td></tr>
<tr><td rowspan="3">Guiding</td><td>General</td><td rowspan="3">Improves user performance in terms of time, workload and precision</td><td colspan="4" rowspan="3">May be confusing when used together with force feedback</td></tr>
<tr><td>Passive</td></tr>
<tr><td>Active</td></tr>
<tr><td colspan="2">Automation</td><td>Shorter execution times and lower operator workload, as long as basic models of the environment exist</td><td colspan="4">Only possible when good models of the system exist</td></tr>
</table>

Figure 3.4: *Matching of the task-primitives of section 2.2 with the operation modes of section 3.2. In the crossing cells are shown indications of the particular use that a certain operation mode can have in micromanipulation tasks. White cells indicate a positive match, light-gray cells indicate a positive match with associated risks, and dark-gray cells indicate a not-possible match.*

minimized by a proper filtering of the feedback signal, while information in other frequency ranges could still be transmitted. The development of micro-force sensing or estimation techniques in multiple degrees of freedom (DOF) is necessary in order to implement this strategy. Nevertheless, existing microforce sensors can already provide useful feedback.

Finally, combinations of automation and guiding modes can become quite useful also in micromanipulation. A partial knowledge of the environment by the HT-Controller is common, with many objects being positioned at known locations, with known shapes, and with clearly defined operations. Since manipulated objects have topologies typically in 2.5 dimensions within a known set of heights, it is often possible to roughly model the stiffness of the environment over the axis normal to the working substrate. In such conditions, it is possible for the HT-Controller to determine an execution plan (at least over some axis or during some operations), and either apply it by automation, or negotiate with the user via guiding and shared control the commands to be issued. The development of better multi-DOF micro-force and position sensors, will improve the environment and interactions modeling, and the resulting automatic planning.

Chapter 4

System requirements related to the presence of the human operator

The system presented in this thesis is meant to be used in a haptic teleoperation configuration, with a human operator commanding its actions and receiving feedback from it. Therefore it is important to consider the requirements and limitations that the operator brings into the system, and optimize the system components with this application scenario into account.

Several studies exist in literature regarding the sensing and acting capabilities of humans. These values vary widely between subjects, between tasks, and within a task depending on several parameters. For certain applications, a refinement of these values can be obtained via application-specific psychophysic studies, but even with such studies it is difficult to find values able to cover for the whole spectrum of application parameters and operator capabilities. Therefore, it is often necessary to extrapolate results from one psychophysic test to other similar situations. Despite their variability, psychophysic studies are the best tool available to asses the impact that different system parameters can have in a the performance of an operator using a device to perform a task. They provide design guidelines to improve the performance of the operator-plus-device system and to optimize the device accordingly.

This chapter gives an overview of several psychophysic parameters of interest to the case studied in this work. Section 4.1 gives a general overview of the characteristics of a micromanipulation operation, when performed by a human operator, and Section 4.2 goes in detail with a report of psychophysic parameters obtained from

literature, giving clues to some systems specifications[1]. Even though the literature on the subject is extensive, some topics still needed to be researched in order to define requirements for the system researched in this thesis. In that sense, section 4.3 studies how uncertainty in the slave device of a teleoperated system affects the performance of the operator while performing certain task-primitives of micromanipulation, while section 4.4 studies the effect of different system configurations on the same performance metrics (i.e. whether fixing the camera to the tool or to the working table has an impact on performance).

4.1 The micromanipulation task from the human perspective

When performing a micromanipulation task in a haptic teleoperation scenario as the one described in this thesis, the operator commands the movements of the slave device though a master device. The operator receives then visual feedback through microscope cameras, whose images are magnified and displayed on a screen, and possibly force feedback from the master device. The cameras provide valuable position information in free-air situations where there is no contact providing force feedback. Images may also provide information in contact situations through the deformation and movement of tools and objects, or through the visible actions of the tool in the environment. The haptic interface provides information in contact situations, when no appreciable displacements are visible or when occlusion impedes the visual supervision of the operations. In the particular case of micromanipulation, and due to the limitations in visual resolution imposed by the Abbe diffraction limit, visual feedback for small features and displacements may become impossible, and haptic feedback would again become an important source of information for the operator.

When executing micromanipulation task though a haptic teleoperation interface, the operator is not provided with exact measurements of the positions of the manipulated objects. The operator commands are also not issued to the system in the form of quantitative displacements or positions instructions. Rather, the operator moves the master device in order to issue the commands, while using the visual and haptic feedback (instead of or additional to numerical displays) to control the trajectory and interactions of the micro tool, together with feed-forward control based on his models of his limbs and the environment. The operator acts as an integrator in the feedback loop, minimizing the position or force error, based on his targets and the feedback received. With that strategy, the error achieved by the operator is only limited by the resolution of the feedback and the tremor and MIM of the guiding limb. In that sense, human operators are robust and adaptable thanks to their learning ability. They are

[1] Sections 4.1 and 4.2 are based on and extended in previous work from the author, appearing in [61].

used to and capable of dealing with imprecise tools, as long as end-point feedback is available to them to correct for the errors introduced by the intermediate devices. They can adapt to coordinate transformations, as is for instance the case of the computer mouse used on horizontal mouse-pads to drive pointers in vertical screens. Even more so, most computer mice change dynamically the scaling of operator movements to pointer movements, improving their usability.

4.2 Some psychophysics of interest

Several studies have reported into the motor control and sensing capabilities of the average human, especially those of the arm and hand. These characteristics are particularly interesting for the case studied in this thesis, since hand-held master devices provide a natural and delicate interface for manipulation tasks. Some relevant results from previous psychophysics studies are listed below.

- The human operator can achieve, with a hand-operated master device, a MIM of about 1 mm over a range of 100 to 200 mm (ratio 100 : 1 - 200 : 1) when moving in free air, i.e. without obstacles. In the presence of stiffness (as would be the case for haptic feedback) a higher precision is possible [48].

- Motion tasks can be carried out with this precision up to a bandwidth of 1 - 2 Hz, in response to unexpected signals. When the motion is faster some of the precision and control is lost. In response to periodic signals, for periodic motion and for learned tasks and trajectories the bandwidth increases to 2 - 5 Hz, while for reflexive actions this bandwidth can go up to a maximum of 10 Hz [18].

- The sensing bandwidth of human operators is much higher, perceiving vibrotactile stimuli up to 1000 Hz [79]. However, providing information on that full range is not necessary in order to achieve a satisfactory performance in certain tasks. Burdea in [20, page 36] comments on several studies showing that sensing bandwidths between 8 and 30 Hz are in many cases sufficient for executing tasks, since they provide meaningful kinesthetic and proprioceptive feedback[2].

- Maximum acceleration for the human elbow flexion are observed to be 5g, whereas consulted experts estimated typical accelerations in the order of 1.25g. Typical velocities that can be reached are 1.1 m/s [18].

- Many human operator specifications are scaled with the magnitude of the stimuli received, the background intensity, or the action been performed, as stated by

[2]Kinesthesia and propioception are the abilities of sensing the body posture, the relative position and motion of parts of the body, and the efforts being employed in moving them [20].

the Weber ratio and confirmed for different stimuli and situations in further studies (for instance [64, 42]). In that way, the human exerted force resolution depends on the exerted force, with values for the hand and arm between 0.7 and 3.35% (with visual feedback present) [79].

4.3 Psychophysic study on the uncertainty requirement

The requirements on uncertainty for the slave robot are considered of particular interest for this work, and are therefore further studied in this section, through a psychophysic study. As commented before, human operators are able and used to deal with changing relations between their commands on a human-machine interface and the movements of the commanded system. Even within their own limbs, feed-forward positioning (with closed eyes) or feed forward force application (without visual indicators) shows after preliminary tests to have uncertainties above 10% of the intended commands. It is the end-point feedback what permits the operator to achieve their final level of performance.

Most micromanipulation systems, on the other hand, use positioners and sensors intended for automatic operation, where high repeatability and low uncertainty are necessary for the realization of the tasks. Even though a low uncertainty is certainly not a negative feature, it constitutes a limiting factor in many device designs, and a contributing factor to its cost and complexity. A proper estimation of the uncertainty requirements on a slave system for haptic teleoperation, and the optimization of such a system for this application, would allow lowering its cost while maintaining the same performance.

An interesting question to answer is therefore what the impact of the slave positioning uncertainty can be on the performance of an operator performing micromanipulation in a haptic teleoperation scenario. One could hypothesize that a certain level of uncertainty can be tolerated in the slave positioning system without a noticeable impact in the performance, and that only high values of that uncertainty would have a significant effect.

4.3.1 Experimental apparatus

In order to test the aforementioned hypothesis, a simulation environment is developed using the Labview programming language from National Instruments, and a Falcon master device from Novint. The simulated environment consist of a needle to be used as a tool, and a work-table where the operations are performed, as can be seen in figure 4.1. The master device commands the needle over the work-table, while presenting force feedback to the operator from the contacts between the table and the needle.

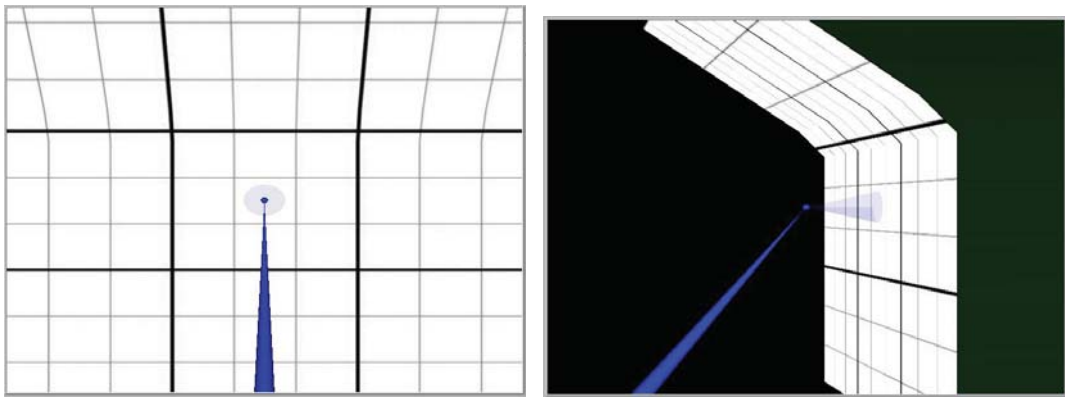

(a) (b)

Figure 4.1: *Top view (a) and side view (b) of the simulation environment. These views are not a technical-drawing projection, but show the views presented to the operator from one camera on top and one camera on the side of the simulation environment. It is possible to see the work-table, with a flat and an inclined section, the needle in blue, and a transparent cone whose projection in the work-table acts as a shadow.*

The system is normally configured to translate the operator commands on the master device in a one-to-one relation to the movements of the simulated needle, representing in this way a perfectly accurate slave system. It is nevertheless possible to introduce distortions in these relations, and by doing so, represent different sources of uncertainty in the system. A positioning robot can have many sources of uncertainty, resulting in command-action relations, each with different position dependency, frequency content, cross-talk, etc. For the purpose of this study, it is of particular interest to consider uncertainties of low frequency content, both in position (bellow 2 Hz, typically representative of sensor non-linearities) and in time (often as a consequence of thermal drift, changes on humidity levels, or change of other environmental conditions), often encountered in positioning systems. The drifts by environmental effects are so slow compared to manipulation times, that they are normally not perceived by an operator during operation. They rather appear as a different system setting each time the system is operated.

The fact that acting and sensing resolutions (or *just noticeable differences, JND*) in human operators tend to be proportional to the magnitude of the stimuli or intended action by the Weber's ration, was taken into account in order to parametrize the distortion applied to the command-action relation. Therefore, the uncertainty on this relation was described by using the maximum values of the derivative of this relation with respect to the commanded position. A derivative of the command-action relation

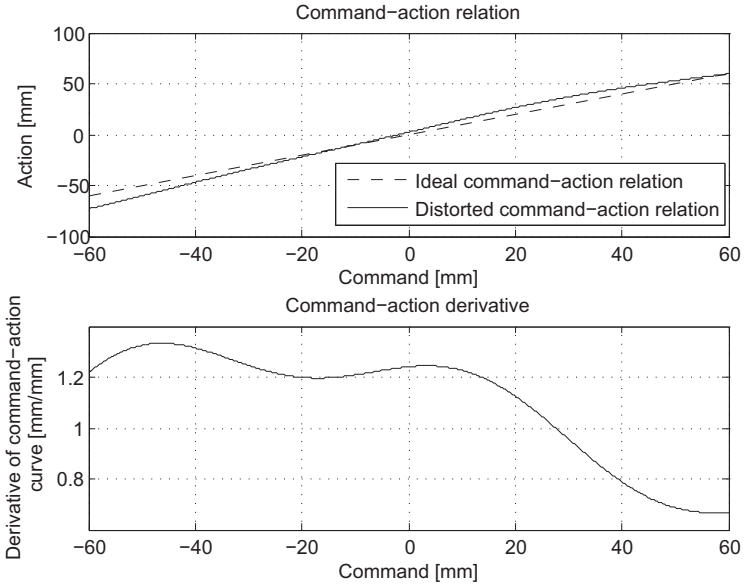

Figure 4.2: *Example of the relation between the commands issued by the operator in the master device, and the displacements of the needle in the simulation. According to the parametrization used in this work, the distortion present in the command-action relation in this case is* $\delta = \frac{1}{3}$*, since the derivative of the relation varies between 67% and 133% of the ideal value of 1.*

constant and equal to 1 represents the system with perfect accuracy, while a derivative varying between $1 - \delta$ and $1 + \delta$ ensures that for any interval d of the command, the action will remain within $d \cdot (1 \pm \delta)$. For this study, this derivative is generated as a random multi-sine with a spatial frequency below 2 Hz (relative to the size of the workspace). By generating a new and random command-action relation for each test, is it possible to emulate the effect of slow drift phenomena. A typical command-action relation, with $\delta = \frac{1}{3}$, can be observed in figure 4.2.

The parametrization of uncertainty used in this work is not standard in the micromanipulation community, but, as a reference, we can extract more standard stage-specifications from it. For instance, from the case with $\delta = \frac{1}{3}$ in figure 4.2, we can

obtain the following specifications:

$$NonLinearity(\%) = \frac{D_{in(max)}}{I_{f.s.}} \times 100 = 8.5$$

Where:

$D_{in(max)} = 10.2$ mm; is the maximum input deviation

$I_{f.s.} = 120$ mm; is the full scale input range

$$Uncertainty(\%) = \frac{D_{out(max)}}{I_{f.s.}} \times 100 = 10.9$$

Where:

$D_{out(max)} = 13$ mm; is the maximum output deviation

$I_{f.s.} = 120$ mm; is the full scale input range

4.3.2 The studied task

The task selected for this study intends to represent some of the situations encountered in micromanipulation, mainly surface scanning tasks, transport tasks and contact establishing as seen in section 2.2. The image depicted in figure 4.3 is set on the work-table to guide the operator movements. The work-table includes a flat section and an inclined section, as indicated in the same figure. With this configuration the operator performs 5 sub-tasks (indicated in figure 4.3):

1. A straight surface scan over a 3D surface.
2. A complex trajectory scan over a flat surface.
3. A straight scan over a single axis.
4. A straight diagonal scan (thus over 2 axes).
5. The equivalent of a 3D transport and contact-establishing operation.

It must be noted how in sub-task 1, the changes on vertical command-action relations are perceived by the operator as changes on stiffness or a non-flat surface profile. Also, in sub-tasks 2, 4 and 5, which develop over multiple axes, a crosstalk effect is perceived: for straight displacements of the master device, a non-straight displacement of the tool occurs (since the command-action relation of each axis varies independently).

Different performance measures can be extracted during the execution of the task:

1. Route error: average distance from the reference line.
2. Time: time taken to complete the subtask.

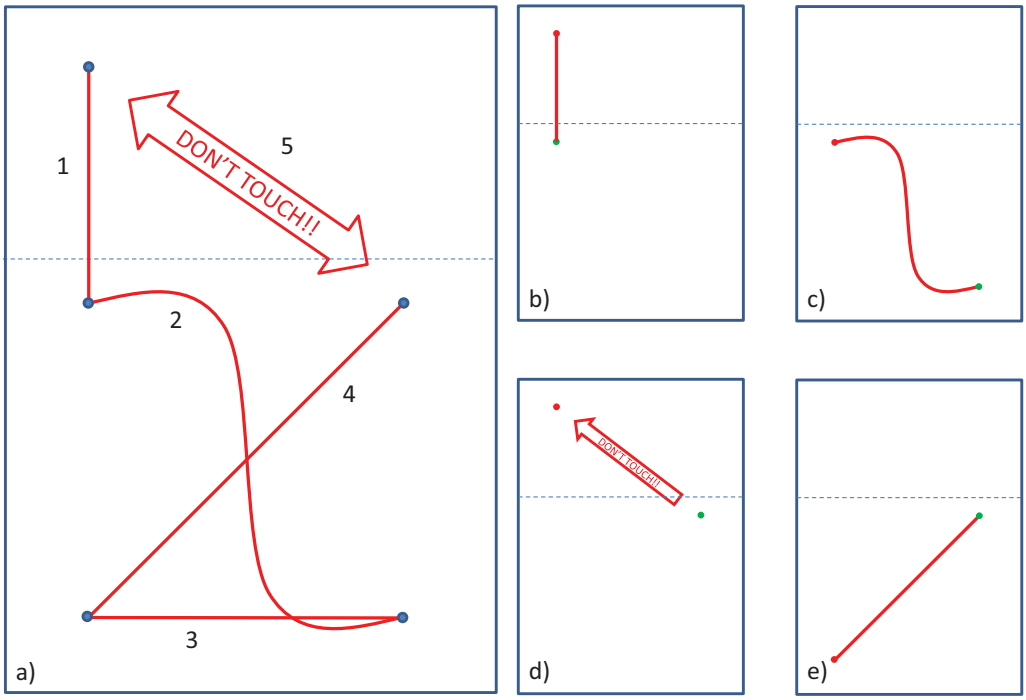

Figure 4.3: *Images presented in the simulated work-table during the user study. The horizontal dotted line represents the start of the slope section of the work-table. a) Full image; b-e) Examples of partial images presented during sub-tasks.*

3. Reversal rate: number of direction changes in the error signal, often used as an indicator of the control effort exerted by the operator.
4. Maximum force: applied by the tool on the work-table.
5. Free-air time: relation between the time the tool expends in free air and the time the tool remains in contact during an operation, which should approach 0 (permanent contact) for sub-tasks 1 to 4, and infinite for subtask 5 (only contact at the target location).
6. Operator workload: as a result of the NASA-TLX Workload Test [37].

4.3.3 Experimental design

Ten operators are asked to perform for this study. Each operator performs the task several times, and with different values of δ. The values selected for δ are $\delta = 0$ (representing the perfect system), $\delta = \frac{1}{3}$, $\delta = \frac{2}{3}$ and , $\delta = 1$ (representing a very distorted command-action relation).

For each operator, the test follows the following steps:

1. The operator is given time to get acquainted with the interface and with the different values of δ for approximately 10 minutes.
2. The system is set for a value of δ, and a command-action relation is generated.
3. The operator is asked to perform sequentially the 5 subtasks.
4. Steps 2 and 3 are repeated four times, for the same value of δ.
5. A NASA workload test is applied to the user.
6. Steps 2 to 5 are repeated for other 3 values of δ.

In order to avoid learning effects, the order of the four different values of δ is randomized between users. Moreover, for each test the initial position within figure 4.3 and the direction of execution of the task is also randomly selected.

4.3.4 Results and discussion

After performing the study with 10 operators, all their data was analyzed using Matlab, and the performance measurements of section 4.3.2 were extracted from this data. These performance-measures were then analyzed using ANOVA, a statistical analysis technique that considers the variance within and between several series of samples to assess the probability of all the series being part of a single Gaussian distribution. Analyzing a group of data-series with ANOVA gives as a result a significance value, often called p, which indicates the probability of all series been actually part of the same distribution. It is normally assumed that p values below 5% are enough to indicate that a significant difference exist between at least two of the studied series.

The intention of this study is to understand from which value of δ (if any) the performance of the operator is significantly affected. Therefore, a first test checks whether there is an effect at all on the performance measures when changing the value of p, via a one-way ANOVA on the data for each sub-task. The only performance measure showing a consistent trend with significance value $p < .05$ are the route error (for sub-tasks 1 to 4) and the NASA-TLX operator workload, whose boxplots are shown in figure 4.4. For those performance measures, a post-hoc test is applied where each distorted case of $\delta > 0$ is compared to the baseline case of $\delta = 0$. Figure 4.5 shows the significance value obtained from these tests, for the pairwise comparison of the baseline to each of the other cases. It is observed how a significant degradation of performance occurs only for the higher values of δ.

In accordance with the hypothesis stated at the beginning of this study, it is possible to notice how distortions up to $\delta = \frac{1}{3}$ do not result on significant degradations of the positioning performance or increases in the reported workload, and even $\delta = 1$

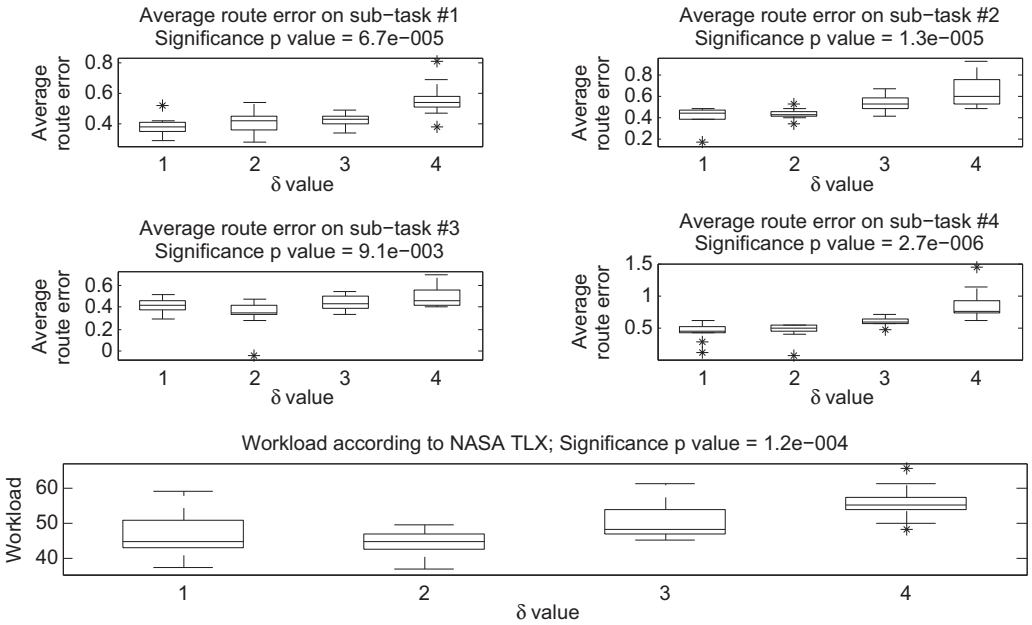

Figure 4.4: *Boxplots of the performance measures showing a significance value higher than 5% in an ANOVA test.*

for other performance measures. These values are normally within specifications even for the most simple positioning stages.

These results must be interpreted carefully, since they are tied to the tasks and performance-measures analyzed in this study, and for the simulated slave characteristics. They nevertheless demonstrate that the accuracy of a teleoperated system does not need to be achieved solely by the slave robot, and that the human operator can make use of haptic and visual information to improve the system accuracy without important impacts in its workload, and without compromises on other performance indexes.

4.4 Psychophysic study on moving tool Vs. moving base

The positioning systems that provide the relative motions required between the tools and the work-plate during micromanipulation tasks can be divided between these two components in the implementation of the micromanipulation system. While in some systems the work-plate is left stationary with the tool set in a manipulator providing all the required displacements, other systems provide all the DOFs in the work plate and leave the tool static, or combine the two approaches. The option of keeping the

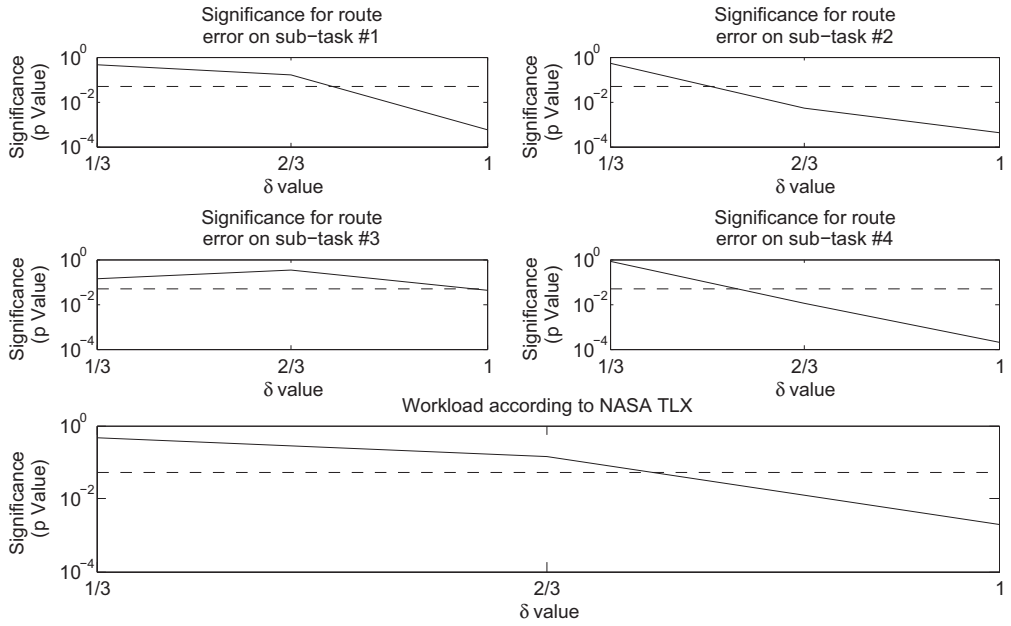

Figure 4.5: *Significance values of t-test between the baseline case of $\delta = 0$ and the cases with $\delta > 0$. The dotted line shows the 5% significance line.*

tool fixed has some advantages, since it allows to keep the vision system focused on the tools-tip (where most actions take place) while the work-plate moves below it, thus achieving constant supervision over a large workspace. Moreover, different, complex or heavy tools can be used as long as their end-effectors can be positioned over the work plate, without needing to design or adapt the positioning system for each tool required by the task.

Simple coordinate transformations allows for achieving the desired relative position by combining the displacements of the work-plate and the tool. This computation is straightforward for the control system to do, but in teleoperation systems it is not clear whether the different configurations may have an effect in the performance of the operator driving the system. Assuming that the vision system is fixed to the ground, the user will perceive the fixed component of the slave system (either the work-plate or the tool) static in the image, while it will observe the movable components traversing the view-field. Equivalently, the camera can be moved together with the moving component, in which case the situation inverses. In either case, with operators used to observe a tool moving on top a fixed work-table, it is interesting to investigate if the opposite situation may result in confusion and degradation of the performance. That is, if observing a fixed tool with a work-plate moving below it results in worse

performance than the natural case of observing a fixed work-plate with the tool moving on top of it.

It is the hypothesis of this study that the performance of the user in both configurations will be equivalent. This hypothesis will be tested by using an experiment similar to that presented in Section 4.3. In particular, the task studied and the experimental design used are the same as in Sections 4.3.2 and 4.3.3 respectively, the only difference been the use of two modes corresponding to the two studied configurations, instead of the 4 modes used in the previous experiment and corresponding to the 4 values of δ. The reader is therefore directed toward Section 4.3 for details on these two aspects of the experiment.

4.4.1 Experimental apparatus

This study utilizes the same simulation environment presented in Section 4.3.1. The simulation is configured in this case with two selectable modes, as shown in Figure 4.6. In the first mode, the probe acting as a tool moves following the displacements of the master device on top of a stationary work-plate. In the second mode, the probe is left stationary in the center of the available views, while the displacements of the master device are negated and applied to the work-plate. That is, a displacement to the left of the master device results in a displacement to the right of the work-plate. Thus, the final relative motion of the tool referenced to the work-plate always follows the user command in the master device, regardless of whether that motion is achieved by displacing the tool in the same direction as the master device (Mode 1) or displacing the work-plate in the direction opposite to that of the master device (Mode 2).

4.4.2 Results and discussion

After performing the study with 8 operators, all their data was analyzed using Matlab, the performance measurements of section 4.3.2 were extracted and analyzed using ANOVA. This analysis showed that none of the performance measurements presented a significant difference (with a p value below 5%) between the 2 studied modes. Moreover, most test-subjects did not realize, until it was explained, the difference between the two modes during the explanation of the test, even if in terms of visualition this difference was obvious. Most users reported a slightly higher mental load when starting the test with Mode 2, but the NASA TLX workload test performed at the of end each study showed that either this problem was solved by learning during the test, or that the difference in workload was not so high as to become significant in the ANOVA analysis.

This study thus verifies the hypothesis that the performance of the operator is equivalent in both system configurations. It must be noted nevertheless that this

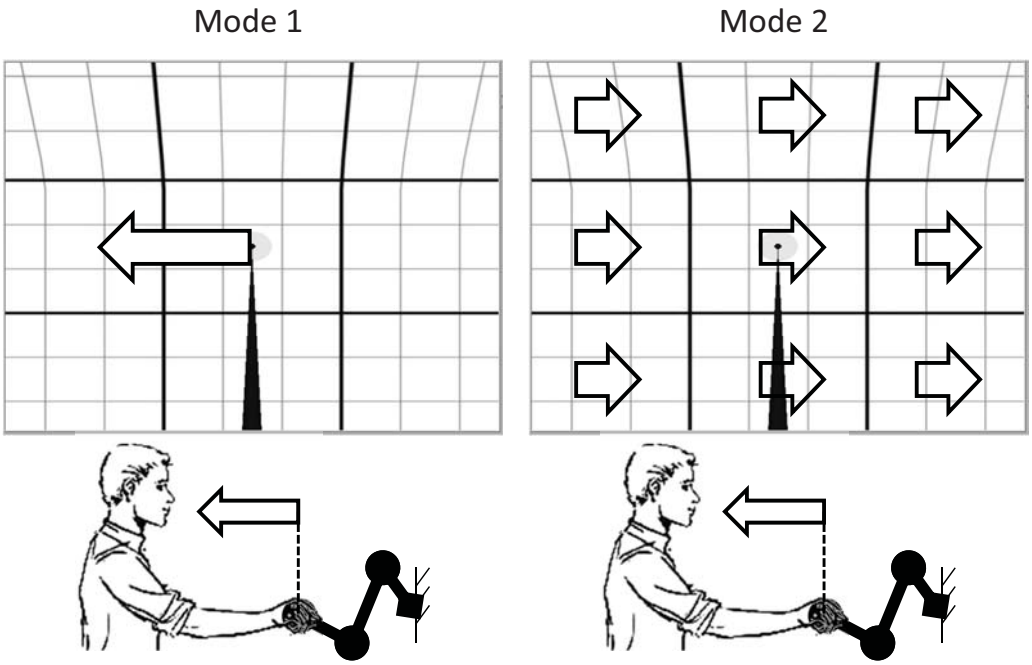

Figure 4.6: *Operation modes in the psychophysic test comparing operation with a moving tool and with a moving base. In Mode 1, master displacements are followed one-to-one by the tool, which moves over a stationary work-plate. In Mode 2, master displacements are negated and applied to the work-plate, while the tool appears stationary in the image.*

study did not consider the rotational DOFs, and further research including them will be necessary before arriving to more general conclusions.

Chapter 5

Final system requirements

Chapters 2, 3 and 4 of this thesis form the basis for the requirements of the haptic teleoperation system for microassembly developed in this work. These requirements and the trade-offs between them are further explored in this chapter. A teleoperation system is primarily divided into the master environment and the slave (or remote) environment, interconnected though the haptic teleoperation controller block. Even though this thesis focuses on the development of devices for the slave side of the system, a master interface and a haptic teleoperation controller are still required for evaluating and demonstrating the slave-side devices and the operation of the system. Moreover, several commercial components are needed for the full operation of the slave side of the system, other than the slave-side devices investigated and developed in this thesis. Even though these master-side and slave-side support components are not developed within this thesis, their requirements are studied in this chapter and reported in so far as it is necessary for the design of the system and for the understanding of this thesis.

Section 5.1 of this chapter introduces the general philosophy followed in the definition of the requirements and the design of the haptic teleoperation system. The main components required for such a system are then described in Section 5.2, together with their requirements. Additional attention is given to two of the system components which are developed within this thesis: the slave positioning stage and a 6DOF force and torque sensor. The requirements for these two components are analyzed in detail in Sections 5.3 and 5.4, respectively.

5.1 Design philosophy and general considerations

Given the application scenario of this thesis, several considerations appear for guiding the design of the haptic teleoperation system. The adaptability of the human operator makes this system particularly useful in the production of prototypes, small assembly series or manipulation in unknown environments, providing a more economical solution than automation would provide for these tasks. Moreover, the entire system is expected to be portable, adaptable, and fit on a table-top. These conditions put limits on the complexity and cost of the system and its components, which should be kept as simple, small and affordable as possible. In order to attain that objective, attention must be given to the system requirements, thus enabling the exploitation of trade-offs between the specifications, cost and complexity of system components.

It is important to keep into account the two environments with which the haptic teleoperation system will interact. When discussing master-side devices attention must be given to the requirements coming from the direct interaction with the user, but also to the requirements imposed by the micro manipulation task at the slave side. Conversely, the slave-side device-requirements are driven partly by the micromanipulation task such devices must perform, and partly by the presence of a human user connected through the haptic teleoperation system. In that sense, many specifications of system components can be kept low, such as operation bandwidth, velocity and accuracy of some components, because the human operator is the limiting factor for these performance figures. The targeted tasks, on the other hand, require a certain level of dexterity, fine MIM values, and the fragility of the manipulated objects calls for low magnitude forces to be used in their manipulation.

It must be noted that the system developed in this project targets a general application field and not one specific task. Therefore many requirements act more as guidelines in the order of magnitudes that must be achieved, rather than as fixed and precise specifications. In the same way, the process to arrive to those requirements follows an empiric approach to obtain figures representative of the application field.

5.2 Required system components

The components required for a haptic telemanipulation system as the one developed in this thesis are presented in Figure 5.1. Starting from the master side, the user interacts with the system through a visual and a haptic interface. A Haptic Teleoperation Controller (HT-Controller) must transmit the user commands from the haptic interface to the slave-side devices (either in position or force), while feeding back information about the interaction forces and displacements in the micro environment to the haptic interface. Once in the slave side, and depending on the haptic teleoper-

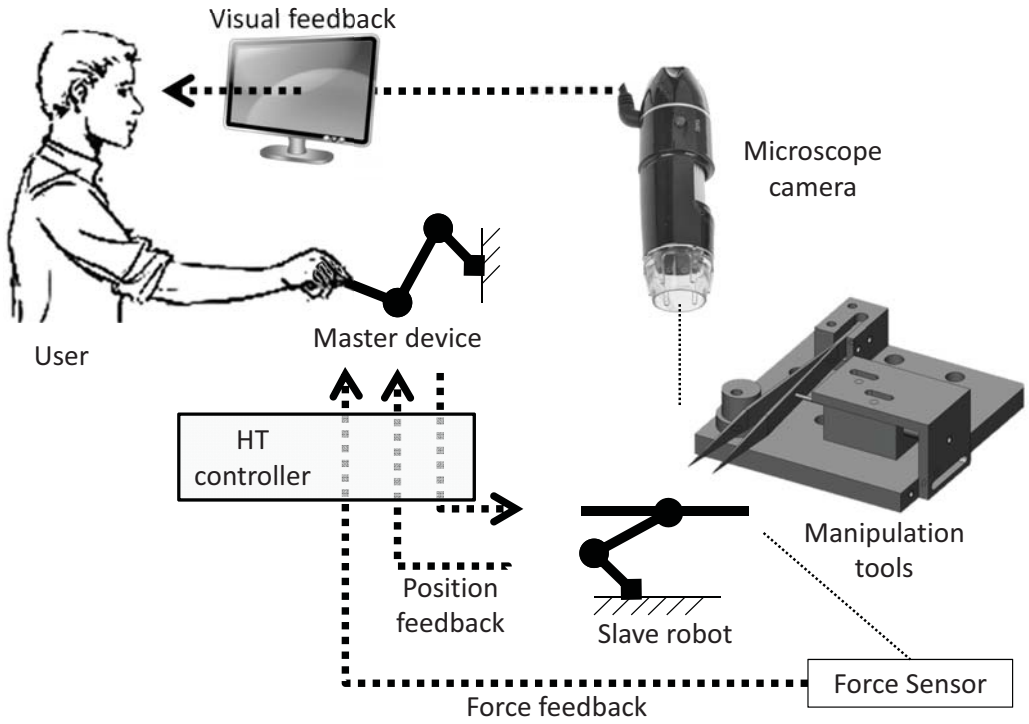

Figure 5.1: *Components of the haptic teleoperated system required for this thesis. Starting from the master side, the system comprises a master device and a visual interface, a Haptic Teleoperation Controller (HT-Controller), a slave robot, manipulation tools, sensors measuring the forces applied by the tools, and a camera system to provide the visual feedback to the operator.*

ation control architecture chosen, the position and the interaction force between the tool and the environment must be actuated by a slave robot, while those same two variables may need to be measured by position and force sensors. Different tools will also be required in order to perform the manipulation task in the micro environment, from simple probes and needles to more complex active devices. Finally, microscope cameras provide the visual feedback from the micro environment to the user.

The requirements for the system components are discussed in the following section. Since a slave robot and a force sensor are developed within this thesis, separate sections deal with their requirements later in this chapter (Sections 5.3 and 5.4 respectively).

5.2.1 Visual feedback

Visual feedback from the operation area provides kinematic information to the user regarding the relative position of objects and tools. It can also provide information about forces through the deformations of the tools and environment and the trace left by the tools in the environment. Given the 2.5D characteristic of many micromanipulation tasks (as explained in Section 2.3), a zenithal view is required for aligning and positioning the tool in the table-plane previous to approaching and contacting it. A secondary view can provide information about distances in the out-of-plane direction. Nevertheless, given the simple out-of-plane characteristics that 2.5D tasks present, this information can be modeled and monitored through other means, like contact-force measurements, shadows or reflexions (more details are given in Section 9.2.2). Using 3D vision systems is always an interesting option, however, given the simplicity of 2.5D tasks, such vision systems are not necessary.

Given the size of the objects targeted in this thesis and their features, a visual feedback resolution smaller than 1 μm is required. For modern optical microscopes, for which the Abbe diffraction limit lies close to 250nm, this is not a problem. On the other hand, part sizes may go up to 1 millimeter, and the working area can even reach some centimeters. Having both a sub-micrometer resolution and a centimeter range, a range-to-resolution ratio of around 10^5, is often not possible with uniform-scale equipment. Furthermore, such a ratio would be impractical for human users whose visual acuity limits them to range-to-resolution ratios below 10^4, and for the use of standard screens with no more than 2000x2000 pixels (based on [5] and [4].

Fortunately, as explained in Section 2.3.1, the range and resolution requirements apply to different kind of operations (transport and mount operations, respectively). It is therefore possible to have one low-resolution vision system to cover the whole range of the workspace, and another fine-resolution microscope to observe the fine details. Moreover, as explained in Section 4.4, if it is possible to keep the focus of the fine-resolution microscope on the tip of the tool, a permanent supervision of the point were the delicate operations are carried out is obtained, with a high level of detail.

5.2.2 Master device

A master device is required for the user to command the slave-side devices. Given the delicacy and dexterity required in micromanipulation, a hand/wrist manipulator is preferred. The characteristics of the tasks at hand call for a device allowing the control of the 3 translational DOFs, plus the rotations around one axis normal to the working plane in the slave-side environment. Moreover, in order to provide force and position feedback to the user from the contacts between the tools and the environment, the master device should provide force feedback in all the aforementioned DOFs. Finally,

many micromanipulation tasks require an additional degree of freedom to operate the tool, such as the closing of a tweezer or the application of glue or heat. In summary, the master device should be able to measure and actuate 5 DOFs: 3 for translations, one for rotation and a last one for the operation of the tool.

5.2.3 Haptic Teleoperation Controller

As mentioned in Section 1.1, there exist several configurations in which the HT-Controller can operate. Even though there are trade-offs to explore within these configurations, for the purposes of this thesis and given the focus on the slave device, there is no constraint in the selection of the control scheme. It is therefore possible to choose a configuration adapted to the sensing and acting capabilities available in both the master and slave sides. It must be noted that independent controllers can be running both in the master and slave sides of the system to drive the different devices that make part of the system. The HT-Controller works then as a supra-controller whose purpose is to connect the local control loops of the master and slave devices.

The haptic teleoperation controller has to transmit the intended operator commands with a maximum bandwidth of 5Hz (Section 4.2). Higher bandwidths are only necessary for reflexive actions, which are not considered useful for the completion of the task dealt with in this thesis. For the information transmitted to the user, at least basic kinesthetic feedback in the same range of 5Hz should be provided to communicate kinematic information and impedance characteristics of the remote environment.

5.2.4 Manipulation tools

The variety of tasks that exists within the micromanipulation field requires as well the use of a variety of tools. Depending on the application, tweezers of different sizes and based on different principles may be needed, such as those using magnetic, electrostatic or capillary forces, friction or, most commonly, vacuum. Other tools are required as well for the application or removal of substances such as glue or conductive paint, for the activation of processes with UV light or electric currents, for characterization or for simply probing, and many more. Even though these tools are meant to actuate over small objects and even smaller features, their support equipment may be much bigger, ranging from a few millimeters for silicon devices to several meters for, for instance, ion beams.

This situation makes it impossible to state unique requirements for the manipulation tool. What it does define is the requirement for the remaining equipment to be able to deal with tools of different characteristics and sizes.

5.3 Requirements for the slave robot

Examining the characteristics of the different groups of micromanipulation operations presented in Section 2.3.1, a strong difference in requirements for each sub-process becomes apparent. In particular, many of the strongest requirements on the mount operation are antagonistic with the strongest requirements of the transport operation. For instance:

- Larger displacements required for transport are difficult to achieve with the low errors required for mounting.
- Higher accelerations require larger actuators forces, which complicates dealing with high force resolutions, only necessary in the mount operation.
- Position sensors have often trade-offs between their resolution and their achievable range.
- Guiding systems able to deal with the smallest MIM, such as flexures or magnetic levitation, are limited in their displacements.

Even though systems exist which are able to cover the requirements of all the groups of operations, the aforementioned trade-offs lead to unnecessarily complex and expensive solutions. Fortunately, these operations take place in different moments of the assembly sequence, which makes it unnecessary to cover for all their requirements at the same time or with the same system. The previous analysis yields naturally to the option of using a dual stage approach, where one system takes charge of the long distance movements of the transport and possibly part of the alignment phase, and another system takes over to perform the more delicate steps of alignment and mounting. In such way, each sub-system can be optimized for its limited set of requirements, instead of for the joint requirement set. In the case of the alignment operation, its requirements are overlapping with those of the other two operations, and can therefore be covered by their associated positioning systems.

In such an approach, it is important for the coarse stage requirements on MIM to be smaller than the fine stage requirements in range by a big factor, in order to cover all the scale levels of the micro manipulation operation. A factor n ensures that for a range R of the fine stage it is possible to reach a position at most $^{\mathrm{R}}/2 \times n$ away from the center of the workspace of the fine stage. The transition area between the fine and coarse stage could of course be moved towards both the course and the fine sides. Nevertheless, it is useful if each operation is covered fully by at least one of the stages, since it would simplify the control during each phase, and allows optimizing the stages only for some of the operations avoiding the aforementioned requirements conflicts. More complex control using both stages at the same time could also be implemented,

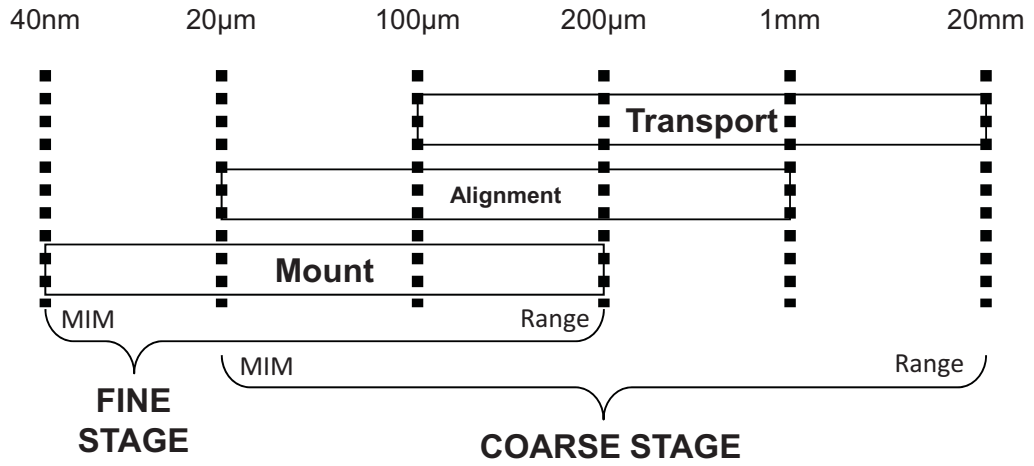

Figure 5.2: *Ranges and MIMs of the coarse and fine stages, superposed to the tree groups of micromanipulation operations of Figure 2.2. The fine stage covers the mount operation with a MIM of 40nm and a range of 200µm, while the coarse stage covers both the alignment and transport operations with a MIM of 20µm and a range of 20mm.*

for instance with the coarse stage following the fine one. In particular, the transport and alignment operations have similar requirements, being mainly focused on free-air movements with little or no contact. Moreover, their combined requirements fit in what is possible to obtain with many of-the-shelve devices. By covering both transport and alignment operations with a coarse commercial stage, research efforts can be devoted to deal with the more difficult requirements of the mount operation in the smallest necessary range.

The distribution shown in Figure 5.2 takes this analysis into account. The coarse stage covers the transport and alignment operations, while a fine stage is in charge of the mount operation. The 1-to-10 relation between the MIM of the coarse stage and the range of the fine stage ensures that the alignment operation can position the tool close enough to the target and in the middle of the range of the fine stage, from where the mount operation can take over for the final positing.

Moreover, some requirements on payload and perturbation rejection in the coarse stage are influenced by the characteristics of the mount operation: the fine stage would be sitting on top of the coarse one, and their interaction must be taken into account when studying their requirements.

The previous analysis has been based on the MIM of the stages, rather than on their accuracy figures as is usual for positioning stages. As explained in Section 4.3,

the fact that this stage is meant to be driven by a human operator via hand movements makes the accuracy requirements almost negligible, as long as it remains stable. A certain level of accuracy is still needed however in order for the the controller to operate properly.

To achieve a fine force resolution in the stage in charge of the mount operations, the use of low-force actuators is advantageous. Furthermore, the moving mass should be as small as possible, to limit the inertia forces. Forces coming from the stage stiffness can also be reduced by the use of compliance in the tool or actuator. This approach has also shown to be particularly useful in haptic teleoperation systems, since it helps maintaining the stability of the system without affecting the performance figures [24]. Nevertheless, other specifications of the system are compromised when the internal stiffness of the slave robot is lowered, like its resonance frequencies, force range and accuracy. A variable stiffness system is therefore an interesting option, given that it can dynamically adjust the trade-offs of stiffness and other specifications.

The main requirements for the 2 stages of the slave robot can then be seen in Tables 5.1 and 5.2, for the fine and the coarse stages respectively.

5.4 Requirements for the force sensor

In the typical fields of application of haptic teleoperated micromanipulation, force measurement ranges of several mN are required, with resolutions close to the μN. For instance in [74] forces of 2 μN are used to manipulate and assemble micro mirrors. Also in the assembly of micro opto-electrical components such as optical fibers, forces must be controlled in the mN range in order to avoid breakage [45]. In cell injection, the applied forces can vary from 0.1 μN to 100mN depending on the type of cell [88, 55, 75]. Moreover, the high positioning resolution required in micromanipulation brings also a requirement on force sensing: when sliding over surfaces, the normal force must be controlled in order to minimize the friction and therefore achieve a smaller MIM. Torque sensing is less reported in literature. Nevertheless, given the size of the objects considered in this thesis it is possible to derive expected torque values between 0.1nNm and 10μNm.

Given the 2.5D nature of the tasks considered in this thesis, sensing in the direction normal to the work plane becomes particularly important, since such measurement provides information about the contact between the tool and the environment, and allows to control the magnitude of such interactions. the strength of this contact typically influences the effect of the tool in the environment (the depth of a groove, the thickness of a paint or glue trace, the quality of an electrical contact), and its mobility over the surface due to friction. Nevertheless, given the multi-DOF nature of micromanipulation tasks, concurrent force sensing in multiple DOFs is as well required.

Table 5.1: *Summary of the requirements for the fine stage of the slave robot.*

Requirement	Value	Reason
Range in X x Y x Z	$>$ 200µm $\times$ 200µm $\times$ 200µm	Expected range of mount operations.
Velocity in X, Y and Z	> 1 mm/s	Ensures following user commands at 1 Hz within the whole workspace.
Acceleration in X, Y and Z	> 5 mm/s^2	Ensures following user commands at 1 Hz within the whole workspace.
Controller bandwidth	> 50 Hz	Ensures following user commands at 5 Hz, and attenuates typical floor vibrations in the laboratory area [40] to the required MIM.
MIM in X, Y and Z	40 – 100 nm	Defined as a safety factor of 2 – 5 relative to the feature sizes.
Motion tracking error, Linearity in X, Y and Z	$<$ 10 nm per every 100 nm	Accuracy over the full range is not necessary, due to the tele-operation mode.
MIM in Θ_x, Θ_y and Θ_z	35µrad pp	Derived from the maximum part size (1mm) and the feature sizes (200nm), considering a safety factor of one fifth.
Rotational range in Θ_x, Θ_y and Θ_z	$\pm$18mrad	Required to correct typical missalignment and manufacturing tolerances in 2.5D, and to perform fine alignment of micro objects.
Actuation force ranges in X, Y and Z	> 10 mN	Enough to hold and accelerate micro objects, overcome forces from capillarity, van der Waals, electro statics or friction (assuming that the normal force can be controlled to the less than 1 mN resolution). Force-fit or other high force tasks are not considered.
Torque range in Θ_x, Θ_y and Θ_z	1 mN/mm	Previously defined forces, in the whole base-space of 10 mm radius. No torque-tasks are defined.

The force sensing principle used in manipulation tasks, should be compatible with the use of micromanipulation tools. The sensor should be as close as possible to the point of interaction, in order to avoid errors introduced by the modeling of any intermediate components, and to avoid loading the sensor with the weight of those

Table 5.2: *Summary of the requirements for the coarse stage of the slave robot.*

Requirement	**Value**	**Reason**
Range in X, Y and Z	$>$ 20mm $\times$ 20mm $\times$ 10mm	Objects are initially scattered in an area of 20mm $\times$ 20mm. The vertical range must be sufficient to move parts over each other and stack them.
Velocity in X, Y and Z	> 10 $^{\text{mm}}/_{\text{s}}$	Traversing the full workspace within two seconds, and following 2 mm peak-to-peak commands at 1 Hz. Distortions will be present, but maximum velocities and end-point position are reached.
Acceleration in X, Y and Z	> 30 $^{\text{mm}}/_{\text{s}^2}$	As before.
MIM in X, Y and Z	< 20 µm	Enough to position the parts within the range of the fine stage.
Rotational range in Θ_z	2π rad	Manipulation and alignment of not-round parts requires full rotation around the Z axis.
Rotational velocity in Θ_z	$\pi/2$ $^{\text{rad}}/_{\text{s}}$	Follow user commands when performing coarse rotations. No scaling is used here since only a coarse alignment is expected.
Rotational MIM in Θ_z	< 2 mrad	Enough to position the parts within the range of the fine stage.

components. The variety of tools necessary for micromanipulation makes it difficult to develop a single force sensor able to deal with all of them. In particular, the abundance of tools based on silicon micro fabrication techniques makes it interesting to develop sensors that can be assembled to those tools in the position of a wrist, or even integrated in their fabrication process.

Part II

System design

Following the requirements outlined in the previous part of this thesis, this part deals with the design of a system for haptic teleoperated micromanipulation. Chapter 6 gives an overview of the designed system, while Chapters 7 and 8 focus on two components of the system: a magnetic levitation positioning stage and a silicon based force and torque sensor.

Chapter 6

Integrated micromanipulation system

Based on the requirements of Chapter 5, the final haptic teleoperation system for micromanipulation is described in this chapter. A general description of the system is given in Section 6.1. Some components of the system had to be custom developed for this application. The overall design and implementation of those components and the arguments leading to their design are explained in Sections 6.2, 6.3, 6.4 and 6.5 of this chapter, focusing respectively on the positioning stages, the force sensing devices, the control architecture and the user interface. Further details about the design of two specific components of the system, a force sensor and a fine positioning stage, are given later in Chapters 7 and 8.

6.1 General system description

The system developed in this thesis implements the elements previously described in Figure 5.1, with the components presented in Figure 6.1. The human interface is managed by a personal computer (PC), which provides the operator with the visual feedback from the manipulation area, with control over system configuration parameters, and enables the operator to monitor the sensors available in the system. This PC also controls the haptic master device and acts as the HT-Controller of the system, transmitting commands from the master device to the slave device, and force feedback in the opposite direction.

A 3 DOF Falcon robot from Novint is used in this work as a master device. In

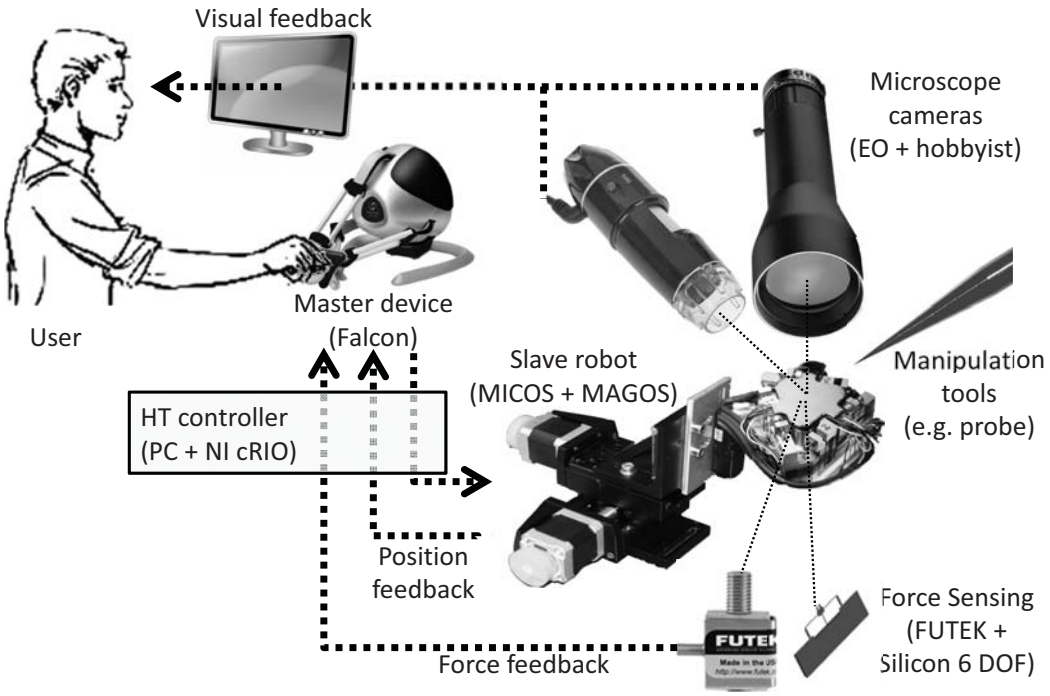

Figure 6.1: *Components of the haptic micromaniplation system. A Falcon robot from Novint is used as a master device, while the slave device is composed by a coarse stage from MICOS and the MAGOS magnetic levitation stage developed in this thesis. Force in the remote environment is sensed through a 1 DOF load cell from Futek. A 6 DOF silicon force sensor is also developed in this thesis for that purpose. An Edmund Optics camera provides a detailed zenithal view of the operation, while a microscope provides an overview and height information. Several micromanipulation tools can be used in the system. The system is controlled through Labview code running between a personal computer (PC) and a National Instruments cRIO controller.*

the future, the master device developed by Patrice Lambert and presented in [51] is planned to be integrated in this system, providing the required 5 DOF: 3 translations, one rotation and one grasping action.

Once in the slave side, a dual-stage system provides coarse and fine positioning to a work-plate of approximately 2 cm in diameter. A combination of PC and real-time Labview programs controls the operation of the positioning stages. Force in the direction normal to the plane can be sensed with a 1 DOF load cell positioned below the work-plate. In order to provide force sensing in additional degrees of freedom, a 6 DOF force sensor is designed within this thesis, but due to its early status of development, it is not integrated into the haptic teleoperation system.

Since all degrees of freedom of the slave robot are implemented in the work-plate, it is possible to use any manipulation tools that can be fixed with their end effectors reaching the work-plate. In particular, during this thesis, tasks were executed using a tungsten probe needle, fine-tip pens and pencils. Exploratory test were made using standard tweezers actuated by an electromagnet and a micro-tweezer from Femtotools.

Two microscope cameras register the visual feedback to be provided to the operator. One EO-5012C color camera from Edmund Optics, together with a 2x magnification lens, provides a detailed zenithal view with a pixel size of 1.1 μm. A hobbyist USB microscope is enough to provide the secondary view. This last camera monitors almost the complete workspace, and is placed at a small angle to the work-plane (typically below 30 degrees) in order to provide information on the distance over the vertical axis between the tool and the work-table.

6.2 Positioners

In order to position the manipulation tools relative to the manipulated objects, it is possible to divide the required DOFs between stages moving the working table were the objects are situated, and stages moving the tool itself. In the case of this thesis, the variety of manipulation tools that the system must support makes it difficult to design stages able to position such tools (Section 5.2.4). Moreover, by having fixed tools it is possible to focus the microscope cameras in the tool-tips, and perform the micromanipulation with constant supervision of the interaction point, while the full size of the work-table can be reached by moving it below the tool. The previous arguments support the option of leaving the tool fixed while moving the work table. Additionally, the low weight of the manipulated objects together with the requirement for low-force actuation and low-moving-mass stages, reinforces the advantage of the aforementioned option. Based on the tests regarding the choice in relative motions of the camera and the micromanipulation tool, and the almost negligible effect of that

choice on operator performance (Section 4.4), it is possible to say that leaving both the camera and tools fixed while moving the work-plate is a safe option.

It must be noted that the previous analysis may not be valid when performing large rotations as part of the micromanipulation sequence. First, the test presented in Section 4.4 considers only translational movements. Preliminary tests performed including rotations showed that operators can become confused when including rotations in the task. Second, mixing rotations and translations in a kinematic chain introduces cross-talks between the different degrees of freedom, and requires very careful calibrations and high accuracy in the system, thus introducing an accuracy requirement not initially present in the tasks. If, on the contrary, the rotations are left in the tool instead of in the work-plate, and care is taken to position the tool-tip over the axes of rotation of the system, it is possible to obtain the same intuitive operation and constant supervision of the interactions described before. Even if the problem with positioning large or heavy tools persists, the approach of keeping the translational DOFs in the work-plate and any large rotations in the manipulation tool must be followed whenever possible.

For this thesis, a dual stage system is obtained by using an off-the-shelve 4 DOF positioner from MICOS as a coarse stage, and mounting a custom-made 6-DOF magnetic-levitation stage on top of it. When possible and necessary, the stage in charge of the coarse rotation around the vertical axis can be separated from the kinematic chain, and used to rotate the tool around its tip. The controlling hardware of both systems is independent, but a common PC application running on Labview allows for coordinating their movements. Depending on the requirements of the task, the fine stage can be separated and the system operated only with the coarse stage as a slave robot, thanks to the fact that the specifications of the coarse stage surpass its original requirements.

6.2.1 Coarse positioning

The coarse stage is implemented by using a stack of four 1-DOF positioners from MICOS. A DT-80 rotational stage provides endless rotation with bidirectional repeatability of 9mrad. On top of this rotation, the horizontal displacements are achieved by two LS65 stages based on a ball-screw and a stepper motor. Each LS65 stage provides 26mm of travel range with 5µm of bidirectional repeatability. The vertical displacements are obtained from a VT-21S stage, working on the same principle and with a bidirectional repeatability of 5µm over a range of 10mm. The rotational stage can be separated from the system and adapted to its use with a specific tool, in tasks where continuous and large rotations are required. This adaptation is not simple, since brackets should be designed to hold each specific tool, position the tool-tip in the axis of rotation, and position that axis within the workspace of the translational

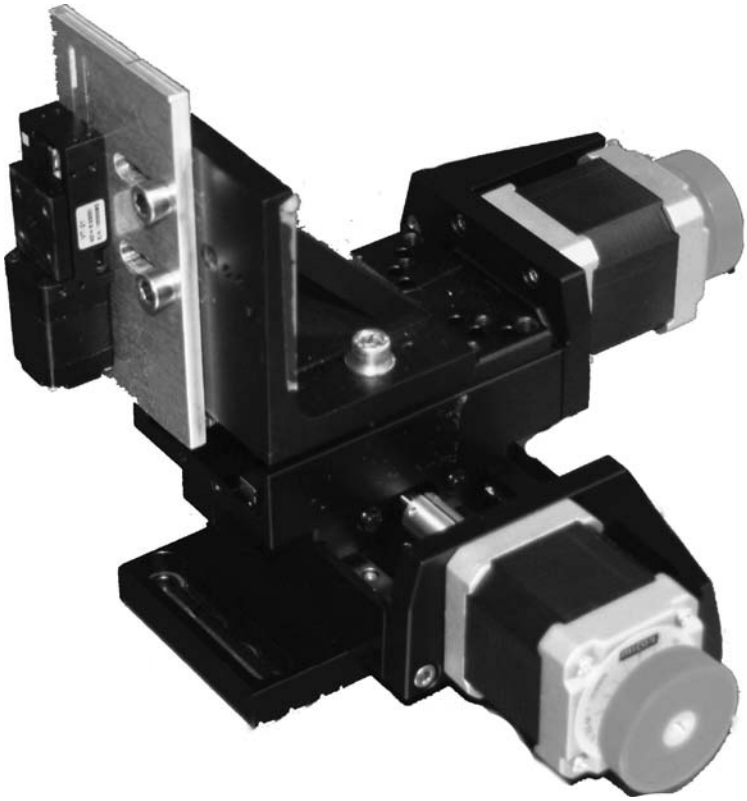

Figure 6.2: *The coarse stage of the slave robot, in its 3 DOF configuration. This stage is implemented by using a stack of 1-DOF positioners from MICOS.*

positioners, while avoiding interference between the different stages. A separate rotational stage can also be used for that purpose. The stage in its 3 DOF configuration (without the rotational stage) can be seen in Figure 6.2.

The 4 stages are controlled by a DMC-2143, 4 axis controller. This controller uses one RS232 port to communicate with a Labview program running on a PC. The controller also has an Ethernet port which could be used to communicate with the cRIO controller of the fine stage.

6.2.2 Fine positioning

A 6 DOF magnetic levitation stage is designed and developed in this thesis as a solution for the fine positioning problem. The combination of magnetic-levitation actuation and optical-sensing generates a system with zero stiffness in open loop, while the closed-loop stiffness can be set by a controller following position references. The moving plate

is completely disconnected from the fixed world and weights only 8.15 gr, ensuring low actuation forces. The whole system weights less than 100 gr and has an overall size of $6 \times 6 \times 4$ cm, allowing an easy integration with the coarse stage. The stage achieves a MIM of 50 nm in translations and 3.5 to 7 μrad in rotations, over a range of 200 x 200 x 200 μm and 18 to 42 mrad respectively. The design, development and performance of this stage are described in detail in Chapter 7.

Positioning stages based on flexure hinges as a guidance principle are also an interesting possibility. An exploratory design for a stage exploiting this principle was investigated within this thesis. More details about this design can be found in [19].

6.3 Force Sensing

Sensing the interaction force between the tool and the objects in the work-plate can be achieved by placing a force sensor either in the tool or in the work-plate. Similar to the situation described before regarding positioning, sensing forces in the work-plate gives flexibility to the system, since it is possible to use the same force sensor independently of the tools needed for the task. This configuration is explored in [56], where a sensorized work table is suggested for measuring the forces applied by the tool in multiple DOFs. This principle has nevertheless one drawback when used to measure forces in several DOFs: in order to reconstruct and separate the force components it is necessary to know the location of the interacting forces at the plate, and any inaccuracies on that position measurement reflects in the force measurement. Thus the method introduces accuracy requirements in the positioning system, additional to those present in the task, and requires recalibration and alignment each time the tool is changed or moved. Moreover, the weight of the work plate and its inertial forces can be relatively high compared to the expected interaction forces, thus increasing the chances of saturating the sensor.

In this thesis, and following the previous analysis, the configuration with force sensing in the work-plate is used only to measure forces in one DOF, normal to the work plate, and only when the operation can be carried out directly over the sensor or with only a lightweight work-plate on top of it. In particular, for tasks which do not require the use of the fine positioning stage, a LSB200-20gram-FSH02667 1 DOF force sensor from FUTEK is fixed on top of the coarse positioning stage. A lightweight work-plate is then positioned on top of it and operations can be carried out while monitoring the vertical interaction forces between the work-plate and the tool.

The second option explored in this thesis is the use of force sensors placed between the tool support and the tool end-effector, equivalent to the position of the wrist between the arm and the hand. In particular, many tools used in micromanipulation, such as micro grippers and probes, are fabricated using silicon micro fabrication tech-

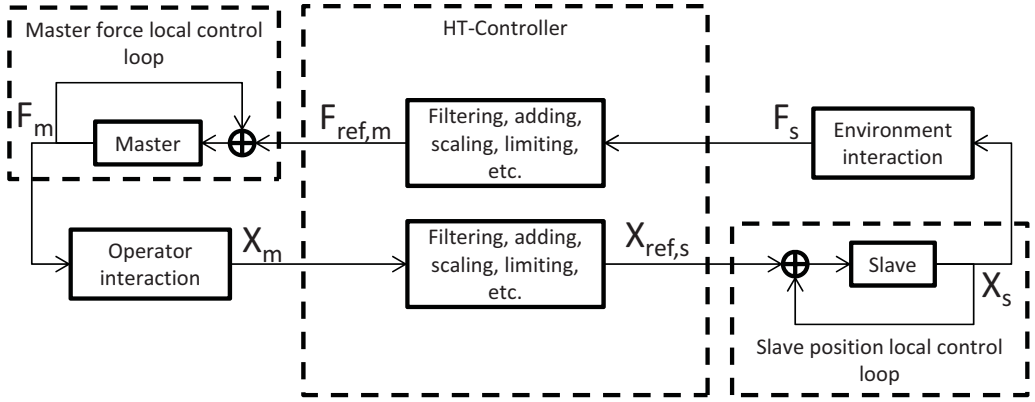

Figure 6.3: *Overview of the control architecture of the micromanipulation system. Two local loops control the force exerted by the master device (F_m) and the position achieved by the slave device (X_s). The HT-Controller takes the force measurements in the slave device (F_s, when available), modify them as needed and transmit them to the master device as a force reference ($F_{ref,m}$). In the other direction, the HT-Controller does the same with the measured position of the master device, resulting on the slave reference position ($X_{ref,s}$).*

niques [25, 29]. It is thus interesting to develop sensors that can be combined with those tools, or even integrated in their fabrication process. Although many silicon-based force sensors can be found in the literature, they are normally not designed with the intention of integrating them with a manipulation tool, thus limiting their applicability to the tasks considered in this thesis. A proof of concept for a 6 DOF force and torque sensor designed for micromanipulation is developed within this thesis, and its detailed description can be found in Chapter 8. Further work is still required for its integration with manipulation tools, and therefore the current version of the sensor is not used as part of the integrated system in this thesis.

6.4 Control architecture

The general architecture of the control system of the haptic teleoperated system for micro manipulation can be seen in Figure 6.3. The control architecture has several levels. At the highest level is the HT-Controller, which is in charge of transmitting information between the master and the slave devices, and in some cases modify this information by filtering, limiting, and scaling it, or by adding new information (as explained in Section 3.2). In this thesis, the chosen implementation follows the position-force architecture, which transmits position commands from the master de-

vice to the slave device, and force commands from the slave device to the master device. Therefore two local control systems are required: one to control the forces exerted by the master device, and one to control the positions achieved by the slave device. These local controllers are depicted in Figure 6.3 as single feedback control loops for simplicity, but can in fact consist themselves of several levels and different architectures. The local control loop of the master device is part of the internal configuration of the Falcon master device used, and is therefore not discussed further in this thesis.

The HT-Controller of this thesis is implemented as a Labview program in a PC running a Windows operating system. Each control cycle takes approximately 20 ms. Thus, the update frequency of the master-force and slave-position references is limited to 50 samples per second. In both master-to-slave and slave-to-master directions, the HT-Controller has low-pass filters that can be configured in order to ensure stability of the system, and to avoid the transmission of involuntary operator movements or unnecessary and disturbing force feedback. Limiters are also available in order to ensure a safe operation of the system and to avoid overloading the slave and master devices. Last, virtual forces can be added to the master force reference to create a virtual impedance field on the master device. This is achieved by measuring the master device position and relating it to an impedance function, which can include position dependent stiffness, damping and inertia.

The local control loop of the slave device is actually composed of two parallel subcontrollers, as shown in Figure 6.4. One controller is in charge of the coarse stages (implemented in the DMC-2143 board) and one in charge of the fine stage (implemented in a cRIO system from National Instruments). When performing transport and alignment operations, or when performing tasks where the fine stage is not necessary, only the coarse stage controller is active. The coarse stage controller operates in feed-forward since the coarse stage is composed of stepper motors without position measurement. While operating the coarse stage with the fine stage mounted on it, the fine stage controller is left to follow a zero reference, thus acting as a compliant work-plate. For performing mount operations in delicate tasks requiring high motion resolution, the coarse stage is left stationary, and the position reference is passed directly to the fine stage control loop, operating with feedback from its local position sensors. More details about the local controller of the fine stage can be found in Section 7.4. The transitions between operating the coarse stage and operating the fine stage can be commanded in different ways from the user interface software. Out of the obvious option of switching between them with a binary control, a continuous transition is also implemented in the system, as explained in Section 6.5.

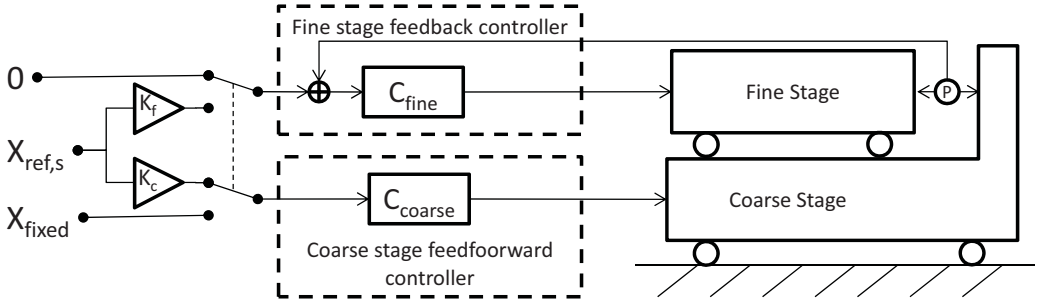

Figure 6.4: *Coarse and fine stage controllers on the slave device. Depending on the kind of operation executed, the reference position* $\mathrm{X_{ref,s}}$ *is passed either to the coarse stage or to the fine stage, after scaling it accordingly (with* $\mathrm{K_f}$ *for the fine stage and* $\mathrm{K_c}$ *for the coarse stage). The stage which is not in use is left following a fixed reference in the meantime.*

6.5 User Interface

Given the modularity of the overall controller, it is easy to configure different interfaces for the operator to command the displacements of the slave robot and receive feedback from the interactions with the environment. The use of a Windows operating system and Labview programing environment further simplifies this process, thanks to the variety of devices, drivers and customizations available to them. Indeed, during this thesis, different interface modules where designed depending on the task or test executed, and on the system modules required for it. It is nevertheless interesting to discuss certain aspects of the user interface which were common to most of the implementations, and supported the operator in performing the tasks. It must be noted that while it is often the case that interaction between teleoperation systems and users occurs through a graphical user interface (GUI), the nature of the system developed in this thesis brings an important part of that interaction into the master device, thus making the user interface mostly haptic.

The basic operation mode of the system consist of the slave device following the scaled displacements of the master device. When force sensors are available in the slave system, the scaled forces are also rendered to the operator through the master device. By using the GUI, it is possible to switch between the coarse and fine stages, as well as adjust the different scalings. It is also possible to command discrete displacements using the GUI.

A first element added to this interface is the possibility of a seamless transition between the fine and coarse stages, with an approach similar to that found in [56]. The displacements of the master device are constrained by a virtual compliant cylinder.

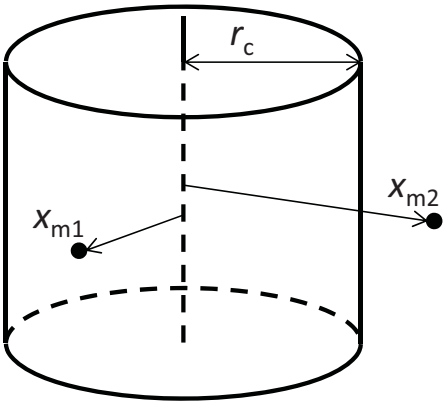

$$F_m = \begin{cases} 0 \text{ if } |x_m| < r_c \\ -k_{f,m} \cdot x_m \cdot \left(|x_m| - r_c\right) \text{ if } |x_m| > r_c \end{cases}$$

$$x_{\text{ref,fine}} = k_f \cdot x_m$$

$$v_{\text{coarse}} = \begin{cases} 0 \text{ if } |x_m| < r_c \\ k_c \cdot x_m \cdot \left(|x_m| - r_c\right) \text{ if } |x_m| > r_c \end{cases}$$

$$x_{\text{ref,coarse}} = \int v_{\text{coarse}} \cdot dt$$

Figure 6.5: *Seamless dual stage operation from the master device. The position of the of the master device x_m is normally transmitted as a reference $x_{\text{ref,fine}}$ to the fine stage of the slave device. When the operator drives the master device outside of a cylinder of radius r_c, a virtual wall appears, in the form of a force F_m dependent by a stiffness constant $k_{f,m}$ on the penetration of the master device into the cylinder walls. A second constant k_c is used to convert this penetration into a velocity reference for the coarse stage of the slave device.*

That is, a position-dependent force equivalent to a linear stiffness is rendered in the master device once the operator drives it outside of a centered cylindric workspace, as can be seen in Figure 6.5. Inside of that cylinder, the displacements of the master device are followed by the fine stage. When the operator pushes against the cylinder walls, the magnitude and direction of the penetration into such walls is transmitted as a velocity command to the coarse stage. In that way the operator can perform delicate tasks using the fine stage, and perform long stroke movements by pushing against the virtual-cylinder walls, without loosing focus and contact with the haptic device.

The second element added to the interface is the presence of a virtual floor. Given the 2.5D characteristics of the tasks dealt with in this thesis, it is often important to have an indication of the presence of contact between the tool and the working plane, and the magnitude of this contact. A natural way to indicate this contact to the operator is by rendering the normal interaction force between the tool and the working plane in the master device. When sensor information is not available, a virtual floor can be implemented, with a position-dependent force-rendering as in the aforementioned case of the cylinder. After calibrating the position of the tool, such that the virtual floor corresponds approximately to the height at which the tool is in contact with the work-plate, operators can use this force information to recognize

when the tool is in contact with the work-plate, and to guide their hand during surface-scanning movements.

The third element added to the haptic interface is the presence of damping. Using the position measurements from the master device it is possible to render a force proportional to the speed of the master device, thus achieving the damping effect. This damping acts on one hand as a stabilizer for the whole manipulation system, reducing the instabilities that are typical of haptic teleoperation systems. Additionally, the damping assists the user to achieve softer and better controlled movements, by reducing the hand tremor, and filtering and slowing down the hand movements. Moreover, when using the aforementioned virtual floor, the damping coefficient is made dependent on the height over the work-plate. In that way, damping is only added when performing delicate operations and when contact is expected, while risk-less transport operations carried out far from the work plate can be performed without the slowing effect of the damping.

Chapter 7

6-DoF Miniature Maglev Positioning Stage[1]

This chapter presents a micro-positioning stage in six orthogonal directions (6-axis) based on magnetic levitation. The stage is custom designed as the positioning system of the slave robot for haptic teleoperated micromanipulation. This application poses a particular set of requirements which are discussed in the introduction.

A novel 2-axis actuator assembly is introduced, in which two fixed coils generate Lorentz forces on a single moving magnet, which is attached to the mover. Three such actuators generate the six forces that are required in the stage. The position of the mover is then sensed by using LED/photo-transistor pairs. The actuator assembly is studied in detail and characterized, both experimentally and through simulations. Non-linearity and position dependency in the transfer functions of the sensor and actuator are identified, characterized and integrated into a dynamic simulation of the system. A Monte-Carlo study is then used to investigate the robustness of the complete system to manufacturing tolerances and the intensity of different noise sources.

The stage is fabricated, including custom electronics for signal conditioning and amplification. With a movement range of 200 x 200 x 200 μm and rotations of 18 to 42 mrad, the achieved Minimum Incremental Motion (MIM) is 50 nm and 3.5 to 7 μrad under closed loop control, and is determined by noise in the sensors and actuators.

[1] Some aspects of design and fabrication explained in this chapter are extended in [61], as indicated within the text.

7.1 Introduction

Several tele-operated micro-manipulation systems have been developed for micro-manipulation, both in the academia [44][67] and in industry [1]. Nevertheless, the reported systems are usually adaptations of existing automatic equipment to the tele-operation application, and thus the hardware components are not optimized for human tele-operation with force feedback. The slave side is commonly implemented by a set of high-stiffness position actuators, which is certainly preferable for most automatic positioning applications. It has been shown, however, that a low-stiffness slave robot can improve stability of haptic tele-operation controllers without a high impact on performance [24]. Moreover, components can be very fragile in the micromanipulation application, and a low stiffness and low mass slave robot ensures a delicate manipulation with low applied forces. Furthermore, the slave systems that are originally designed for automatic manipulation are in many aspects over-specified with respect to the use that a human operator will present in a tele-operation scheme. These specifications come at a high cost, undermining one of the main advantages of using tele-operation over automatic systems for prototyping or working in unstructured situations. Existing systems do not take into account the intelligence and adaptability that the operator adds to the system as a whole. Automatic positioning stages are designed to perform several operations per second, at control bandwidths much over what the users require: human movements generally remain below 5Hz [18] achieving just a few simple operations per minute. The high accuracy level in positioning and force application that is required in automation, becomes also worthless when the commands are presented by the inaccurate user limbs, which in open-loop can present large errors compared to the force and displacement values intended by the user. On the other hand, the user acts as a complex, adaptable and intelligent controller, using visual and haptic feedback to drive the actions of the end effector. As such, humans are used to and capable of dealing with inaccurate actuators (as in the case of human limbs), and can perform complex tasks with low-performance hardware components.

In this work, the MAGOS stage (acronym for MAGnetic levitation and Optical Sensors) is presented as a possible solution to the aforementioned problems. On the one hand, the magnetic-levitation actuation and optical-sensing principles used in this work keep the moving part completely disconnected from the fixed world. With this method the positioning system achieves zero stiffness in open loop, while the closed-loop stiffness can be set by a controller following position references. With a model of the system, the controller effort can be used as an estimator of the forces that are applied in the environment. The system can also be controlled by providing force references and using the system in feed-forward configuration to generate those forces, as required by certain haptic tele-operation schemes, contrary to the practice of setting

Table 7.1: *Main specifications for the positioning stage.*

Specification	Specified value
Translation range	200 x 200 x 200 μm
Translation Noise level	40 − 100 nm pp
Rotation range	±18 mrad, vertical axis
Rotation Noise level	35 μrad pp
Force range	10 mN
Payload	1 g
Controller bandwidth	>50Hz

force-control loops on top of position loops [34]. On the other hand, attention is given to keeping the system inexpensive and small, while maintaining the requirements set by the tele-operation scheme and the intended application.

7.2 Requirements and specifications for the magnetic positioner

The application scope is taken into account in the definition of the specifications of the stage. The stage is intended for sub-millimeter sized objects, in assembly operations where minimum incremental motions (MIM) below 1um and 35 μrad are required to overcome problems by tight clearances and to avoid damaging the objects. The full assembly operation may require a large workspace in order to move objects and tools within the workspace and pre-align them, but this stage is intended for the delicate contact interactions that only occur at a sub-millimeter level. This means that the stage is designed for a workspace of 200 x 200 x 200 μm^3 and rotations of about ±18 mrad, operating in a two-stage scheme together with a standard coarse stage, which will take care of any large displacements. The mass of the manipulated objects is typically very small, as are also the interaction forces. In order to provide a delicate manipulation and to maintain a clear relation between the actuation forces and the interaction forces, the moving part of the stage is optimized for a low mass and low driving forces. As a final requirement, the upper face of the slave robot must remain completely open, in order to avoid visual occlusion or interference with the manipulation tools. A summary of the main specifications of the stage, derived from these requirements, can be seen in Table 7.1.

7.3 Conceptual design

Several magnetic levitation stages can be found in literature, achieving some of the specifications that are targeted in this work. Systems with reluctance actuators are commonly used when high forces are needed [53][26], while commutated Lorentz actuators with Halbach magnet arrays are used in cases requiring long travel ranges [89][41]. For applications with small travel ranges and lower force-density requirements, Lorentz actuators provide a fairly linear current-force characteristic. In a Lorentz actuator, a current is driven through a wire in the presence of a magnetic field, generating a force between the wire and the origin of the magnetic field. When using cheap permanent magnet material, the resulting heavy permanent magnet part is in most cases left stationary, while the lighter coils are attached to the moving components. This approach requires several connections to the moving part, compromising its modularity and adding actuator stiffness. By mutually exchanging the coil and permanent magnet, no connections are required in the mover, but care must be taken to keep the moving mass low. This is possible with modern permanent-magnet materials like NdFeB. Of particular interest for this work are the stages presented in [46]. Kim et al. achieves 6-axis actuation with only 3 moving magnets, by using a 2-axis actuator in which a single magnet in the mover and 2 stationary coils provide 2 perpendicular forces [82]. The position sensing in maglev stages is commonly achieved by capacitive, inductive or interferometric sensors in order to avoid contacting the mover. These sensing methods are very accurate (down to nanometer accuracy), but at the same time they are expensive and space consuming, and in some cases require electric grounding of the mover.

The MAGOS stage presents a similar architecture to the stage that was exhibited in [46], but uses a novel type of a compact 2-axis Lorentz actuator that is explained in section 7.3.1. It uses photo-transistors for position sensing. Figure 7.1 shows a schematic view of the stage.

6 SFH-9201 infrared reflective sensors, composed of a LED and a phototransistor, are mounted on the stationary base. Three sensors point upward and are in charge of measuring the vertical position z and the rotations around the x and y axis. The other 3 sensors measure a horizontal displacement to determine the x and y positions and the rotation around the z axis. As long as the information coming from the sensors is linearly independent, it is possible to reconstruct the 6-axis position of the mover from their readings. This kind of sensors presents a short linear measuring range and they have a much lower price than more accurate options. In view of the requirements that are outlined in section 7.2, they perfectly fit this application, in spite of their limited performance on noise and drift.

3 coil assemblies are also mounted on the base, and provide the actuation forces

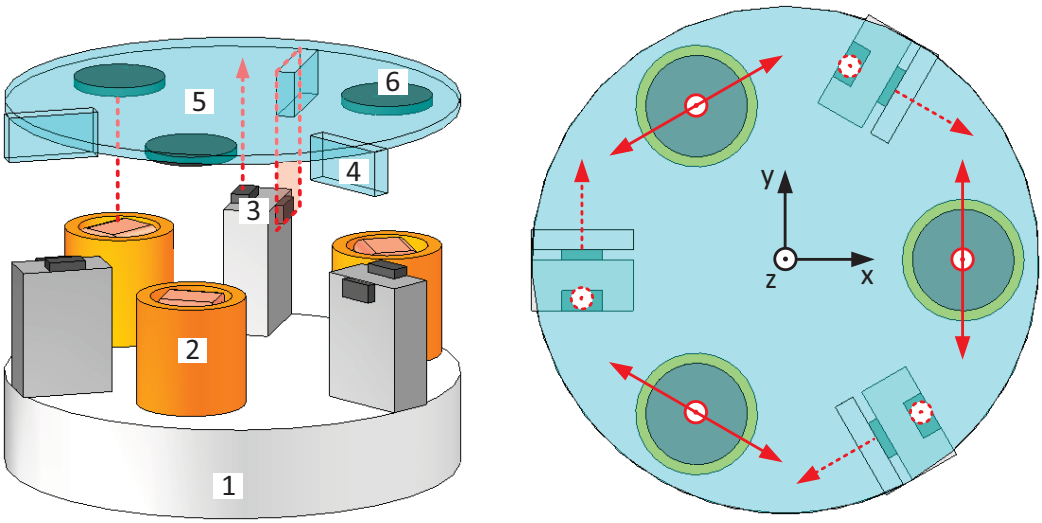

Figure 7.1: *Conceptual design of the magnetic-levitation 6-axis stage. a) Exploded lateral view with (1) Base structure, (2) Actuator coils, (3) Sensor holders with sensors, (4) Sensor Targets, (5) Floating disk and (6) Actuator magnets. b) Top view with the 3 in-plane and 3 out-of-plane lines of actuation of the forces (solid arrows) and lines of measurement of the distance sensors (dotted arrows).*

with the magnets that are located on the mover directly on top of the coils. The mover also holds the targets for the position sensors, and includes a thin layer of ferromagnetic material for improving the magnetic flux direction near the coils and reducing the magnetic flux above the disk.

7.3.1 2-axis Lorentz actuator assembly

In section 7.3 a compact magnetic levitation actuator was introduced. In this section we will further analyze, dimension and test such an actuator.

2-axis actuator concept

The 2-axis Lorentz actuator that is used in the stage is composed of a square coil, nested inside a cylindrical coil, that are both located below an axially magnetized cylindrical magnet (Figure 7.2). The upper section of the square coil profits from the strong and almost vertically directed magnetic field near the surface of the magnet, and generates a lateral force. The lower parts of the square coil generates a counteracting force, but due to its distance from the magnet surface this force is much smaller than the contribution of the upper part. The round coil uses a different area of the magnetic

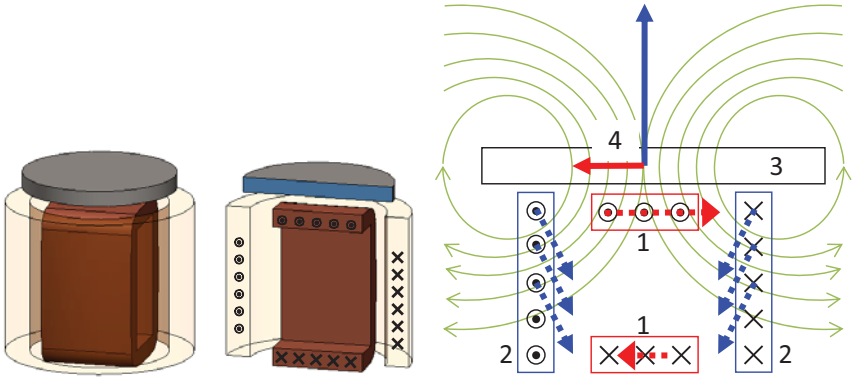

Figure 7.2: *2-axis compact actuator. a) The 3D coil assembly with the magnet on top, and section view of the coils indicating the direction of the currents; b) A cross section of the actuator with the square coil (1), the round coil (2), the magnet (3), the Lorentz forces on the coils (dotted arrows), and the reaction forces on the magnet (4, solid arrows).*

flux. In that area, most of the flux travels horizontally and radially, which together with the current (also horizontal but with circular trajectory) generates a vertical net force.

2-axis actuator dimensioning

In principle it would have been useful to count with an analytical mathematical description of the current-to-force relation of the actuator. Given that the magnetic flux is not constant in space, the calculation includes a double integration of magnetic charges on the surface of the magnet to obtain the magnetic flux in the surrounding space, and a triple integration of that flux in the coil volume to obtain the forces, as shown in equation (7.1) (more details in appendix A).

$$F = \frac{\sigma_{\text{sm}}}{4\pi} \int\limits_{V_{\text{coil}}} J(r) \times \left(\int\limits_{S_{\text{mag}}} \frac{(x-x')\,\hat{i} + (y-y')\,\hat{j} + (z-z')\,\hat{k}}{\left[(x-x')^2 + (y-y')^2 + (z-z')^2\right]^{1.5}} ds' \right) dv$$

Where:
$\sigma_{\text{sm}} = \pm\mu_0 M$ = Surface magnetic charge density (7.1)
$\pm$ Depending on the magnet surface
M = Magnetization
S_{mag} = Surfaces of the magnet
V_{coil} = Volume of the coil

Such an integral has to be solved numerically, like is done in [82]. In our work, the ferromagnetic back-plate adds further complexity to the problem, and therefore a simulation using finite elements modeling was used instead, to obtain the current to force relation.

For the FEM simulations, COMSOL software is used. The simulation includes the 2 coils, the magnet and the ferromagnetic plate. A parametric study was run in order to select the dimensions of the different elements of the actuator. The parameters in table 7.2 where used in the simulation. The height of the coils was not changed during the studies. An increase of the height of the coils corresponds to an increase of resistance and the related power loss, while the force at a certain current level also increases. Nevertheless, above a certain value this force increase becomes negligible due to the distance from the permanent magnet. Figure 7.3 shows for instance a particular case for the horizontal actuator, and it can be seen how after 10 mm the added force becomes almost negligible. Similar results where obtained for different sets of parameters and for the vertical actuator, and since there was no design-constrain on the heights of the coils, those were left in 10 mm.

Figures 7.4 and 7.5 show the results of the parametric studies, indicating the configurations within the design space that generate enough force at the nominal operation point. For a given actuator force, there is a trade-off between the dimensions of the coil and the magnets. A smaller magnet reduces the moving mass, but also requires bigger coils. This increases their footprint on the mover, and consequently the mover size and mass. Furthermore, the square coil must fit inside the round coil, creating an additional trade-off between their dimensions. All of these trade-offs were explored in order to determine the definitive coil and magnet dimensions, such that the size of the assembly would remain practical, with force generation according to the requirements and a limited moving mass. The final dimensions of the coils can be seen in Table 7.3.

Table 7.2: *Parameters used in the parametric study of the vertical and horizontal actuators.*

Parameter	Values	Comment
Magnetic field within the magnets	1.2 [T]	Value of standard magnets
Current density on copper cables	6e6 [A/m]	
Fill factor	0.8	Achievable with orthocyclic winding
FOS	2	Necessary to cover for differences between model and measurements in preliminary test
Minimum vertical force	$\frac{\frac{115[mN]}{FOS}}{3} \approx 75[mN]$	Including extra force to cope with crosstalk
Minimum horizontal force	$\frac{\frac{15[mN]}{FOS}}{\sqrt{3}} \approx 17[mN]$	Including extra force to cope with crosstalk
Magnet radius	4 to 6 [mm]	
Magnet height	0.5 to 2 [mm]	
Round coil internal radius	3 to 6 [mm]	
Round coil thickness	0.5 to 2.5 [mm]	
Square coil side	4 to 8 [mm]	
Square coil thickness	0.1 to 0.2	As a proportion of the coil side dimension
Coil to magnet distance	1 [mm]	Worst case

2-axis actuator characterization

Using the previously selected dimensions, a second parametric study was run, exploring the current-to-force relation over the positioning workspace of the actuator. Figures 7.6 and 7.7 show the value of the forces and torques in all 6 DOF of the vertical and horizontal actuator at a constant current, in the area around the nominal working position. Due to the non-homogeneity of the magnetic field, position-dependent gains and cross-talk terms were observed, and polynomial functions were fitted to those relations. Such effects generate variations of up to a 10 % in the intended forces and torques over the workspace. More details about these position to force relations can be found in [61].

A measurement setup was built to validate the current-to-force relations obtained

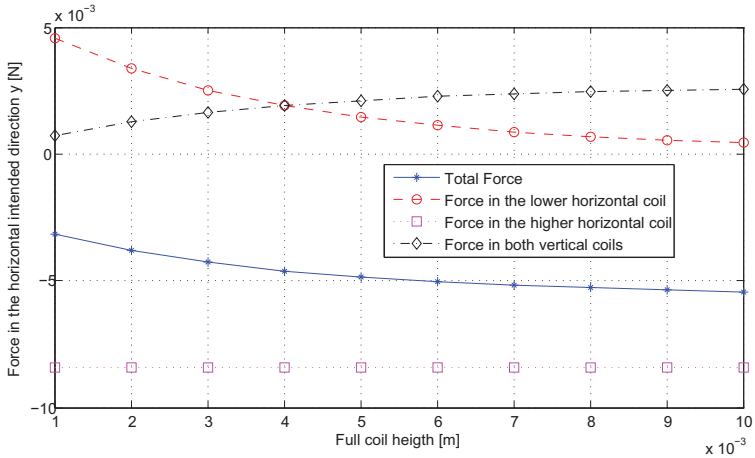

Figure 7.3: *Force in different sections of the coil of the horizontal actuator as a function of the coil height. It can be seen that after 10 mm the additional force is almost negligible, due to the low field strength far from the magnet.*

in the FEM simulations. A cylindrical magnet was mounted to a load cell, such that the force in the actuation direction could be measured. A square and a cylindrical coil where placed on a 3-axis positioning stage with a positioning resolution of 5µm, and energized with a constant current. The coil and the magnet were centered by searching for the symmetry axis of the force. The workspace of the actuator was then explored while recording the force values measured by the load cell. The data obtained from this experiment showed current-to-force relations with shapes similar to those obtained in the FEM simulations, but with a scaling factor of around 1.3. This scaling factor could be attributed to tolerances in the component properties, especially the magnetization of the magnet, the fill factor, the shape and homogeneity of the coil windings, and the coil to magnet distance.

7.4 Controller design and system simulation

A model has been made of the complete system using the SimMechanics package of Simulink. This model includes the inertial properties of the stage, the current-to-force characteristics of the actuators as obtained from FEM modeling (section 7.3.1), a model of the sensors and the external disturbance forces (i.e. floor vibrations and assembly interaction forces). Internal vibration modes are not considered since the eigen frequencies of the components lie far above the operating bandwidth and are assumed to be sufficiently damped and filtered from the sensor signals.

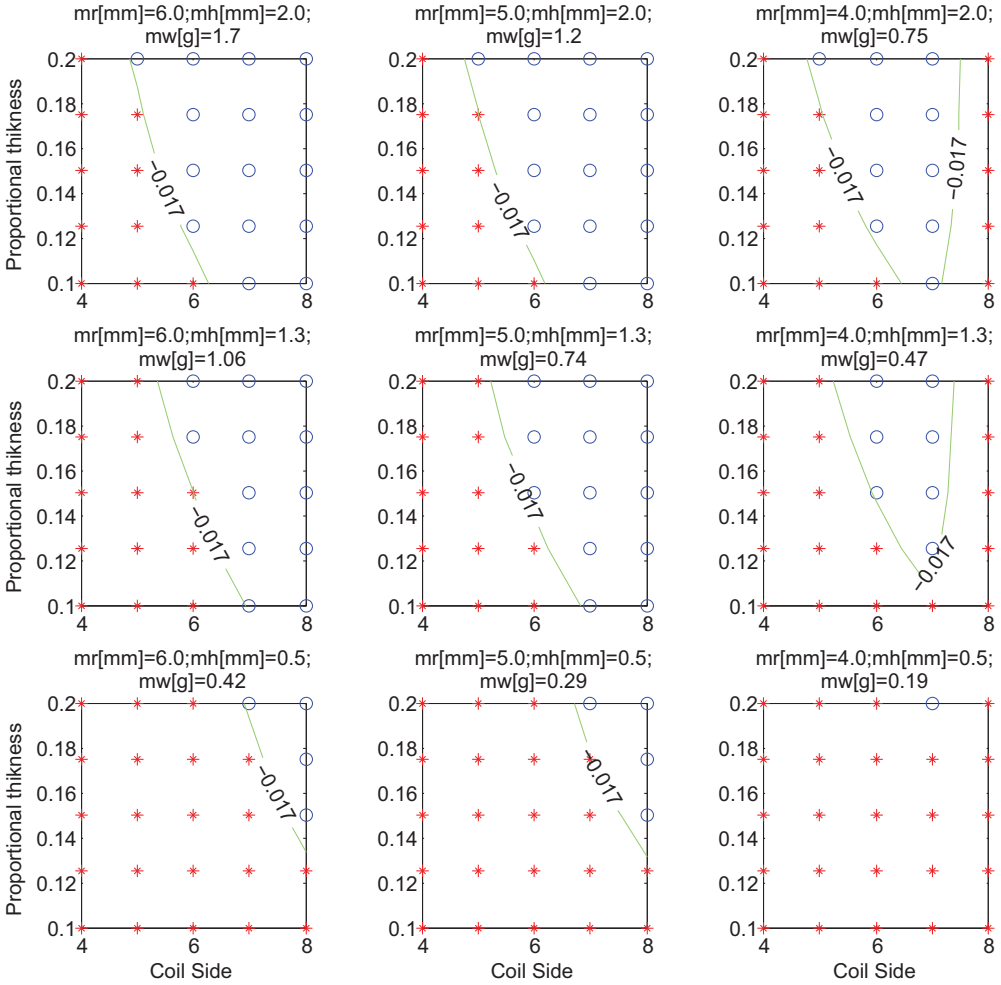

Figure 7.4: *Parametric study of dimensions for the horizontal actuator. The circles indicate the configurations generating enough force, while the asterisks indicate those generating insufficient force. The interpolated limit-force line in mN is also indicated. The titles of each subplot indicate the magnet radius (mr), its height (mh) and it weight (mw).*

In the SimMechanics model of 7.8, the controllers feedback-matrix $G_F B$ receives a set-point in the six orthogonal world coordinates and monitors the 6-axis position in the same coordinate system. The controller then outputs the necessary forces to be applied on the CoM (Centre of Mass) of the mover. A gain balancing matrix G_B transforms the forces and torques required in the CoM to the 2-axis forces applied by each actuator [62], and a force-to-current matrix $G_F J$ uses the characteristics of the

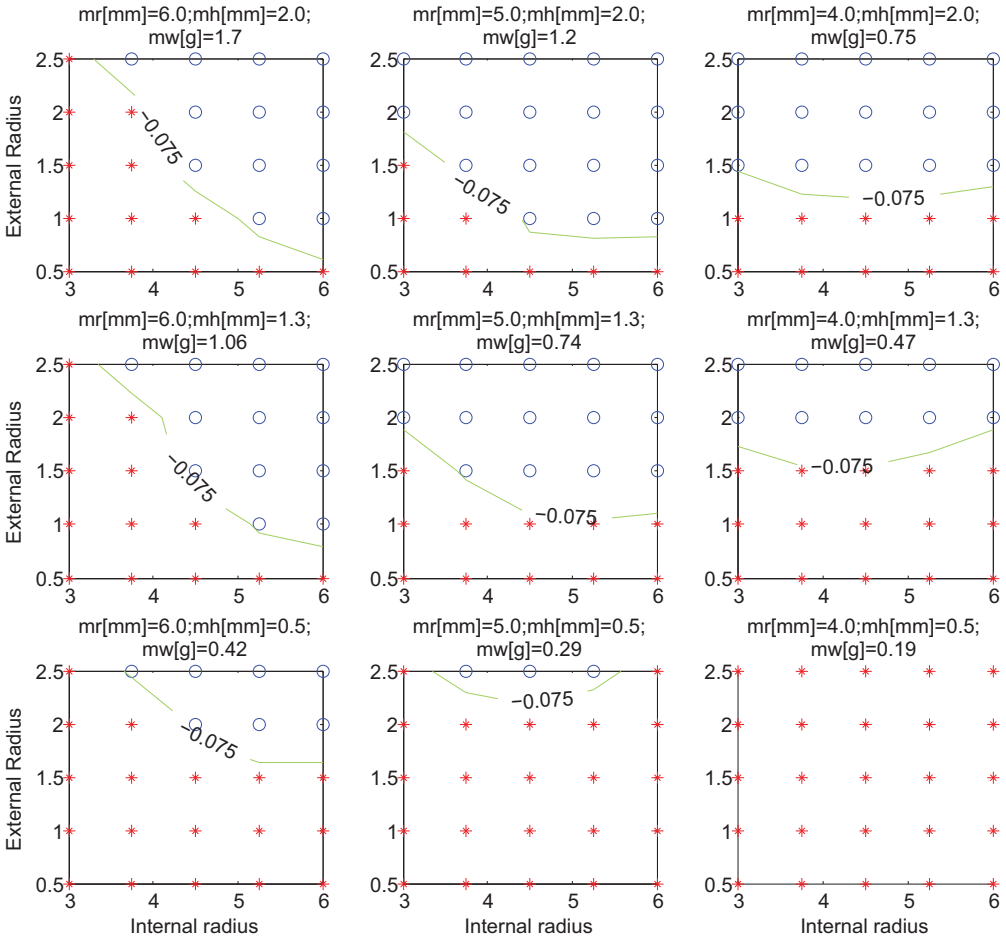

Figure 7.5: *Parametric study of dimensions for the vertical actuator. The circles indicate the configurations generating enough force, while the asterisks indicate those generating insufficient force. The interpolated limit-force line in mN is also indicated. The titles of each subplot indicate the magnet radius (mr), its height (mh) and it weight (mw).*

actuators to obtain the currents to be applied to the coils. Due to the inherent crosstalk of the actuator (as explained in section 7.3.1), a position dependent crosstalk appears at this level, which is modeled by the current-to-force matrix G_JF. This matrix is updated during the simulation, as a function of the measured position. The forces are then applied to the moving mass, which also receives the external disturbance forces. The position sensors are modeled according to their experimentally observed characteristics, including non-linearity, saturation and noise. Finally, and since the

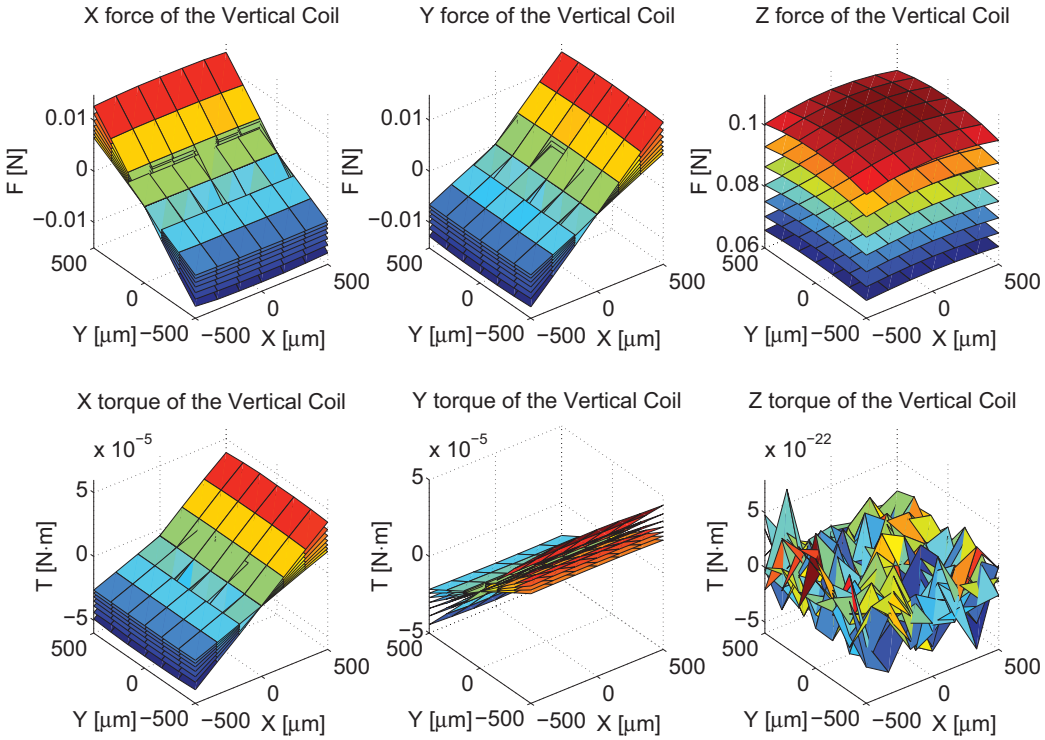

Figure 7.6: *Force-displacement characteristic of the vertical coil as calculated by the FEM model. Units on the x- and y-axes are [m], units on the vertical (z-) axis are [N] for the upper row and [Nm] for the lower row. The seven planes in in each graph correspond to different coil-magnet distances, from 0.25 to 1.25 [mm].*

position sensors are not measuring directly the CoM position, a matrix S is used to transform the measurements from the sensors axes to the world coordinates.

Despite the actuator cross-talk, the simulation shows that six independent SISO controllers can effectively control the system. This approach is also taken in the control of existing 6-axis maglev stages by various groups [46][50][35]. Assuming small rotations and using a linear model of the system, PID controllers are tuned for an open-loop unity-gain cross-over frequency of 50Hz. Since the system is open-loop unstable, the derivative and integral components must be carefully chosen to ensure enough phase margin at the unity-gain cross-over frequency. Figure 7.9 shows the open-loop Nyquist and Bode plots of the controlled system in the x axis, both for a continuous and for a discrete model of the system with a sampling frequency of 1kHz. It is possible to notice how the discrete controller achieves considerably less phase margin due to the relatively high crossover frequency compared to the loop period of the controller. Other axis were similarly tuned.

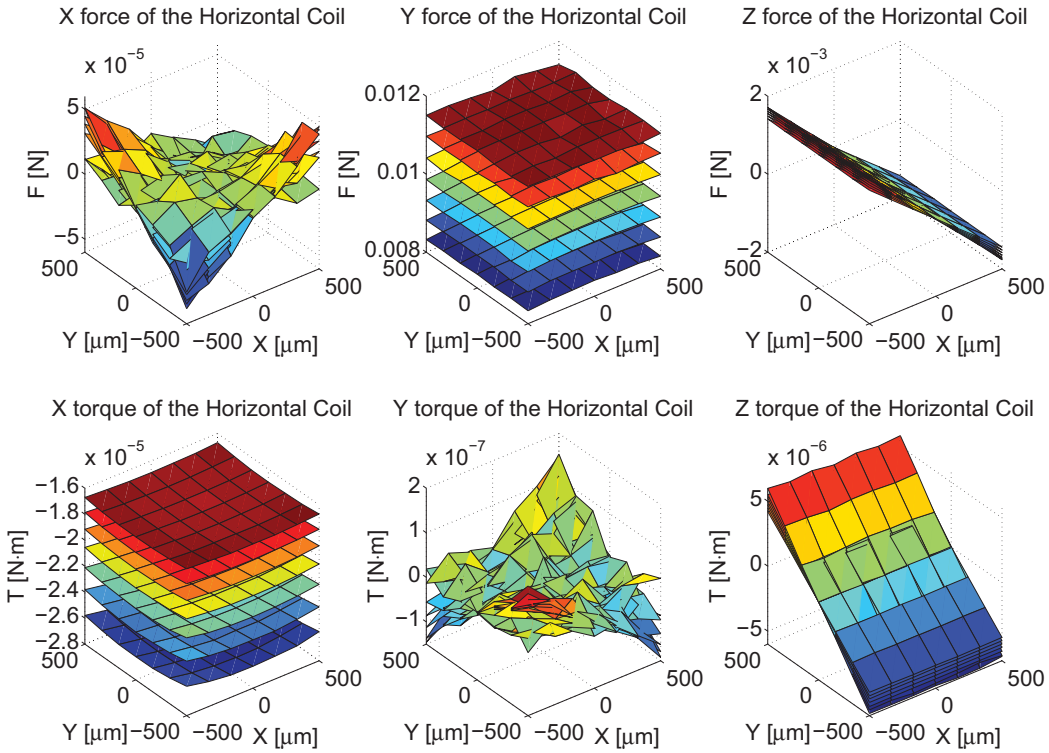

Figure 7.7: *Force-displacement characteristic of the horizontal coil as calculated by the FEM model. Units on the x- and y-axes are [m], units on the vertical (z-) axis are [N] for the upper row and [Nm] for the lower row. The seven planes in in each graph correspond to different coil-magnet distances, from 0.25 to 1.25 [mm].*

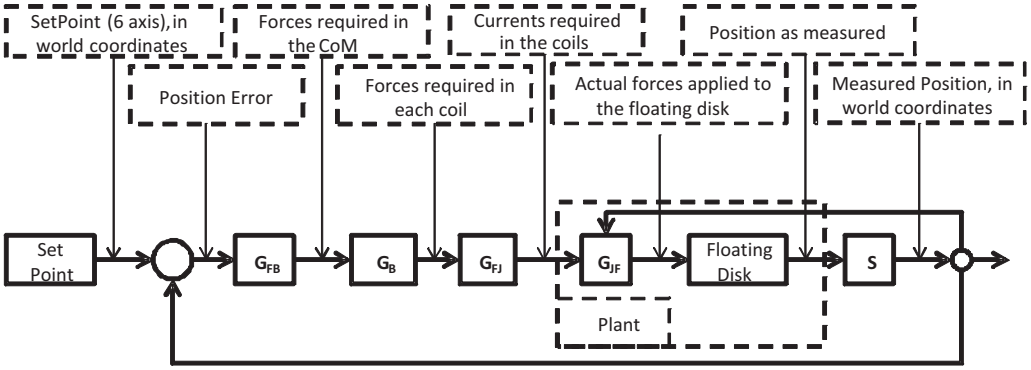

Figure 7.8: *Schema of the simulation of the system and its controller.*

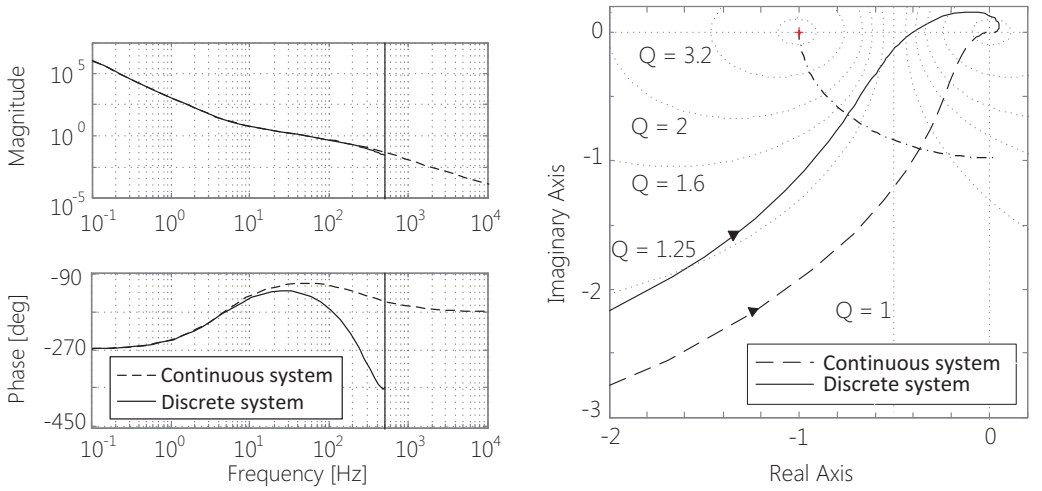

(a) **(b)**

Figure 7.9: *Open loop Bode (a) and Nyquist (b) plots of the controlled system in the x axis, both for a continuous and for a discrete model of the system with a sampling frequency of 1kHz. It is possible to observe the phase contribution at 50 Hz to ensure stability, provided by the derivative zero. The derivative action is canceled by a pole at 250 Hz to avoid amplifying high frequency noise.*

The effect of manufacturing and assembly tolerances on stage performance has been investigated in [61] using the system model in a Monte Carlo-type simulation. The results show that the stage can be built with standard manufacturing technology, provided that extra care is taken during assembly of the coils and their alignment to the magnets.

7.5 Components design and fabrication

The fabricated mechanical structure (Figure 7.10) is composed of two separate assemblies: the stationary base and the mover. Dimensions and specifications of the components are given in Table 7.3. More details on the design and fabrication of the system components can be found in [61].

The base structure is fabricated from an aluminum block by 5-axis CNC milling. It contains alignment features for the positioning of the coils, and attachment points for the sensor mountings. Since the measuring range of the sensors is just as large as the required workspace, the overlapping region leaves only a few μm of clearance. For that reason, the sensors are mounted on adjustable parallel guides with flexure

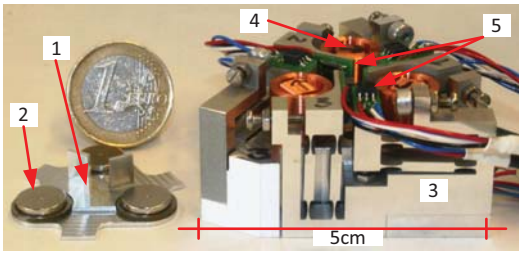

(a)

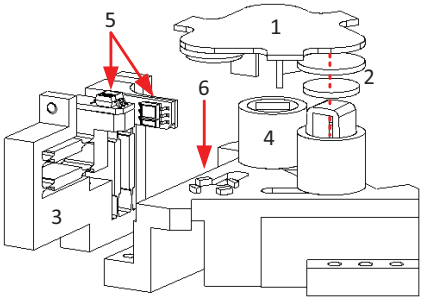

(b)

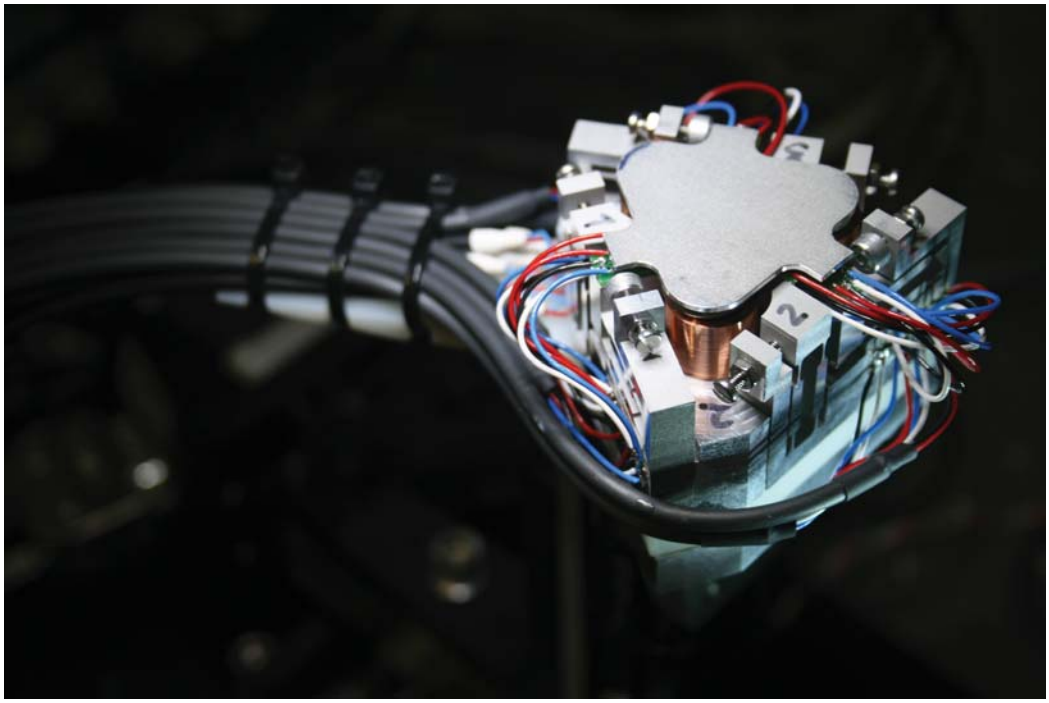

(c)

Figure 7.10: *Components of the system in both (a) the fabricated stage, and (b) an exploded view with some components removed for clarity: 1) Mover; 2) Magnet and iron assembly; 3) Adjustable sensor mount; 4) Coils assembly; 5) Horizontal and vertical position sensors; 6) Coil alignment features. The assembled system can be seen in (c).*

hinges. Two of these guides are combined into a single block, which holds a vertical and a horizontal sensor. The block is fabricated from high-strength aluminum alloy by a combination of CNC milling and wire EDM.

Table 7.3: *System dimensions and components characteristics*

Specification	Achieved value	Remarks
Sensor range	210 µm	
Sensor noise	15 – 28 nm pp	Depending on the distance.
Actuator force	160 mN peak vertical	Larger values can be obtained for short periods.
	20 mN peak horizontal	
Actuator size	12 (h) x 10 (r) mm cylindrical coil assembly	
	10 x 1.5 mm moving magnet (0.88 g mass)	
Mover first resonance frequency	7 kHz	
Overall size	6 x 6 x 4 cm	
Overall mass	<100 g	
Moving mass	8.15 g	
Mover moments of inertia	500 gmm^2 around the horizontal axes (x,y)	
	1000 gmm^2 around the vertical axis (z)	

The mover, milled from a single piece of aluminum, consists of a 1 mm thick plate with six flaps that serve as horizontal and vertical sensor targets. Attached to its bottom side are three stacks, each one composed of a 1 mm thick iron disks for magnetic flux guiding, and one magnet. FEM simulations show that the first eigenmode has an eigenfrequency of 7.7 kHz. During the assembly process, and after fixing the coils to the base structure, additional tools are used to align the magnets to the coils. The same alignment tools and calibrated shims are used to center the position sensors to the middle of the desired workspace using their adjustable mounts. To demonstrate the possibility of using less expensive fabrication methods, a second mover was fabricated by using standard 3D printing techniques with plastic material, and centering the magnets with guides outlined in the same fabrication process. Detailed characterizations of the systems were not performed with this mover, but the system behaved stably and could follow position references with this mover installed, even while using the controller-coefficients designed for the metallic mover.

Custom electronics were designed and fabricated to condition the sensor signals and amplify the coil currents [61]. These electronics were tailored to our application, thus ensuring the required specifications at lower cost and complexity than equivalent

general purpose electronics. The sensors are excited by an active current source using a Diode-Zener pair as a reference. The sensor signal is then amplified and filtered at 1kHz. For the amplification of the coil currents, a Widlar bilateral current source is implemented. Power OpAmps could be used as output stage thanks to the small currents required to drive the coils. Four 3 channel PCB's were fabricated, two for conditioning of sensor signals and two for amplification of coil currents. All components are selected for low noise operation.

7.6 Control Architecture

For controlling the device, a real-time compact RIO (cRIO) system from National Instrument is used. The sensor signals are digitized with 24 bits of resolution, while the coils are commanded with 16 bits. The controller runs with a loop period of 1 ms in the cRIO controller. Data acquisition (DAQ) and digital filtering of both the acquired signals and the user commands are performed in the cRIO FPGA at a loop frequency of 50 kHz. A user interface runs in a PC connected to the real-time controller via TCP/IP.

7.6.1 System identification for crosstalk reduction

The stage can be initially controlled with the controller coefficients that are obtained from the system model, but differences between the model and the real device will limit the achievable performance. The system dynamics in the bandwidth of interest are very simple, consisting of linear and rotational inertia factors actuated by forces and torques. These dynamics are therefore assumed to be correct, although the fabrication tolerances and FEM errors will introduce variations in the static current-to-force gains. As mentioned previously, the actuator characteristics vary depending on the position of the magnet relative to the coils, and this variation is significant within standard fabrication tolerances. These misalignments additionally generate parasitic forces on the actuators, in the directions where they are supposed to behave passively. Moreover, a geometric distribution is assumed when converting forces required in the CoM to forces applied by the coils, and any differences in the assembled device will introduce additional crosstalk in the system. Finally, the forces obtained in the FEM simulations may differ from the real ones, due to numerical errors, simplifications made during the simulation and, again, tolerances in fabrication and material properties.

The aforementioned model inaccuracies can be incorporated in the model by introducing a gains and crosstalk matrix $\mathrm{C_t}$ in the force-to-acceleration relation, such that $\mathbf{C_t} \cdot \mathrm{F} = \mathbf{M} \cdot \mathrm{A}$. With a perfect model, $\mathbf{C_t}$ should be an identity matrix. Since that is not true in this case, it is necessary to identify the $\mathbf{C_t}$ matrix. It is then possible

Table 7.4: *Summary of system performance figures*

Specification	Achieved value	Remarks
Translation range	210 x 210 x 210 μm	Smaller range when tilted
Translation Noise level	40 nm pp	With vibration isolation table
Rotation range	±21 mrad, vertical axis	Not simultaneous
	±9 mrad, horizontal axis	
Rotation Noise level	3.5 μrad pp, vertical axis	With vibration isolation table
	7 μrad pp, horizontal axis	
Force range	>10 mN	Interaction force
Payload	>3 g	
Controller bandwidth	50Hz	

to calculate a correction matrix $\mathbf{C_c} = \mathbf{C_t}^{(-1)}$ to be multiplied by the requested forces, such that $\mathbf{M} \cdot \mathrm{A} = \mathbf{C_t} \cdot \mathbf{C_c} \cdot \mathrm{F} \Rightarrow \mathbf{M} \cdot \mathrm{A} = \mathrm{F}$. In order to do so, and since the system is open-loop unstable, the device is operated for several seconds while following arbitrary position signals in all six directions, and both the requested forces and the measured positions are recorded. The recorded position is double-differentiated to obtain the accelerations, and filtered to eliminate the numerical error that appears in the process. Then, the $\mathbf{C_t}$ matrix is obtained by a linear least-square fit of $\mathbf{C_t} = \mathbf{M} \cdot \mathrm{A} \cdot \frac{1}{\mathrm{F}}$ to the acquired data, such that the root mean squared error (RMSE) between observed and fitted values is minimized. After including the correction matrix in the control architecture, and calculating a new $\mathbf{C_t}$ matrix, average improvements of a factor 100 are observed in each crosstalk term, while the diagonal terms come close to 1. Repeated cycles of calculating $\mathbf{C_c}$ matrices from the $\mathbf{C_t}$ matrix of the previous cycle proved ineffective in further reducing the crosstalk of the system. It must be noted nevertheless that this calibration only holds locally, since both the current-to-force relation and the cross-talk terms vary depending on position.

7.7 System operation and performance

The performance specifications of the MAGOS stage are summarized in Table 7.4.

Figure 7.11 shows the stage response to step-changes of the reference in the x axis. In Figure 7.11a the steady-state noise level shows to be 40 nm peak-to-peak allowing a position resolution of 50 nm. Figure 7.11b shows a larger 10 μm step and allows to observe the step response of the system, with a settling time of 60 ms (up to 5 % error over the step size).

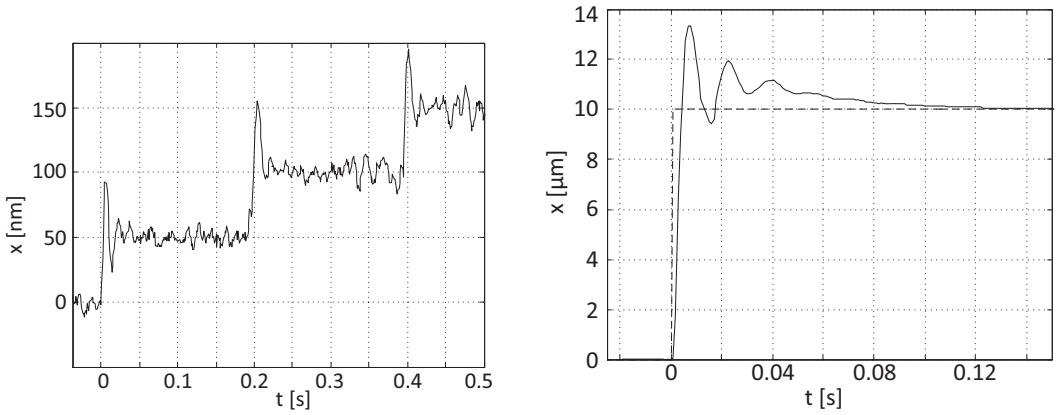

(a) (b)

Figure 7.11: *Position of the stage and error against reference, when following steps of a) 50nm and b) 10*µm.

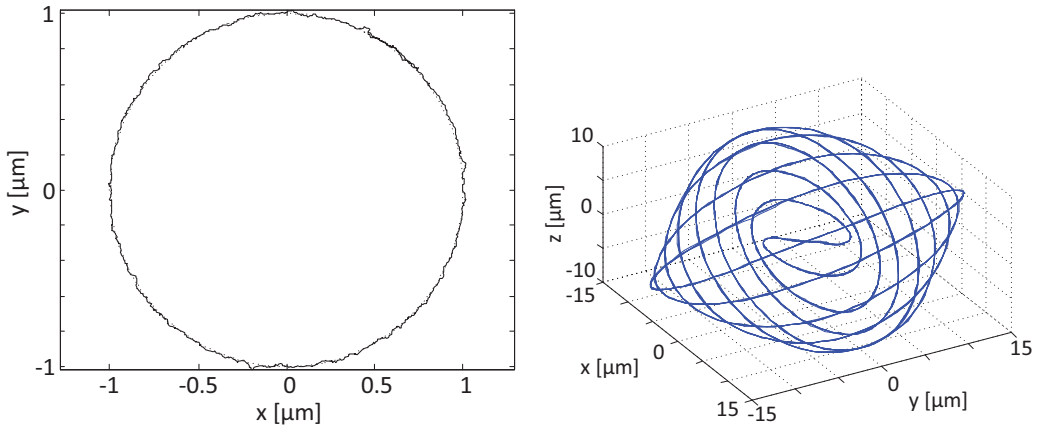

(a) (b)

Figure 7.12: *Multi-axis trajectory of the mover following (a) a 1* µm *circle in x and y axis ; (b) A reference signal of 8 Hz in the x axis, 9 Hz in the y axis and 10 Hz in the z axis, with 10* µm *amplitude.*

The system is able to follow multi-axis trajectories, despite some crosstalk that remains after the calibration explained in Section 7.6.1. Figure 7.12a shows the system behavior when following a circular trajectory, simultaneous in x and y. Figure 7.12b shows a more complex task, in which the stage draws a 8 Hz : 9 Hz : 10 Hz Lissajous curve in x, y and z axis simultaneously.

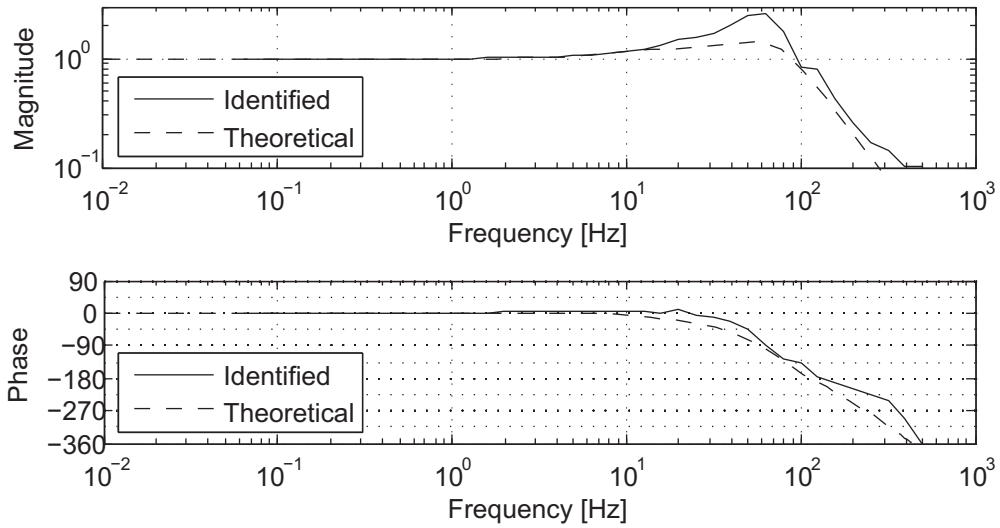

Figure 7.13: *Closed-loop frequency response calculated for the simulated discrete model (dashed line), and transfer function obtained from the device (solid line).*

A dynamic system identification of the controlled system was also performed. A frequency sweep was applied as a reference for the system to follow in the x axis, and the input and outputs were recorded and compared to obtain the frequency response of the system. Figure 7.13 shows the obtained frequency response together with the calculated one. It is possible to observe how the measurement closely follows the prediction. The magnitude of the gain of the system at 50Hz is nevertheless higher than expected, possibly due to inaccuracies in the model, and to the aforementioned position dependencies present in the system. Similar results were obtained in the remaining axes.

7.8 Conclusions

The presence of a human user in a haptic teleoperated micromanipulation scenario and the way in which he interacts with the system, creates an infrequently exploited niche of specifications for positioning stages. Even though this manipulation can be achieved with standard positioning stages, the common specifications of these positioners limit the potential micromanipulation scenarios and the achievable performance of the user. Moreover, a lack of attention on the capabilities of the user often results in the use of over-specified and over-priced components.

The MAGOS magnetic levitation positioning stage, presented in this work, takes

into account both the requirements coming from typical micro-manipulation tasks and those from the presence of the human tele-operator and the tele-operation controller schemes. The concept of the device ensures a low-stiffness operation, allowing for a compliant manipulation of delicate parts, and contributing to the stability of the haptic control loop. Moreover, the lack of contact and low moving mass of the mover ensures low and transparent operation forces, and it is therefore possible to estimate the forces, that the system is applying in the environment, from the commanded actuation forces. The mover is a simple and disconnected structure allowing for modular operation with multiple movers, and the free upper side maximizes the accessibility of tools to the working area. All these requirements have been met with low-cost sensing and actuation components, which despite their limited performance are still suitable for the intended application. The fabrication techniques, although expensive for a custom device like the one presented here, could become affordable when fabricating this device in series. Moreover, as demonstrated by using the 3D-printed mover, the possibility of using less precise fabrication techniques could also be investigated for this application.

The Lorentz actuators introduced in this work provide a compact method for 2-DoF actuation requiring a single magnet. The actuators behave rather linearly in a limited position range, but the current-to-force relation changes notably for larger displacements. It is therefore important to determine the size of this variation and the robustness of the control system against it.

The device was fabricated and tested, achieving a range of 210 μm in the translations and between ±9 and ±21 mrad in the rotations. The measured noise levels stayed below 40 nm and 7 μrad peak-to-peak respectively, allowing for a positioning resolution of 50nm and 10 μrad. The stage was controlled using PID controllers tuned to a bandwidth of 50Hz. Despite the use of simple SISO controllers, the system was able to follow multi-axis trajectories with limited crosstalk, thanks mostly to the correction introduced on the gain balancing matrix of the controller.

Chapter 8

Silicon based 6 DOF Force and Torque Sensor[1]

This chapter presents the design, fabrication and characterization of a piezoresistive 6 Degrees of Freedom (DOF) force and torque sensor to be used in the slave unit of the haptic teleoperation system for micro-manipulation. The device has been fabricated with an IC-compatible process and contains 24 piezoresistors as sensing elements. Its partly asymmetric mechanical structure consists of 7 suspended beams providing force sensing functionality on a probing area, which includes a calibration structure. Thanks to this asymmetrical structure, micro-manipulation tools such as micro-grippers or probes can be easily implemented in the same substrate as the sensor, replacing the calibration structure. The geometry of the beams and the location of the piezoresistors in the structure are designed using finite element modeling to provide independent force measurements (i.e. low crosstalk) and high sensitivity, with limited geometrical size. The mechanical structure is 3 x 1.5 x 0.03 mm^3 in size and its first resonance frequency is estimated to be 4500 Hz, as computed with a dynamical analysis. A calibration of the device is experimentally performed, and a linear regression model is fitted to the calibration data to extract the forces and torques from the resistance variations detected in the piezoresistors. The data acquisition system is programmable, allowing for dynamic adjustments of the trade-offs between noise levels, measurement error and bandwidth. Depending on the axis, the linear range of the sensor reaches 4 to 30 mN in forces and 4 to 50 μNm in torques. During on-line measurements, noise

[1] Some aspects of design and fabrication explained in this chapter are extended in [12], as indicated within the text.

levels up to 13 to 27 $\mu N/\sqrt{Hz}$ and 11 to 43 $nNm/\sqrt{Hz}$ were observed, respectively, for forces and torques.

8.1 Introduction

Force and torque sensing is essential in micro-manipulation, both to execute operations reliably and to avoid damaging fragile objects. Force and torque information is used in automatic handling systems to prevent that micro-grippers and other micro-tools exert too high forces on the manipulated objects. In human tele-manipulation such detected forces can be fed-back to the user through haptic interfaces, or used by a computer controller in a shared control scheme, as was explained in Chapter 3. Typical fields in which the control of the forces and torques are needed, include handling and assembly of MEMS and MOEMS [74], life sciences (cell manipulation) [75] and minimally invasive surgeries [39, 57, 15, 80]. In these applications components have typical dimensions in the micrometer range (up to a few hundreds of micrometers), and due to their fragility the force and torque to be controlled are respectively in the mN and μNm range with μN and nNm resolution.

Several micro force-sensing devices have been described in literature, realized both with precision manufacturing techniques [2, 59, 54] and with silicon based processes [16, 27, 73]. Usually there is a trade-off between the range of detectable force and the sensing resolution: the bigger the detectable range of force, the worse is the resolution [66]. The devices realized with traditional manufacturing techniques and strain gauges fixed on the mechanical structure have a big range of detectable force and torques (N and tens of mNm ranges) but low resolution (mN and μNm ranges). Sensing devices which are able to measure force in the mN range with μN resolution, are silicon based devices using the capacitive [16], piezoresistive [27], and piezoelectric [73] principle. Most of such devices measure the forces in a limited number of degrees of freedom (DOFs) [25, 69] and only a few are able to monitor loads along 6 DOF [27, 17]. Moreover, most of the developed sensing devices adopt symmetric structures to eliminate crosstalk between the different DOF [54, 25, 69]. Despite the advantages of this design principle, it often limits the access to probing points and the integration of manipulation tools. The only asymmetrical 6 DOF micro-force sensor known by the authors is the capacitive sensing device developed in [17].

In this work, an asymmetrical 6 DOF micro-force and torque sensor based on piezoresistors is presented. Thanks to its IC and MEMS compatible production process and its asymmetrical structure, the device can be integrated in the same fabrication flow of many existent silicon micro-grippers and probes, which already require similar fabrication steps (e.g. [25, 29]). The device has the capability of detecting forces and torques in the mN and μNm range, with μN and nNm resolution, respectively.

Section 8.2 of this chapter explains the design process leading to the dimensions of the device. Section 8.3 summarizes the silicon processing steps used in the fabrication of the device. In Section 8.4 the experimental calibration of the device and the generation of its calibration matrices is described. Using those calibration matrices, the device can operate on-line with the system described in Section 8.5. Noise levels and sampling rates when operating on-line are reported also in this section. Section 8.6 summarizes the results of this works and comments on the future developments.

8.2 Device Design

The proposed device (shown in Figure 8.1) is intended to measure 6 DOF forces and moments referenced to the probing point, indicated as *c*. The device consists of a silicon structure with implanted piezoresistors to measure the stress induced by the application of loads. The 6 DOF sensor, with a total dimension of 3 x 1.5 x 0.03 mm^3, features a partly asymmetrical geometry composed of 7 suspended beams connecting the bulk material to the sensor probing point *c*. The first resonance frequency of the device, computed with a dynamic analysis of the model by Finite Element Method (FEM), is 4500Hz. 16 measuring piezoresistors (indicated in red numbers from 1 to 16 in Figure 8.1) are implanted in the high stress concentration regions of the beams and 8 reference piezoresistors (indicated from a to g in black letters in Figure 8.1) in the low stress concentration areas of the device. A T-shaped structure (*calibration structure*) is fabricated surrounding the probing point *c* for experimental testing and calibration purposes. The calibration structure can be replaced by micro-manipulation tools during the fabrication process, such as micro-grippers or probes reported in [25, 29].

The calibration structure presents micro-fabricated features (calibration points) to apply the calibration forces in precise locations (Figure 8.2). Each calibration force applied to one of the calibration points shown in Figure 8.2 generates a different combination of loads in the probing point *c* of the device as shown in the Table of Figure 8.2. The matrix in Equation (8.1) relates the 6 calibration forces (F_1 to F_6) to the 6 pure loads (F_x, F_y, F_z, M_x, M_y, M_z) in the probing point *c*. The distance l_x and l_y appearing in the matrix are the distance, along the x and y axis respectively, between the calibration points and the probing point *c*. Since this matrix is invertible, the 6 calibration forces indicated provide enough information for a complete 6 DOF calibration. Additionally, given the symmetry of the calibration structure around the yz plane, 3 more calibration forces (F_{3s}, F_{4s} and F_{6s} symmetric to the F_3, F_4 and F_6 respectively) can be used to apply both positive and negative loads in the corresponding directions, for a total of 9 calibration points. These 3 forces (F_{3s}, F_{4s} and F_{6s}), although not necessary for the calibration of the sensor, duplicate the

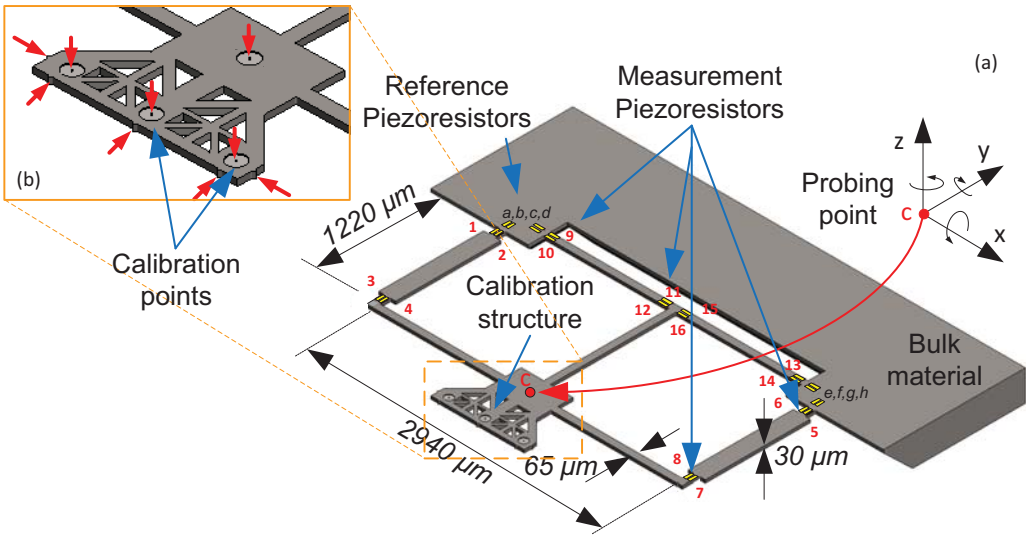

Figure 8.1: *a) Designed structure for the 6 DOF force and torque sensor. Measurement piezoresistors are indicated with red numbers, while reference piezoresistors are indicated with black letters; b) Details of the calibration structure with highlighted the calibration points and the calibration forces (red arrows). The calibration structure can be replaced by micro-manipulation tools.*

achievable range of calibration forces in F_x, M_y and M_z, while using the same force probe, and provide additional calibration and validation points in the remaining DOFs. The application of loads that are symmetric to F_1, F_2 and F_5 is not possible during the experimental characterization of the device, due to the characteristics of the force probe used and to the asymmetry of the structure around the xz and xy planes.

$$\begin{bmatrix} F_x \\ F_y \\ F_z \\ M_x \\ M_y \\ M_z \end{bmatrix} = \begin{bmatrix} 0 & 0 & 0 & 1 & 0 & 0 \\ 0 & 0 & 0 & 0 & 1 & 1 \\ -1 & -1 & -1 & 0 & 0 & 0 \\ 0 & l_y & l_y & 0 & 0 & 0 \\ 0 & 0 & l_x & 0 & 0 & 0 \\ 0 & 0 & 0 & l_y & 0 & l_x \end{bmatrix} \cdot \begin{bmatrix} F_1 \\ F_2 \\ F_3 \\ F_4 \\ F_5 \\ F_6 \end{bmatrix} \tag{8.1}$$

8.2.1 Device Dimensioning

The geometry of the device is designed to obtain different stress distributions for each loading direction, and thus provides independent force measurement (i.e. low crosstalk). Then, the number and location of the piezoresistors are selected through a FEM study to achieve the force and torque range, resolution, stiffness and resonant

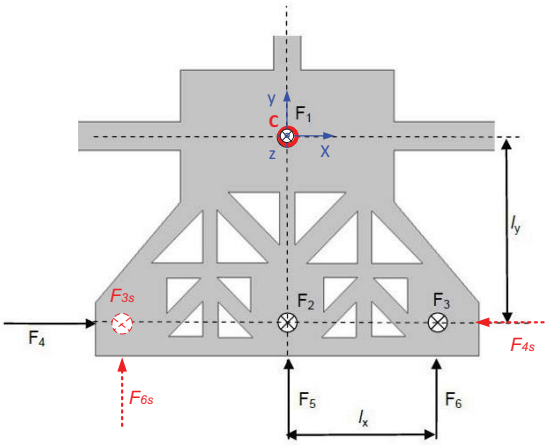

Force applied	Load at the probing point *c* of the device
F_1	$F_z = -F_1$
F_2	$F_z = -F_2 \; ; M_x = F_2 \cdot l_y$
F_3	$F_z = -F_3 \; ; M_x = F_3 \cdot l_y \; ; M_y = F_3 \cdot l_x \; ;$
F_4	$F_x = -F_4 \; ; M_z = F_4 \cdot l_y$
F_5	$F_y = F_5$
F_6	$F_y = F_6 \; ; M_z = F_6 \cdot l_x$
F_{3s}	Symmetric to F_3
F_{4s}	Symmetric to F_4
F_{6s}	Symmetric to F_6

Figure 8.2: *Relation between force applied in the calibration points and respective loads applied in the probing point* c *of the calibration structure.*

Table 8.1: *Device specifications*

Parameter	value	units
Force resolution	< 100	µN
Force range	> 5	mN
Torque resolution	< 50	nNm
Torque range	> 2	µNm
Stiffness	> 50	N/m
Resonant frequency	> 1000	Hz

frequency given in Table 8.1, while aiming for the maximum sensitivity. These values of force/torque resolution and range are typical in delicate micro-handling tasks as reported in [74, 75, 39, 57, 15, 80]. A minimum value of stiffness and resonant frequency is also set to avoid large deformations and to keep the first resonant frequency of the device much higher than the intended operational frequency. The operational frequency is estimated 10 Hz maximum for manual micro-handling tasks [18] and one order magnitude higher for automatic tasks.

The initial step of the design process is the choice of a partly asymmetrical structure for the proposed sensor to facilitate the integration of a micro-tool. Additionally, measuring locations are identified such that each loading direction results in a different distribution of stresses on the device. This allows to differentiate the 6 independent loads and minimize any potential crosstalk coming from non-linearity in the sensor. Table 8.2 shows the stress distributions for the selected device geometry, by indicating

Table 8.2: *Relation between the 6 applied loads and the sign of the stress generated in the measuring locations indicated in Figure 8.1. Double and simple signs give indication of the relative magnitude of the stress for each loading direction.*

Loads	Measuring Piezoresistors 1 to 8							
	1	2	3	4	5	6	7	8
Fx	++	- -	-	+	- -	++	+	-
Fy	-	+	++	- -	-	+	++	- -
Fz	++	++	+	+	++	++	+	+
Mx	++	++	++	++	++	++	++	++
My	++	++	-	-	- -	- -	+	+
Mz	- -	++	++	- -	++	- -	- -	++

Loads	Measuring Piezoresistors 9 to 16							
	9	10	11	12	13	14	15	16
Fx	+	-	-	+	-	+	+	-
Fy	- -	++	++	- -	- -	++	++	- -
Fz	+	+	-	-	+	+	-	-
Mx	- -	- -	++	++	- -	- -	++	++
My	+	+	-	-	-	-	+	+
Mz	++	-	- -	++	- -	+	++	- -

the signs and order of magnitude of the stress in each measurement location for all loading directions.

The next step is the selection of the dimensions (length, width and thickness) of the beams and the number and position of the piezoresistors, through a parametric FEM study. The goal is to achieve a structure as small as possible, while satisfying all the previously set specifications, as reported in Table 8.1. Given the dimensions, the resulting model is studied with a FEM analysis using the software COMSOL. In the FEM analysis, the possible 6 DOF loads are applied to the probing point c and the longitudinal stresses generated in the structure are analyzed, since the piezoresistors are more sensitive to that loading direction. The stress distribution is computed and the number and location of the measuring piezoresistors is determined. These locations are chosen such that the measuring piezoresistors are implanted in the regions subjected to highest stress for each of the 6 DOF loads, and the reference piezoresistors are implanted in the no-stress regions of the device. Figure 8.3, for instance, reports the stress generated in the structure by the load F_x.

It is then checked if the modeled device satisfies the stiffness, resonant frequency and stress specifications. The resonance frequencies and the stiffness are derived from the FEM dynamic analysis of the model. The stress conditions are essentially three. First, the maximum stress in the device has to be always below the yield stress of the

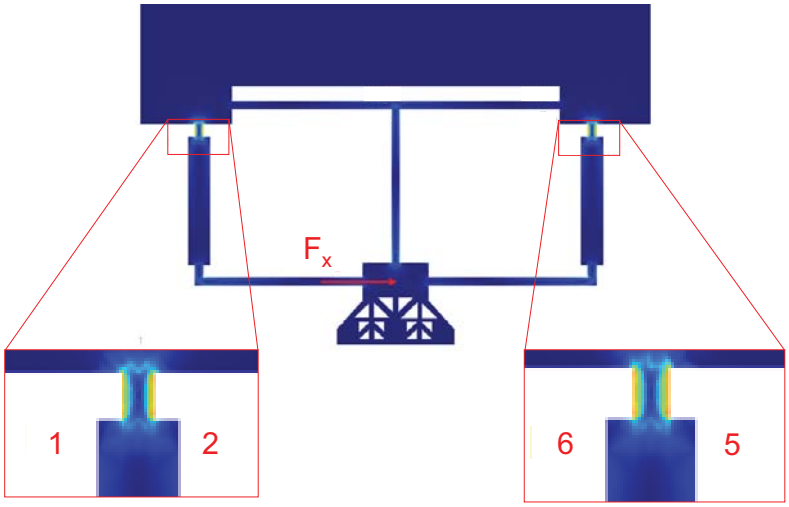

Figure 8.3: *Stress distribution in the structure for the load* F_x *applied at the probing point* c. *The locations subjected to the higher stress are highlighted.*

material (7 GPa according to [65]) in order to avoid mechanical failure. Second, the strain in the piezoresistors should remain below 10 % for the intended measurement range in order to remain within the linear behavior of the piezoresistive sensing elements [29] and simplify the processing of the signals. Last, when the device is excited by forces at the required resolution, the resulting stress has to be detectable by at least one piezoresistor. In order to check this third condition, the resistance change in piezoresistors is related to the change in local stress (computed with the FEM analysis in the positions of the structure where the piezoresistors are inserted), according to the following equation:

$$\frac{\Delta R}{R} = (\pi_l \cdot \sigma_l + \pi_t \cdot \sigma_t) \approx \pi_l \cdot \sigma_l \tag{8.2}$$

where ΔR is the resistance variation in the piezoresistor due to the applied stress, R the zero-stress resistance of the piezoresistors , π_l and π_t the longitudinal and transversal piezoresistive coefficients, σ_l and σ_t the longitudinal and transversal stress in the piezoresistor. Since the beams are long compared to their deflection, the stress σ_t in the transverse direction can be neglected [72].

The stress that can be measured by one piezoresistor ($\sigma_{l,\min}$) depends on the voltage noise (U_{noise}), the input voltage (U_{input}) and the piezoresistive coefficient (π_l depending on the type and orientation of the piezoresistor on the silicon crystal) according to Equation (8.3) [86].

$$\sigma_{l,\min} = \frac{4 \cdot U_{\text{noise}}}{\pi_l \cdot U_{\text{input}}} \tag{8.3}$$

With an input voltage of 1 V and a noise voltage of 10 μV (as observed for a similar setup in previous works by [85]), the minimum detectable stress for a single piezoresistor is 40 kPa.

If the conditions for stiffness, resonant frequency and stress are satisfied, a forces-to-stress matrix $\sigma(\mathrm{F})_{n\times 6}$ is obtained using COMSOL, relating the stress in the n measured piezoresistors (16 in the case of this work) to the 6 DOF loads applied to the probing point c. Using Equation (8.2), the expected change on resistance of the piezoresistors as a function of the applied forces, $\frac{\Delta \mathrm{R}}{\mathrm{R}}(\mathrm{F})_{n\times 1}$, is obtained. A calibration matrix $\mathbf{C}_{6\times n}$ can then be calculated that converts the measured resistance change due to the strains back to our estimation of the applied forces, $\mathbf{U}_{6\times 1}$.

$$\begin{gathered} \mathbf{U}_{6\times 1} = \mathbf{C}_{6\times n} \cdot \frac{\Delta \mathrm{R}}{\mathrm{R}}(\mathrm{F})_{n\times 1} \\ n = \text{Number of piezoresistors} \end{gathered} \tag{8.4}$$

Using Equation (8.4) it is possible to predict the force range, resolution and sensitivity of the device. The trade-offs between these specifications were explored resulting in the shape and dimension of the structure presented in Figure 8.1, such that the device can cover all specifications, while remaining small and achieving a good balance between range and resolution [12].

8.3 Fabrication

An IC-compatible process is used to fabricate the proposed structure (refer to [85] for a detailed description), allowing the integration in the same fabrication process of IC-compatible micro-manipulation tools such as the ones shown in [29, 86]. The starting material is a (100) p-type silicon wafer with a 1 μm thick n-type epitaxy layer. The piezoresistors are created by using a second epitaxy layer (500 nm, boron, $1.1 \cdot 10^{18}$ atoms/cm^3). Reactive ion etching (RIE) is used to define the dimension of the piezoresistors (Figure 8.4a). Both the sensing and reference resistors are oriented along the [110] direction in (001) plane. The resistors are isolated from each other by the reversed biased n-type epitaxy layer and p-type isolation rings created by ion implantation (Figure 8.4b). After metalization and passivation, cavities are anisotropically etched on the back side of the wafer to define the thickness of the suspending structures (Figure 8.4c). A deep reactive-ion etching (DRIE) is then performed on the front side to define the lateral geometry of the structures, where a pre-deposited

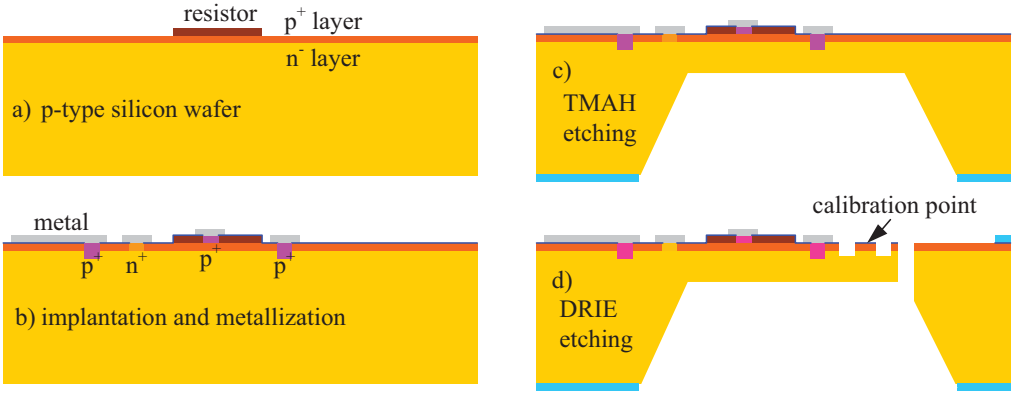

Figure 8.4: *Main fabrication steps of the device.*

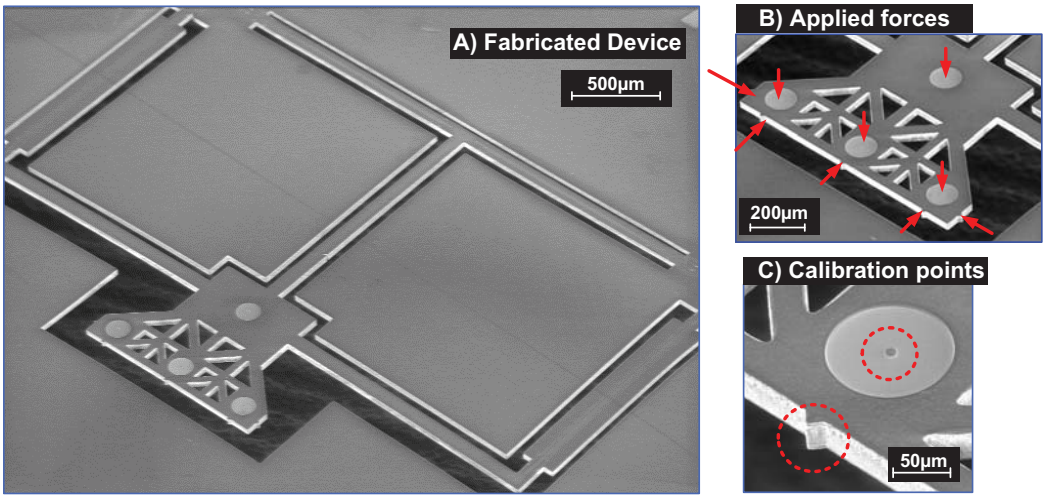

Figure 8.5: *a) SEM images of the fabricated sensor; b) the calibration structure with the locations of applied calibration forces; c) the micro-fabricated features on the calibration structure for the application of the calibration forces.*

aluminum layer inside the cavity functions as a mechanical support and etch-stop (Figure 8.4d). Another short DRIE step is used to define the in-plane calibration points. Finally, by removing the aluminum layer, the device is released. Individual sensors are detached from the wafer by a scribe and break process, aided by the presence of anisotropically etched scribe lines.

A SEM picture of the realized device is shown in Figure 8.5 with a detailed image of the calibration structure and the micro-fabricated features (calibration points).

8.4 Device calibration

The sensor is characterized with the strategy shown in Figure 8.6. The fabricated device is glued and wire-bonded to a PCB board, which is fixed on top of a vibration isolation table. A 1 DOF force probe from Femtotools [32] is pushed against the microfabricated features (calibration points) of the calibration structure by a motorized stage, in steps of 100nm. This force probe was selected because of its resolution of 0.4 μN, which exceeds the resolution expected from the fabricated device. The 2 mN range of the force probe, on the other hand, remains below the range expected from the 6 DOF sensor. This is nevertheless not a problem as long as the device is utilized within the linear range of the piezoresistive sensing elements, estimated at 10 % according to [29]. The calibration is therefore only valid up to the aforementioned 10 % strain in all piezoresistors, which then determines the sensor range.

After applying a force, the piezoresistors are connected, one at a time, to an external Wheatstone Bridge through a National Instruments PXI2536 crosspoint matrix switch. In this way, all resistances are measured with a single amplifier and DAQ channel. The amplifier board is custom made using a INA125P instrumentation amplifier. Commercial amplifiers available (including a lock-in amplifier) are not used because the filtering used in most of them introduces an important delay in the measurement after each change in the switch configuration. The Wheatstone Bridge is excited by a 1 volt potential. Since the piezoresistors have a typical resistance of 90 kohms, and are connected only one at a time, the power consumption within the device is approximately 2.5 μW.

Force ramps are applied several times to the nine testing points of the calibration structure, resulting in a total of 1000 calibration samples. The resistance of all piezoresistors is recorded, together with the applied 1 DOF force. For each calibration sample, the 6 components of the load $\mathbf{F}_{\text{applied},6\times1}$ are calculated from the 1 DOF force measurement, taking into account the relations on Equation (8.1). This acquisition generates then 2 matrices: the matrix $\frac{\Delta R}{R}(F)_{24\times1000}$ of changes in the 24 resistors for each calibration sample, and the matrix $\mathbf{F}_{\text{applied},6\times1000}$ of 6 DOF loads applied in the probing point.

Using the acquired data, a linear relation is fitted between the variation of the values of the piezoresistors and the applied loads. A calibration matrix $\mathbf{C}$ is obtained by a linear least-square fit of Equation (8.4) to the acquired data, such that the root mean squared error (RMSE) between observed values and fitted values, $\text{RMSE}\left(\mathbf{F}_{\text{applied},6\times1000} - \mathbf{U}_{6\times1000}\right)$, is minimized.

Figure 8.7 shows the relation between the reference loads applied to the structure ($\mathbf{F}_{\text{applied},6\times1000}$) and the calculated loads ($\mathbf{U}_{6\times1000}$), obtained by using the calibration matrix $\mathbf{C}$ and Equation (8.4). The remaining fit-error can be attributed to several

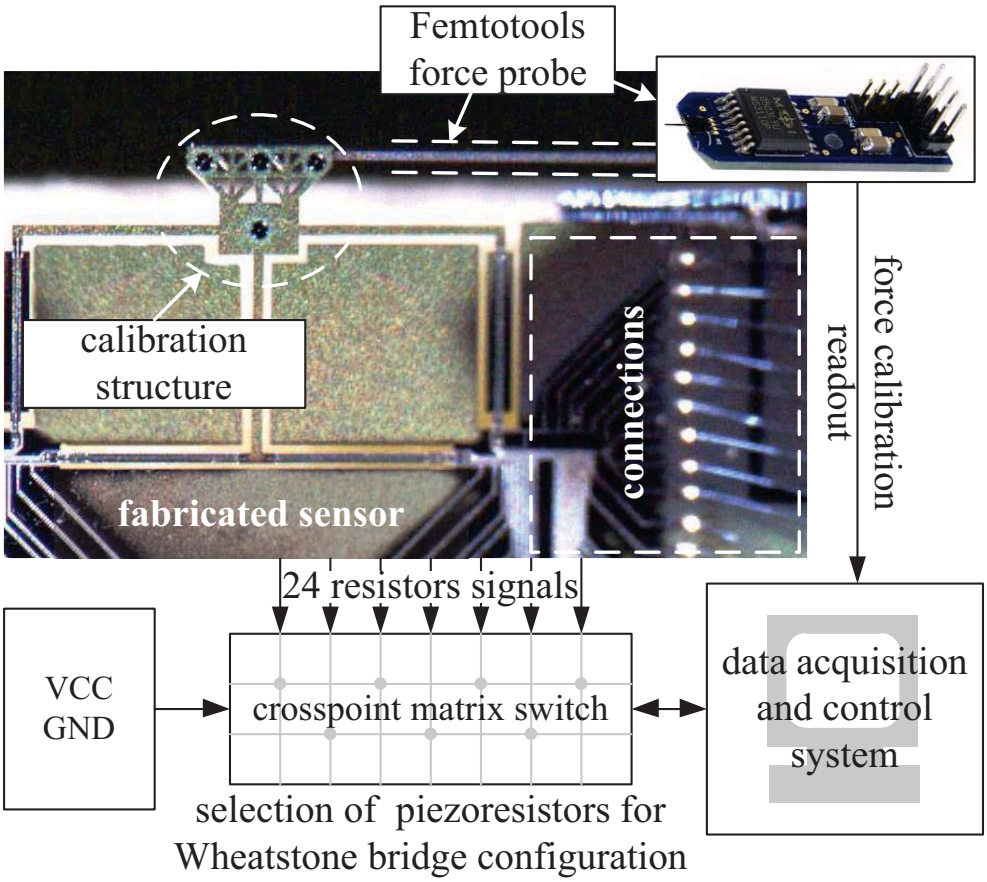

Figure 8.6: *Calibration procedure. The sensor is bonded to a PCB and all resistors are connected to a crosspoint matrix switch. A single readout channel is used to measure all piezoresistors.*

causes that can be classified in three groups: i) errors related to the resistance value; ii) errors due to the measuring and calibration set up; and iii) errors related to the calibration method.

The measurement error in the resistance value is related to the presence of thermal noise, and to the sensitivity of piezoresistors to drift of the applied voltage (BIAS voltage), temperature and light. The thermal noise is estimated to be in the range of 10 μV, as observed in this setup and similar setups in previous works [85]. With regard to the sensitivity to light, temperature, and drift of the BIAS voltage, no-load reference measurements allow for compensating these errors. During calibration, this is done by comparing the values of the piezoresistors to a non-contact measurement obtained

before the application of each force ramp, and after calibration this is achieved by using the reference piezoresistors. Given the high sampling rate of the system compared to the slowness of temperature, light and BIAS variations, only insignificant changes occur in these conditions during a calibration or measurement cycle, and their effect in the measurement can be compensated up to the level of the noise in the measurement of the resistors.

The calibration setup also contributes to the errors in the measurement, due to characteristics intrinsic to the force probe, to mechanical misalignments between the force probe and the calibration structure, and to uncertainties in the measurement instrumentation. Out of any inaccuracies present in its own calibration, the reference force-probe showed sensitivity to light. In order to cancel this effect, the measurements from the force-probe were referenced to a non-contact measurement obtained before the application of each force ramp. With regard to the mechanical misalignments between the probe and the calibration structure, care is taken to align both devices, and the micro-fabricated calibration points ensure low positional misalignment relative to the size of the calibration structure. Nonetheless, visual angular misalignments estimated in the range of 1 or 2 degrees are still present, generating errors between 1.7 to 3.5 % of the range of the applied forces. These values are similar to the root mean square error (RMSE) values observed in the calibration, thus indicating that most of the measurement error could be caused by such misalignments. The switch matrix used introduces an additional path resistance, which changes on time and depends on the particular switch used, and the load of the switch. This value is normally below 10 ohms, and therefore has little effect on the force estimation.

The last source of measurement errors is related to the calibration method. The regression model used assumes a linear relation between the applied forces and the resistance variations. Even though this relation is mostly linear in the studied range, characterization of individual piezoresistors showed non-linearities up to 1.5 % of the full range, for strains below 0.1. This non-linearity has an effect in the crosstalk of the system. That is, when applying force in a single DOF, the system will report small force measurements also in the remaining DOFs. Given the combination of measurements that occurs when calculating the applied forces, it is not possible to directly translate the non-linearity of single resistors to the force-estimation obtained by the system. Simulations showed that these non-linearities generate crosstalk below 2 % of the corresponding output ranges. Only Fz showed a deviation of 4 % of its range when applying load in Mx.

With 16 measured piezoresistors and only 6 output signals, the system is over-determined: 6 piezoresistors giving linearly independent values are theoretically enough to measure the 6 loads. The over-determination provides redundant information, which helps on reducing non-correlated noise from the measurements. Thanks to the cross-

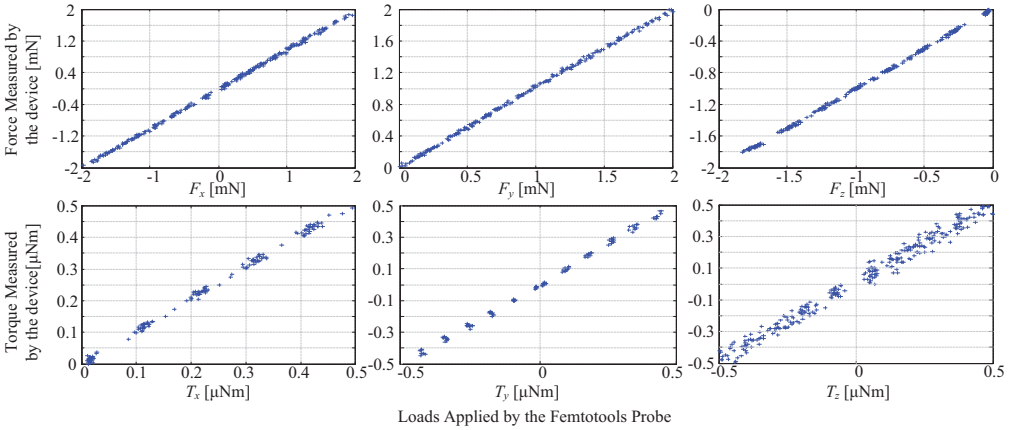

Figure 8.7: *Loads applied in the 6 DOF by the Femtotools force versus loads measured by the calibrated device.*

point matrix switch, the system is flexible and can be configured to measure different numbers of piezoresistors. A calibration matrix calculated for a sub-set of the 16 piezoresistors available can then be used for converting the resistance measurements to load estimations (according to Equation (8.4)). This matrix is obtained using the same strategy explained at the beginning of this section, but limiting the linear fit to the resistance changes of the sub-set of piezoresistors.

In order to choose which piezoresistors to use when the number of acquired signals must be limited, all possible sub-sets for a certain number of piezoresistors are tested and compared. A weighted sum of the RMSE components resulting from the linear fit of Equation (8.4) is used for this comparison. The weights on the sum of the RMSE components are chosen to bring the torque RMSE values (typically in the range of 1×10^{-9} Nm) and the force RMSE values (typically in the range of 1×10^{-6} N) to a comparable range. In that way, the performance index becomes an average of the force error measured in µm and the torque error measured in nNm. Other performance indexes could be used to select the sets of piezoresistors, depending on the requirements of specific applications. For instance, more weight could be given to a particular loading direction if the application requires so, or attention could be given to maximize the measurement range or sensitivity of the device.

Figure 8.8 shows the performance index for different numbers of piezoresistors used. It can be noticed how the performance improves noticeably faster between 6 and 8 piezoresistors, than between 8 and 16. This result suggests that there are 2 additional degrees of freedom in the calibration, out of the 6 measured forces, thus supporting the hypothesis that a big part of the error observed during the calibration would be

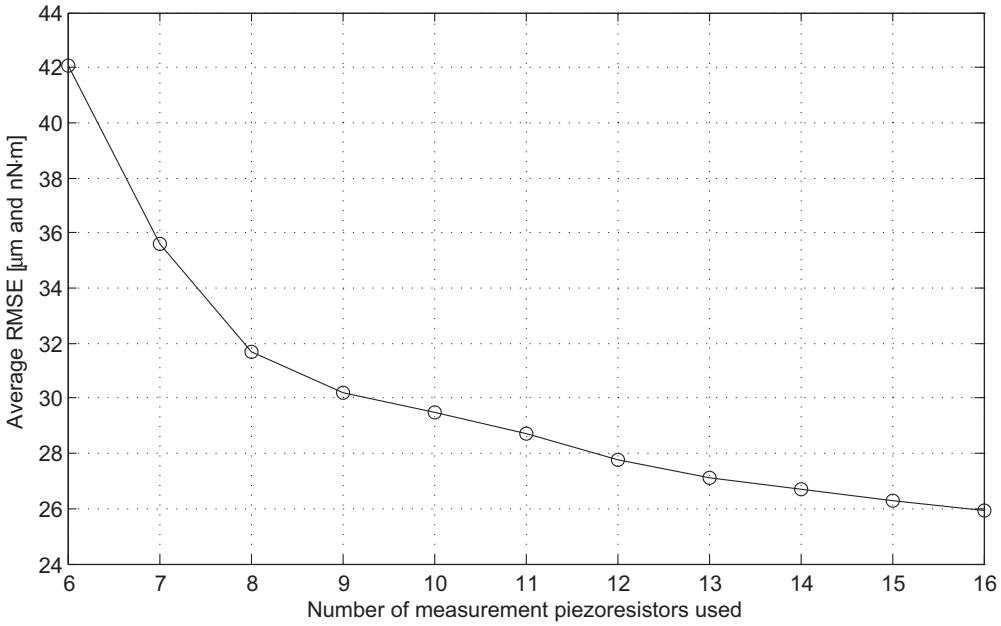

Figure 8.8: *Best performances obtained among all possible combinations for each number of piezoresistors used. The performance index represents an average of the force error measured in µm and the torque error measured in nNm*

caused by the misalignment of the probe in the two non-axial angles.

8.5 Device operation and performance

In order to operate the force sensor on-line and test its performance, a LabView application is developed. The application operates the crosspoint matrix switch, the DAQ board, and calculates the applied loads from the resistance measurements. Depending on the number of measurement piezoresistors requested by the user, the application chooses a set of piezoresistors based on the lists previously obtained in Section 8.4, and loads the corresponding calibration matrix. The user can also specify how many of the available 8 reference piezoresistors will be used for temperature and bias voltage compensation. In each measurement cycle, the LabView application connects through the matrix switch all measurement and reference piezoresistors to one external Wheatstone Bridge, and calculates their resistance. The values of the measurement piezoresistors are first adjusted by an average of the resistance change in the reference resistors, in order to compensate for changes in temperature, illumination, or in the bias and excitation voltages in the device. The remaining resistance variation is then multiplied

by the calibration matrix to obtain the estimation of the force and torque applied on the sensor (as shown in Equation (8.4)).

After the connection of each piezoresistor to the DAQ system and due to the latency of the switches and the low pass characteristics of the amplification and acquisition stages, one millisecond is required for the measurement signal to stabilize. These delays are added to the processing time and the latency of the Windows environment, to obtain the final sampling rate of the system. With the system utilized in these experiments, a reliable sampling rate of 20ms was obtained when using 7 piezoresistors (1 for reference and 6 for measurement), and a sampling rate of 65ms was obtained when using all 24 available piezoresistors. Once the sampling rate has been defined, a digital filter can be applied to the signal to minimize the effect of noise.

The flexibility on the operation of the sensor and on the number of piezoresistors used, introduces a series of trade-offs that can be exploited depending on the application. Altogether, the use of more measurement piezoresistors and lower filtering bandwidths results in a slower sensor, with a better calibration fit and robustness against temperature and bias voltage changes, and therefore a lower measurement error. On the other hand, the use of less piezoresistors allows for faster measurements, but it also increases the error of the sensor fit, and the use of higher bandwidths on the filter allows for more thermal noise to reflect on the output. Therefore, at higher sampling rates, the accuracy and resolution of the sensor are limited. Table 8.3 shows a summary of the specifications of the fabricated device, when operated with different numbers of piezoresistors and at different filtering bandwidths.

8.6 Conclusions

A 6 DOF micro force/torque sensor with piezoresistive sensing elements integrated in a partly asymmetrical micro-structure has been developed and experimentally characterized. With outer dimensions of 3 x 1.5 x 0.03 mm^3 and the first resonance frequency at 4500 Hz (as obtained from FEM simulations), the 6 DOF sensor achieves a range of 4 to 30 mN in forces and 4 to 50 μNm in torques. Noise levels up to 13 to 27 $\mu N/\sqrt{Hz}$ and 11 to 43 $nNm/\sqrt{Hz}$ are achieved, depending on the filter applied at the output of the device. The calibration and processing of the measured data successfully cancels the coupling between the measured signals, caused by the asymmetrical geometry of the sensor. The partly asymmetrical geometry of the device makes it innovative, allowing the fabrication of micro-tools in the same substrate as the sensor. The process used for the fabrication simplifies the integration of a wide range of micro-tools, which are based on steps similar to those used in this sensor, and include IC fabrication techniques for the instrumentation together with DRIE for defining the mechanical structure.

Table 8.3: *Main sensor specifications in the 6 DOF's. The range is estimated assuming linearity of the piezoresistors up to a 10 % strain [29]. The calibration root mean squared error (C-RMSE) is obtained for different amounts of used measurement piezoresistors, in sets defined in Section 8.4. The sensor noise is specified at different sampling rates (SR), filter bandwidth (BW), number of reference piezoresistors (Nrpr) and number of measurement piezoresistors used (Nmpr). Sensor noise is also specified as a function of the bandwidth of operation.*

Specification	Fx	Fy	Fz	Tx	Ty	Tz
Linear Range (mN, μNm)	13	30	4	4	7	50
Stiffness (N/m, nNm/rad)	1363	1695	97	137	306	1955
C-RMSE (μN, nNm)						
6 Piezoresistors	47	44	44	40	25	55
10 Piezoresistors	50	29	17	14	19	48
16 Piezoresistors	48	26	16	13	16	39
Noise Levels (μN, nNm)						
SR = 50; BW = 20Hz; Nmpr=6; Nrpr=1;	108	122	58	50	60	170
SR = 22; BW = 10Hz; Nmpr=12; Nrpr=4;	82	86	42	36	44	132
SR = 14; BW = 1Hz; Nmpr=16; Nrpr=8;	27	21	12	9	13	50
Noise Level as a function of bandwidth ($\mu N/\sqrt{Hz}$, $nNm/\sqrt{Hz}$)	26	27	13	11	14	43

The use of a linear fit permits to measure micro loads in multiple degrees of freedom, with neither fully decoupled signals coming out of the sensing elements, nor explicit theoretical descriptions of the relations between these signals and the applied loads. A simple post-processing of the acquired signal, consisting only of a matrix multiplication, can decouple the measurements and profit from sensor redundancy. Even though this technique has been applied in previous work, it must be noted that in many cases the design of sensing devices is guided and constrained by requirements in signal decoupling. The use of the linear fit gives increased freedom in the mechanical design of the devices by eliminating symmetry constrains, at a limited cost in the signal-processing architecture.

The use of the matrix switch allows for a dynamic adjustment of the trade-offs existent between fit error, measurement noise and sampling rate. This functionality is very

useful when testing sensor concepts, or in applications with changing requirements.

The natural evolution of the developed 6 DOF sensor is the integration of micro-tools in the same substrate of the sensor. Care must be taken when designing such tools to include micro-fabricated features for calibration, like the features included in the calibration structure of the device presented in this thesis. A calibration can then be performed using any point within the device as the device probing point (possibly the end effector of the tool), as long as an invertible relation exist between the 6 calibration loads and the 6 loads in the device probing point. In such way a fully sensorized system for micro-manipulation can be obtained and tested in micro-handling tasks.

Part III

System validation and conclusions

The following two sections summarize the result of this thesis, by characterizing, validating and demonstrating the designed system in Chapter 9, and giving the conclusions of this thesis and recommendations in Chapter 10.

Chapter 9

System properties and validation

In this thesis, a system for haptic teleoperated microassembly was realized based on custom-developed and commercially available components, as described in previous chapters. This chapter first gives a summary of the performance and properties achieved by the system in Section 9.1. Section 9.2 demonstrates these properties, by using the system to perform micromanipulation tasks.

9.1 System properties

The following list summarizes the properties achieved by the system designed in this thesis.

- The system allows haptic teleoperated manipulation in 3 translational DOFs, while the 3 rotational DOFs are still controllable through the graphical user interface, or can be left following zero references and act as a tunable compliance. By using a master device with more DOFs, all the DOFs of the slave robot could be controlled via the master device.

- The slave robot can be positioned to within a workspace of 25mm $\times$ 25mm $\times$ 10mm, with Minimum Incremental Motions of 50 nm. In the rotations, the system achieves a range of 18 to 42 mrad, with MIMs between 3.5 and 7 μrad.

- Force sensing in the vertical direction is achieved using a load cell with a range of 200mN. This load cell can only be used when operating solely with the coarse stage, and not when the fine stage is added to the system.

- Force sensing in 6 DOF is achieved through a custom developed silicon sensor, even though this sensor is still not integrated into the system. The sensor achieves a range of 4 to 30 mN in forces and 4 to 50 μNm in torques, with noise levels up to 13 to 27 $\mu N/\sqrt{Hz}$ and 11 to 43 $nNm/\sqrt{Hz}$, respectively.

- Zenithal visualization is achieved with a microscope camera with a pixel size equivalent to 1.1μm in th object plane, while a secondary camera provides a side view of the whole workspace.

- Several tools can be used with the system, as long as they can be fixed with their end-effector onto the work-plate. Special brackets are necessary when the task requires large rotations from the tool (over the rotational range of the fine stage of the slave robot), or when a force sensor must be adapted to the tool in order to provide force feedback.

- Through the user interface, the operator can command the system with discrete commands in the GUI or directly through displacements of the master device. The master device can render the force coming from the vertical force sensor to the user. It can render a virtual plane that the operator can use as a reference of contact with the work-plate, as well as a height-dependent damping which provides a stabilizing effect.

9.2 Operational validation

Several tests were performed in order to validate the ability of the system developed in this thesis for performing micromanipulation tasks. This section reports on two of those tests. The first subsection demonstrates the manipulation by pushing of microspheres. The second subsection shows the results of a study that was executed with several operators in order to asses the effect of vertical force feedback on operator performance, and compare it with the option of providing only visual feedback. In doing so, this second test both demonstrates the capabilities of the system on micromanipulation tasks, and assesses the enhancement in performance that the user can achieve by using such a system.

9.2.1 First demonstration: Pushing microspheres

A typical task in micromanipulation is that of pushing objects over a flat surface. When micro objects must be sorted out of a mixture, aligned, or assembled over a plane, pushing them is a viable and common option since the objects remain always in the intended plane and at the proper height, and no gripping is required. Moreover, the

Figure 9.1: *Logo of the Delft University of Technology, composed of microspheres. The spheres are brought into place by pushing them with a probe, while the system is controlled by an operator through the haptic teleoperation interface.*

lack of constraints in the planar DOFs (out of friction) ensures a delicate manipulation where only enough force to move the object is applied by the tools. This tasks is also one in which the human operator is normally needed, since the option of developing automation algorithms is often complex. The local variations in friction force and the distribution of this force below the manipulated objects make it difficult to predict the object trajectory, and corrections must be permanently applied to the tool trajectory in order to bring the objects to the intended location. These corrections are performed using visual feedback, thus additionally requiring computer vision algorithms in the system when intending to use automated systems [43].

In the case of this demonstration, micro-spheres are sorted out of a mixture and arranged to form the logo of the Delft University of Technology (TUDelft), as can be seen in Figure 9.1.

In a first demonstration, the system is configured using the coarse stage and with the 1 DOF load cell between the stage and the work-plate. A layer of gelpak is set over the work-plate to provide adhesion between the spheres and the work-plate and avoid the sticking of the spheres to the manipulation tool. Silicon spheres of 100 µm of diameter are spread over the work-plate. Using a copper probe, the spheres are pushed out of the mixture and arranged to form the logo of the TUDelft with a total width of 700 µm. During the test, the user receives force feedback from the vertical force sensor, thus receiving a natural indication of the contact between the tool and the work-plate. Additionally, virtual damping is added in the master device to stabilize the hand movements.

In a second demonstration, the system is configured using the fine stage together with the coarse stage. The two stage system is driven by the method explained in Section 6.5, in which the center area of the master-device workspace is constrained by a virtual cylinder and drives the fine-stage position, while the positions outside

this virtual cylinder drive the coarse-stage velocity. Since no force sensor is used in this case, a virtual floor is rendered in the master device to indicate to the user the position in the master device workspace equivalent to that of the work-plate in the slave environment. This position must be calibrated at the beginning of the test. Virtual damping is also added to the master device for stability and better operator-control. In this case, glass spheres with diameters between 20 and 60 μm are sorted and used to create the TUDelft logo, with a total width of 370 μm (or 450 μm when including the μsymbol).

In both cases, the developed system allowed the operator to achieve resolutions impossible to reach by the un-assisted hand. At the same time, the task execution developed in an intuitive way for the operator, who could guide the system movements directly with his hand movements through the 3D master device, while been guided, stabilized and informed about the contact with the work-plate thanks to the force feedback provided through the master device. This force feedback also ensured the safety of both the tool and the environment during the execution of the task, by limiting the force developed between the work-plate and the tool.

9.2.2 Second demonstration: Visual feedback Vs. Haptic feedback in contact perception

One of the difficulties found in performing teleoperated tasks is the perception of depth, presence of contact and intensity of contact, out of the provided visual information. The teleoperation system proposed in this thesis offers to the operator one additional feedback channel, thanks to the measurement of forces between the environment and the tool, and its presentation in the master device: the haptic cue. In order to asses one of the possible benefits of providing such a feedback to the users, this section compares the performance of users when performing a representative micromanipulation task by using visual cues, haptic cues, or both.

Humans normally rely on a variety of visual cues to perceive the distance to an object, and the relative distances between objects. In most teleoperated systems, and particularly in those targeted to micro-environments, many of these cues are lost. For one thing and unless a binocular vision system is available, the convergence and stereopsis cues are not available to the operator. Many monocular cues are not useful due to the small distances being judged (which rules out long range indicators like the texture gradient), the distortions and scaling introduced by the lenses (which for instance complicate a correct understanding of perspective), and the lack of movement of the viewpoint (which rules out dynamic cues like the motion parallax). 3D vision systems are not common in the field, except for those were visualization is achieved through a virtual-reality representation of the environment [67, 11]. The operators

are left nevertheless with some cues to understand the relative depths of objects in the micro environment. For the tasks studied in this work, which develops mostly in 2.5D, the most commonly used cues for depth perception, contact presence and contact intensity are:

- Shadow and reflection: The shadows and reflections of a tool on a surface, seem to approach the tool when the tool approaches the surface. When the tool is in contact with the surface, it also seems to be in contact with its reflected image or shadow. This principle is used for instance in [84] to estimate vertical distances in an automatic system.

- Depth of field: When a lens is focused on an object, other objects at approximately the same distance of the lens also appear in focus. Therefore, the difference in focus of two objects gives a cue of their relative depth relative to the lens.

- Side views: Secondary cameras provide a direct image of the relative depth of the objects. The user must nevertheless continuously switch between the two views in order to use this information, as mentioned in [84].

- Deformations: If either the environment or the tool are flexible, their deformation can be used to identify the presence and intensity of contact.

- Trace (or, in general, tool effect): If the tool leaves a visible effect over the environment (a trace or scratch for instance), it can also be used to identify the presence and intensity of contact.

This study tests the hypothesis that haptic feedback in the vertical direction is a viable alternative to the aforementioned visual cues when performing contact and surface scanning tasks. The study also tests whether the performance-improvement obtained from visual cues is independent of that obtained from haptic cues.

Experimental apparatus

For this study, the micromanipulation system is configured using the coarse-stage, as can be seen in Figure 9.2. On top of the stage, the 1 DOF load cell is placed in order to measure the normal forces applied by the tool on the work-plate. The work-plate is suspended over the load cell through 3 springs, in order to avoid damaging any components during the study, and to improve the stability of the bilateral controller. On top of the work-plate, a block of foam is glued in order to provide a surface profile for the study. A mechanical pencil is fixed, such that the whole work-plate area is accessible to the pencil through the movement of the MICOS stages.

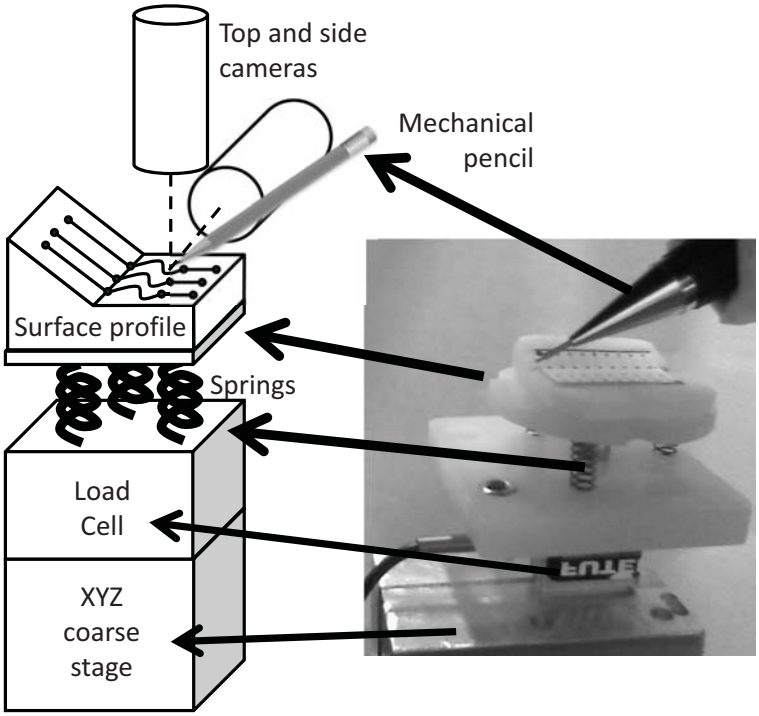

Figure 9.2: *Configuration of the slave system for the test comparing visual feedback and haptic feedback in contact perception. The coarse stage drives the work-plate below a fixed mechanical pencil. Between the work-plate and the stage, a force sensor is placed, together with a set of spring for protecting the system components. Over the work-plate, a foam block provides a surface profile over which a drawing is placed for the operator to follow with the pencil.*

For observing the operation, two cameras are used. One camera provides a top-view of the scene while the second provides a second view with an angle of approximately 10 degrees to the plane of the work-plate. The top camera includes a coaxial light source. A second light source is included to provide a side illumination, thus introducing a noticeable shadow of the tool on the work-plate.

Thanks to the modules used in this system and to their configurability, it is possible to test 2 conditions for the visual feedback and 2 conditions for the haptic feedback:

- Visual feedback:

    1. Basic visual feedback: The user is presented a top view of the scene. The illumination is provided through a coaxial light source, thus providing only a light shadow. The aperture of the camera lens is set as small as possible

in order to maximize the depth of field. The user counts additionally with the indications coming from the presence of a trace left by the pencil on the work-plate, from the darkness of this trace, and from the deformations of the compliant work-plate.

2. Enhanced visual feedback: The user is presented a top and a side view of the scene. The illumination is provided through a coaxial light and a lateral light sources, thus providing a strong shadow. The aperture of the camera lens is set as big as possible in order to minimize the depth of field. The user still counts with the trace and deformation cues.

- Haptic feedback:

1. Without haptic feedback: The user commands the system through the Falcon master device, but the only forces present are gravity compensation and a light damping to stabilize the operator hand.
2. With haptic feedback: In addition to gravity compensation and damping, the user is presented with an amplified reproduction of the force measured in the vertical axis by the force sensor in the slave robot.

The task

The task presented to the operator in this study is similar to that explained in section 4.3.2, and is representative of some of the situations encountered in micromanipulation, mainly surface scanning tasks, transport tasks and contact establishing, as seen in section 2.2. An image depicted in Figure 9.3 is set on the work-plate to guide the operator, who is asked to follow the lines with the pencil, always keep contact with the image, and, especially, keep the contact force as low as possible. The work-plate includes a flat section and an inclined section, as indicated in the same figure. With this configuration the operator performs 4 sub-tasks separated by black circles (from top to bottom in the figure):

1. A contact-establishing operation when trying to touch the uppermost black circle of a line.
2. A straight surface-scan over a 3D surface.
3. A complex trajectory surface-scan over a flat surface.
4. A straight surface-scan over a flat surface.

The operations can also be performed backward (from bottom to top).

During the execution of the task, the following performance measures are extracted:

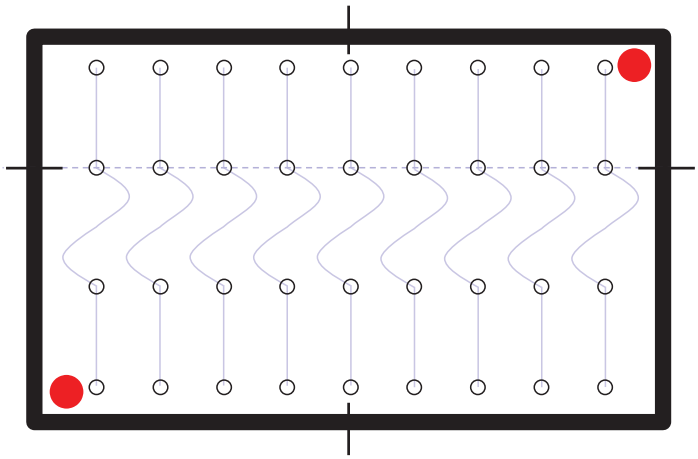

Figure 9.3: *Images presented in the work-plate during the user study. Each line represents a task, and is divided by black circles in 3 sub-sections. The horizontal dotted line represents the start of the slope section of the work-plate. The whole image occupies an area of 2 cm × 1 cm.*

1. Time: time taken to complete the subtask.
2. Maximum force: maximum force applied by the tool on the work-plate.
3. Free-air time: relation between the time the tool expends in free air and the time the tool remains in contact during an operation, which should approach zero (permanent contact) for the sub-tasks of painting on the surface, and infinite for the contact sub-tasks (only contact at the target location).
4. Operator workload: as a result of the NASA-TLX workload test.

Experimental design

This study follows a factorial experiment design, in which all combinations of the 2 conditions for the visual feedback and the 2 conditions for the haptic feedback are tested. The resulting four modes in which the system is tested are shown in Figure 9.4.

Ten operators are asked to perform for this study. For each operator, the test follows the following steps:

1. A new printed image is placed over the work-plate.
2. The operator is given 5 minutes to get acquainted with the system, and performs 2 practice runs of the task under each mode.

	Basic visual feedback	Enhanced visual feedback
Without haptic feedback	1. The reference mode with basic visual feedback and without haptic feedback	2. Enhanced visual feedback without haptic feedback
With haptic feedback	3. Basic visual feedback with haptic feedback	4. Enhanced visual feedback with haptic feedback

Figure 9.4: *The four modes in which the system is tested, by combining the 2 conditions for the visual feedback and the 2 conditions for the haptic feedback.*

3. The system is set to operate in one of the 4 test modes, and a new image is placed on the work-plate.
4. The operator is asked to contact the circle at either extreme of one of the lines.
5. Once in the circle, the operator must press a button in the master device, and trace a line (following the one printed in the guiding-image) until the other extreme of the guiding-line, indicating each black circle with a click.
6. The previous step is repeated six times (or more in case of extreme failures, like the breakage of the pencil lead).
7. A NASA TLX workload test is applied to the user.
8. Steps 3 to 6 are repeated for the other 3 test modes.

In order to avoid learning effects, the order of the four different test modes is randomized between users. Moreover, for each test the direction of execution of the task is alternated.

Results and discussion

After performing the study, all the data is analyzed using Matlab. Using two-way ANOVA, it is possible to recognize whether including haptic feedback has a significant effect on the operator performance, whether the visual cues have a significant effect on that performance, and whether these two effects are independent and therefore add-up

when the two types of feedback are used together. As with other ANOVA analysis, the p value obtained for each value of the manipulated variables indicates how significant is the effect of that variable in the result of the experiment. It is common to assume that a value of $p < 0.05$ indicates a significant relation between the manipulated variable and the dependent variable.

In the case of this study, significant relations are only observed with the maximum force applied by the tool on the table, with the time taken to complete the subtasks number 2, and with the results of the NASA TLX workload test. As can be seen in Figure 9.5, the use of haptic feedback has a significant effect on lowering the force applied during all subtasks, slightly improving the execution time of subtask number 2 and lowering the subjective workload, showing a significance value p_{h} much lower than 0.05 in most aforementioned cases. Improved visual feedback only has a significant effect in the force applied by the tool during the contact subtask and in the subjective workload, where $p_{\mathrm{v}} < 0.05$. The significance of the interaction, p_{i}, remains always far over 0.05, thus indicating that the effects produced by the two kinds of feedback are mostly independent. That is, that the change in performance from combining the two feedback modes is equivalent to the sum of the effects of each individual feedback mode.

The result indicates that both haptic and visual cues can provide useful information to the user in this kind of micromanipulation situations, thus proving the hypothesis set at the beginning of this study. It also shows that once contact has been established between the tool and the environment, the small relative displacement between the two components limits the information that the operator can get from visual feedback, and therefore haptic feedback becomes a very useful tool. Even when some visual feedback was still available thanks to the darkness of the trace on the paper and to deformations of the compliant work-plate, only the haptic feedback provided enough information for the users to control the force applied by the tool during the task execution. In the two cases where visual feedback had a significant effect, the haptic feedback produced a similar result. This indicates that haptic feedback can substitute improved visual feedback in situations where the latter is not possible. Moreover, the interaction significance remained always above 0.05, showing that haptic feedback can improve performance even in cases in which advanced visual feedback is already available.

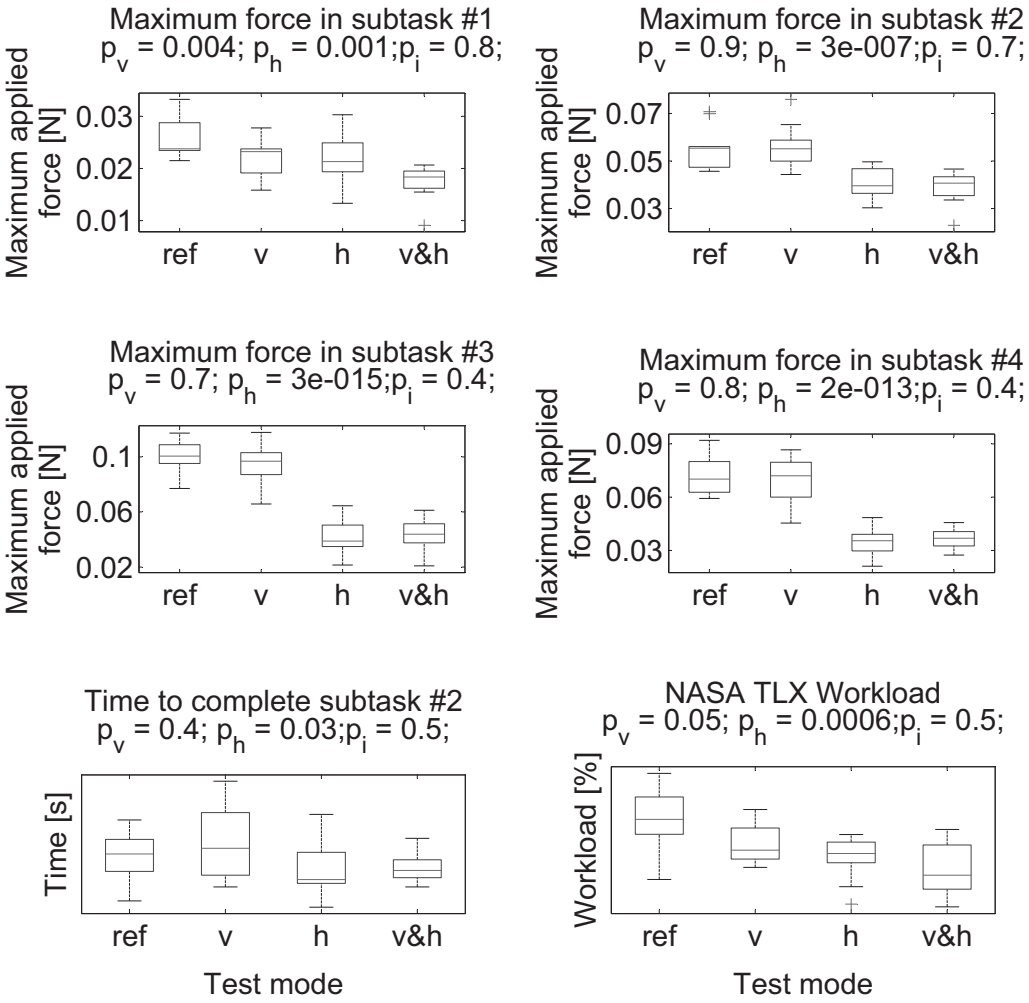

Figure 9.5: *Boxplots of the performance measurements which experimented a significant effect from the 4 studied modes, in each subtask. The use of haptic feedback has a significant effect in several subtasks, where it shows a significance value* $p_{\mathrm{h}} < 0.05$. *Improved visual feedback only affects the force applied during contact subtask and the subjective workload, as indicated by* $p_{\mathrm{v}} < 0.05$. *The significance of the interaction,* p_{i}, *remains always far over 0.05, thus indicating that the effects produced by the two kinds of feedback are mostly independent.*

Chapter 10

Conclusions and recommendation

The main goal of the research presented in this thesis was to understand how to better support a human operator performing micromanipulation tasks, and based on that understanding develop a system for teloperated micromanipulation, focusing on the slave-side devices. The first stage of this research was an in-depth analysis of the requirements coming from the kind of tasks which the system must deal with, from the support that is possible and useful to give to the human operator, and from the abilities and limitations of that user. Following those requirements, a system concept was developed, which consisted of the integration of carefully selected commercially available products with custom developed components. In particular, a 6 DOF magnetic levitation stage was developed as a fine positioning stage for the slave robot, and a silicon based 6 DOF force sensor was developed to explore possibilities for force and torque sensing during micromanipulation. The system was integrated and characterized, and its usefulness was demonstrated through the performance of micromanipulation tasks by human operators.

A general conclusion drawn from this research is that in order to make haptic teleoperated micromanipulation systems a viable and competitive option, it is vital to identify the kind of tasks for which haptic teleoperated micromanipulation systems can be a solution, and to optimize such systems and its components for these applications and for the haptic teleoperation scenario. In order to do so, one must understand both the advantages and limitations that this approach offers compared to its main competitors: automatic manipulation, self assembly, unaided manipulation by hand, among others. In particular, the highest potential of teloperated systems is on dealing with uncertain situations, thanks to the reasoning abilities of the human operators. Therefore, the use of these systems in structured and repetitive tasks does not consti-

tute a fair demonstration of their advantages. Likewise, the use of components meant for automatic manipulation which often over-perform some of the motor abilities of the user, results in systems which are more complex and expensive than required, thus undermining some of the main advantages of using teleoperated systems.

Following that reasoning, this work placed particular attention to the definition of the requirements. By carefully studying the consequences of including a human operator in the system, and the special needs arising from the tasks and support modes, it was possible to optimize system components for this particular niche. Thus, the resulting system can deal with the situations normally encountered in teleoperated micromanipulation, without incurring in significant costs or complexities often found in systems intended for automatic manipulation, and without having to compromise properties useful for this application.

10.1 Conclusions

Even though partial conclusions were given in the preceding chapters, a summary of the conclusions of the thesis is given in the following list:

- Typical tasks encountered in manipulation can be decomposed in primitives. They can be classified by analyzing the force-application or positioning goal of the operator and the impedance of the environment in which such tasks must be performed. In the particular case of micromanipulation, they can be further divided in 3 groups depending on the level of detail and delicacy required in performing them: the transport, alignment and mount operation groups. It is then possible to design systems able to perform such task-primitives, and exploit the system capabilities when performing more complex tasks. Thus, the primitives can be used as a source for the system-requirements and as a benchmark for assessing its performance, while ensuring the flexibility of the final system in terms of applications.

- The separation of the tool in a master and a slave side in teleoperation scenarios, and the introduction of the HT-Controller in between, generates a set of channels through which information (in the form of commands or feedback) must flow, between the master device, the slave device and the controller. By enabling, modifying or augmenting the information flowing in those channels it is possible to create an inventory of modalities in which a teleoperation system can operate, the impact these modalities can have on performance during assembly tasks, and the requirements they set for the system components. This inventory becomes then a useful tool when assessing the applicability of haptic teleoperation to a certain problem. In particular, this inventory is used to show

that teleoperated micromanipulation systems can obtain several benefits from different haptic teleoperation modes.

- Psychophysic tests show that operator performance does not get affected by small levels of inaccuracy in the positioning stages of the slave robots. Only large distortions of the relation between position reference and achieved position have a significant impact on the performance of the user. Even though this result is specific to the tasks and performance measures considered in this study, they do demonstrate that the accuracy of a teleoperated system does not need to be achieved solely by the slave robot. The human operator can make use of haptic and visual information to improve the system accuracy without important impacts in its workload, and without compromises on other performance indexes.

- Psychophysic test also show that human operators performing micromanipulation tasks achieve a similar performance when using systems with the camera fixed to the same frame as the work-plate (and therefore see the tool moving and the work-plate fixed), and when using systems with the camera fixed to the same frame as the tool (and therefore see the tool fixed, and the work-plate moving behind it). This study supports the option of fixing the tools while moving the work-plate, which brings many additional advantages in terms of operation-monitoring and reachable-workspace. Even though this is a common approach in micromanipulation, this study provides validity to that decision from the perspective of the human-operator.

- A proper understanding of both the task characteristics and the operator capabilities and limitations leads to an adjusted requirement set compared to automatic manipulation systems, which permits the use of concepts otherwise disregarded. This generates designs with exceptional capabilities only in the aspects that are necessary, while permits to save costs and avoid compromises arising from aspects which are actually not necessary for this application.

- The analysis of the requirements revealed two slave-side devices that can profit from further developments, namely the positioning robot and the force sensor.

  - Positioning robots used in current systems are not optimized for teleoperation, thus often over-performing the capabilities of the human operators. Moreover, most positioners are also not intended for manipulation of very small and lightweight objects, thus requiring for their operation much higher forces than those required by the task.
  - Force sensors currently available and able to measure the loads encountered in micromanipulation are difficult to integrate with tools, due both to the

use of incompatible fabrication technologies and to the use of symmetric structures which leave no open-access for the tool to be integrated and operate on the environment.

- The magnetic levitation scheme presented in Chapter 7 proved to be a suitable option as a positioning robot for teleoperated micromanipulation. This system allows positioning of micro-objects in 6 DOF, with high resolution, completely contact-less, with low moving mass, low actuation forces, and keeping the top-side open for access by tools and for monitoring. The position measurement principle, based on infrared reflective sensors, is small, light and has low cost, while providing high resolution and ensuring enough accuracy and stability for the system to remain stable. The inaccuracies and drift of these sensors did not represent a problem for using the system in this application, since the human operator could correct these errors using visual and haptic feedback.

- The force sensor presented in Chapter 8 demonstrates the feasibility of piezoresistor-based silicon force-sensors in wrist-position to measure the 6 DOF loads arising from the contact between a tool and the environment during micromanipulation. The mechanical structure used leaves one side of the sensor open for the integration of tools, while the fabrication method is compatible with many existent grippers and probes. The calibration method, by fitting a linear regression model, proved capable of providing independent load-measurements, even if due to the mechanical design the signals coming from the piezoresistors are coupled. The measurement instrumentation uses a programmable switch-matrix, thus enabling dynamic adjustments of the trade-offs between accuracy, noise and sampling rate.

- The haptic channel is an effective way to communicate information on contact and interaction forces to the user in typical micromanipulation tasks. When compared to visual information, the haptic channel showed to be at least equally effective for the tasks investigated in this thesis. For permanent-contact situations where no appreciable displacements can be observed between the tool and the environment, the user performance increased thanks to the presence of haptic feedback, as compared to visual feedback. Moreover, the performance improvements coming from both types of feedback are independent, and the two operation modes can therefore be combined for an even higher performance.

- The integrated system proved to be a useful tool in micromanipulation. Human operators could perform manipulation of microspheres with different configurations of the system. The users managed resolutions in this manipulation which would have been impossible by the un-assisted hand, while keeping both the tool

and the environment safe, and keeping a low workload thanks to the natural interface provided by the 3D master device and the available force feedback.

10.2 Recommendations

Haptic teleoperation systems for micromanipulation have many aspects where improvement can be achieved, and the variety of applications and operation modes available creates new directions for development and optimization with each problem. Regarding the topics touched by this thesis, the following aspects should be further researched in order to advance in the field:

- Based on the decomposition of tasks presented in Chapter 2, standardized benchmarks could be clearly defined and parametrized, as well as the metrics used to assess the systems intended for solving them. These benchmarks would permit comparing different micromanipulation solutions and describing their performance using indicators relevant to the field. Once defined and realized, these benchmarks could be even distributed to groups working in micromanipulation to ensure homogeneity of the reported results.

- Psychophysic tests such as those presented in Sections 4.3 and 4.4 generate important inputs for the definition of requirements for haptic teleoperation systems. Such tests should be extended to other tasks and other parameters. In particular:

  - The psychophysic test regarding accuracy of the slave system should also be executed considering the accuracy of the slave-side force sensors. Other sources of inaccuracy with different bandwidth and amplitude characteristics should also be considered, such as the floor vibrations often encountered in the 1 to 10 Hz band.
  - The psychophysic test regarding the fixation of the camera to either the work-plate or the tool should be extended to consider rotational DOFs, and the different modes in which it is then possible to map the position of the master device to that of the slave device.

- The control signals driving the coils of the magnetic levitation stage presented in Chapter 7 can provide a reference of the forces arising from the interaction between the tools and the objects in the work-plate, thus acting as a force sensor. The low moving-mass and lack of friction or flexion of components make this an interesting approach, since the interaction forces would not be masked by large actuation forces. This method was investigated during the development of this

thesis and difficulties were found due to the position dependency of the current-to-force relations in the stage. An exploratory study showed that a calibration of the current-to-force relations performed for the center of the workspace is only valid in the vicinity of that position, and that considerable cross-talk and inaccuracies appear when deviating a few micrometers from that location. A position-dependent calibration could solve this issue, by calibrating the sensor in several locations across its workspace and fitting a function to describe the position dependency. It must be noted nevertheless that the magnetic levitation principle used makes the current-to-force relations also dependent on the distribution of magnetic materials around the stage. The problems gets amplified by the drift and inaccuracies present in the position sensors. Therefore this method would only be useful if automatic and fast calibrations can be made just before operation, and if any magnetic materials around the stage remain motionless after such calibration.

- The force sensor presented in Chapter 8 demonstrates a technology that could facilitate the integration of silicon tools and force-sensors. The natural step forward is the demonstration of this capability, by integrating existent micro-tools in the same substrate of the sensor. Care must be taken when designing such tools to include micro-fabricated features for calibration, like the features included in the calibration structure of the device presented in this thesis. It is also important to consider the effect that the actuation principle of the tool can have in the operation of the force sensor. In particular, thermally actuated tools may generate uneven heat distributions in the device and interfere with the measurements. In that case, heat transfer models must be used to estimate the temperature in each piezoresistor, based on the reference piezoresistors available and the historical data regarding the activation of the heat-actuator. Another option, suggested in [12], is to place reference piezoresistors in small silicon-flaps near the measurement piezoresistors. These flaps would not be subjected to strain, and would provide a more realistic reference of the temperature-induced resistance-change of the piezoresistors in their vicinity.

- The system developed in this thesis showed its usefulness through the demonstrations described in Section 9.2. In particular, the psychophysic study of Section 9.2.2 gives an empirical validation of the capability of the system to support human operators in micromanipulation tasks. That test is just an appetizer of what can and should be studied with this and similar systems. Performing similar test with different tools, tasks, support modes and system settings would improve the understanding of the factors influencing operator performance in teleoperated micromanipulation tasks. In particular, the system developed in

this thesis must be tested in tasks using rotational DOFs, more complex interactions, and more complex tools such as grippers or glue dispensers, in order to asses its usefulness for a wider set of tasks. This recommendation goes hand-in-hand with the recommendation regarding standardized benchmarks at the beginning of this section, since those benchmarks would provide clearly defined metrics to assess, share and compare the results of the psychophysic studies.

Appendix A

Lorentz force calculation in the 2DOF actuator for magnetic levitation

The actuator proposed in section 7.3.1 is based on Lorentz forces, which act on charges moving through a magnetic field, as stated by Lorentz law:

$$F = \int (J \times B) dV \tag{A.1}$$

where J is the current density and B is the magnetic flux density. This simple definition must be exploited to calculate the force produced by the magnet on the actuator coils.

Following [38], a first integral must be calculated to obtain the value of B in the area surrounding a flat magnet, from the definitions of the B caused by differential magnetic charges. The magnetic potential produced by a differential magnetic charge can be expressed as:

$$\begin{aligned} &d\Psi = \tfrac{\rho_m(r')dv'}{4\pi\mu_0|r-r'|} \\ &\text{Where:} \\ &\rho_m = \text{ Magnetic charge density} \\ &dv' = \text{ A differential magnetic volume} \\ &r' = \text{ Position of the magnet } dv' \\ &r = \text{ Position of the observer} \end{aligned} \tag{A.2}$$

Then, we can express the magnetic field as a function of the magnetic potential:

$$\begin{aligned} &H = -\nabla\Psi \\ &\text{Where:} \\ &H = \text{ Magnetic field} \\ &\Psi = \text{ Magnetic potential} \end{aligned} \tag{A.3}$$

And taking the magnetic potential caused by a magnetic charge, we can obtain the resulting magnetic field:

$$\begin{aligned} &dH = -\nabla d\Psi = -\frac{\rho_m(r')dv'}{4\pi\mu_0}\left(\frac{\partial}{\partial x}\frac{1}{|r-r'|}, \frac{\partial}{\partial y}\frac{1}{|r-r'|}, \frac{\partial}{\partial z}\frac{1}{|r-r'|}\right) \\ &\text{Where:} \\ &|r-r'| = \sqrt{(x-x')^2 + (y-y')^2 + (z-z')^2} \end{aligned} \tag{A.4}$$

Expanding equation A.4:

$$\begin{aligned} dH &= -\frac{\rho_m(r')dv'}{4\pi\mu_0}\left(\frac{(-1/2)(2)\left[(x-x')\hat{i}+(y-y')\hat{j}+(z-z')\hat{k}\right]}{\left[(x-x')^2+(y-y')^2+(z-z')^2\right]^{1.5}}\right) \\ dH &= \frac{\rho_m(r')dv'}{4\pi\mu_0}\left(\frac{(x-x')\hat{i}+(y-y')\hat{j}+(z-z')\hat{k}}{\left[(x-x')^2+(y-y')^2+(z-z')^2\right]^{1.5}}\right) \\ dH &= \frac{\rho_m(r')dv'}{4\pi\mu_0}A\left(r,r'\right) \\ &\text{Where:} \\ A\left(r,r'\right) &= \frac{(x-x')\hat{i}+(y-y')\hat{j}+(z-z')\hat{k}}{\left[(x-x')^2+(y-y')^2+(z-z')^2\right]^{1.5}} \end{aligned} \tag{A.5}$$

The magnetic field due to a magnetic volume is then the superposition integral of the previous to the volume of the magnet:

$$\begin{aligned} &H = \int\limits_{Vmag} \frac{\rho_m(r')A(r,r')}{4\pi\mu_0}dv' \\ &\text{Where:} \\ &Vmag = \text{ Magnetic volume} \end{aligned} \tag{A.6}$$

By using a permanent magnet with flat faces and uniform magnetization, all the charge density is in the surface and independent of the position within it. One face is modeled as cumulating the "negative" charge density and the other the "positive" charge density, both adding 0 in order to ensure that there are no monopoles. With this assumption, equation A.6 simplifies to:

$$\begin{aligned} &H = \frac{\sigma_{sm}}{4\pi\mu_0}\int\limits_{Smag} A\left(r,r'\right)ds' \\ &\text{Where:} \\ &\sigma_{sm} = \pm\mu_0 M = \text{ Surface magnetic charge density} \\ &\pm \text{ Depending on the magnet surface} \\ &Smag = \text{ Surfaces of the magnet} \\ &ds' = \text{ A differential of surface of the magnet} \end{aligned} \tag{A.7}$$

Outside of the magnet, the magnetic flux B is finally:

$$\begin{aligned} B &= \mu_0 H = \tfrac{\sigma_{sm}}{4\pi} \int\limits_{Smag} A\left(r, r'\right) ds' \Rightarrow \\ B &= \tfrac{\sigma_{sm}}{4\pi} \int\limits_{Smag} \tfrac{(x-x')\hat{i}+(y-y')\hat{j}+(z-z')\hat{k}}{\left[(x-x')^2+(y-y')^2+(z-z')^2\right]^{1.5}} ds' \end{aligned} \tag{A.8}$$

With the magnetic flux defined, we can include it in equation A.1. We obtain then 5 nested integrals to calculate the total Lorentz force in a coil, depending on its position relative to the magnet.

$$\begin{aligned} F &= \tfrac{\sigma_{sm}}{4\pi} \int\limits_{Vcoil} J(r) \times \left(\int\limits_{Smag} A\left(r, r'\right) ds' \right) dv \Rightarrow \\ F &= \tfrac{\sigma_{sm}}{4\pi} \int\limits_{Vcoil} J(r) \times \left(\int\limits_{Smag} \tfrac{(x-x')\hat{i}+(y-y')\hat{j}+(z-z')\hat{k}}{\left[(x-x')^2+(y-y')^2+(z-z')^2\right]^{1.5}} ds' \right) dv \end{aligned} \tag{A.9}$$

In equation A.9 two integrals superpose the magnetic flux of the differential magnetic charges through the surface of the magnet. The remaining three integrals cumulate the forces applied to the differential volumes of the coil through the coil's volume.

Bibliography

[1] Applications - production systems. http://www.nanomotor.de/aa_production_system.htm. [cited at p. 76]

[2] ATI industrial automation: Robotic end effectors and automation tooling. http://www.ati-ia.com/. [cited at p. 98]

[3] Motion basics and standards. http://www.newport.com/Motion-Basics-and-Standards/140230/1033/content.aspx. [cited at p. 22]

[4] Viewing distance calculator - metric. http://myhometheater.homestead.com/ viewingdistancemetric.html. [cited at p. 54]

[5] Visual acuity webvision. http://webvision.med.utah.edu/book/part-viii-gabac-receptors/visual-acuity/. [cited at p. 54]

[6] David A. Abbink. Neuromuscular analysis as a guideline in designing shared control. In *Advances in Haptics*. 2010. [cited at p. 26, 32, 33]

[7] J. Abbott, P. Marayong, and A. Okamura. Haptic virtual fixtures for robot-assisted manipulation. *Robotics Research*, page 4964, 2007. [cited at p. 2, 25, 32, 33]

[8] J.J. Abbott, Z. Nagy, F. Beyeler, and B.J. Nelson. Robotics in the small, part i: Microbotics. *Robotics & Automation Magazine, IEEE*, 14(2):92–103, 2007. [cited at p. 32]

[9] I. Aliaga, A. Rubio, and E. Sanchez. Experimental quantitative comparison of different control architectures for master-slave teleoperation. *Control Systems Technology, IEEE Transactions on*, 12(1):211, 2004. [cited at p. 19]

[10] R.O. Ambrose, H. Aldridge, R.S. Askew, R.R. Burridge, W. Bluethmann, M. Diftler, C. Lovchik, D. Magruder, and F. Rehnmark. Robonaut: NASA's space humanoid. *Intelligent Systems and their Applications, IEEE*, 15(4):57–63, 2000. [cited at p. 2]

[11] F. Arai, T. Sugiyama, P. Luangjarmekorn, A. Kawaji, T. Fukuda, K. Itoigawa, and A. Maeda. 3D viewpoint selection and bilateral control for bio-micromanipulation. In *IEEE International Conference on Robotics and Automation, 2000. Proceedings. ICRA '00*, volume 1, pages 947–952 vol.1. IEEE, 2000. [cited at p. 6, 7, 10, 120]

[12] Jesse Bank, Pablo Estevez, Marcello Porta, and Jia Wei. *Development of a novel 6 DOF interaction force sensor for micro-gripper applications.* MSc thesis, Delft University of Technology, Delft, The Netherlands, June 2010. [cited at p. 97, 104, 134]

[13] S Bargiel, K Rabenorosoa, C Clvy, C Gorecki, and P Lutz. Towards micro-assembly of hybrid MOEMS components on a reconfigurable silicon free-space micro-optical bench. *Journal of Micromechanics and Microengineering*, 20(4):045012, April 2010. [cited at p. 5, 6, 7]

[14] Cagatay Basdogan, Alper Kiraz, Ibrahim Bukusoglu, Aydin Varol, and Sultan Doganay. Haptic guidance for improved task performance in steering microparticles with optical tweezers. *Optics Express*, 15(18):11616–11621, 2007. [cited at p. 32]

[15] P.J. Berkelman, L.L. Whitcomb, R.H. Taylor, and P. Jensen. A miniature microsurgical instrument tip force sensor for enhanced force feedback during robot-assisted manipulation. *Robotics and Automation, IEEE Transactions on*, 19(5):917–921, 2003. [cited at p. 5, 98, 101]

[16] F. Beyeler, S. Muntwyler, and B. J Nelson. Design and calibration of a microfabricated 6-axis force-torque sensor for microrobotic applications. In *IEEE International Conference on Robotics and Automation, 2009. ICRA '09*, pages 520–525. IEEE, May 2009. [cited at p. 98]

[17] F. Beyeler, S. Muntwyler, and B. J Nelson. A Six-Axis MEMS Force-Torque sensor with Micro-Newton and Nano-Newtonmeter resolution. *Journal of Microelectromechanical Systems*, 18(2):433–441, April 2009. [cited at p. 98]

[18] T.L. Brooks. Telerobotic response requirements. In *Systems, Man and Cybernetics, 1990. Conference Proceedings., IEEE International Conference on*, pages 113–120, 1990. [cited at p. 29, 39, 76, 101]

[19] Ron Bruinen, Pablo Estevez, and Robbert Munnig Schmidt. Design and analysis of a flexure based 3-DOF micropositioner for haptic teleoperated micromanipulation. Deflt, The Netherlands, May 2011. [cited at p. 68]

[20] Grigore Burdea. *Force and touch feedback for virtual reality.* John Wiley & Sons, 1996. [cited at p. 39]

[21] Jongeun Cha, Ahmad Barghout, Julius Kammerl, Eckehard Steinbach, and Abdulmotaleb El Saddik. Improving spatial perception in telepresence and teleaction systems by displaying distance information through visual and vibrotactile feedback. *Presence: Teleoperators and Virtual Environments*, 19(5):430–449, December 2010. [cited at p. 33]

[22] S. K Chollet, F. Bourgeois, L. Benmayor, B. Moll, C. Wulliens, and J. Jacot. A flexible microassembly cell for small and medium sized batches. In *Proceedings of the 33rd ISR (International Symposium on Robotics) October*, volume 7, page 11, 2002. [cited at p. 6, 7, 8, 9]

[23] Christiansson, Van der Helm, Mechanical Maritime and Materials Engineering, and TU Delft. Hard master, soft slave haptic teleoperation, October 2007. [cited at p. 3]

[24] Gran A. V. Christiansson and Frans C. T. van der Helm. The Low-Stiffness teleoperator slave - a trade-off between stability and performance. *The International Journal of Robotics Research*, 26(3):287 –299, March 2007. [cited at p. 58, 76]

[25] Z Chu, P.M Sarro, and S Middelhoek. Silicon three-axial tactile sensor. *Sensors and Actuators A: Physical*, 54(1-3):505–510, June 1996. [cited at p. 69, 98, 99]

[26] David P. Cuff. *Electromagnetic nanopositioner*. Thesis, Massachusetts Institute of Technology, 2006. Thesis (S.M.)–Massachusetts Institute of Technology, Dept. of Mechanical Engineering, 2006. [cited at p. 78]

[27] D. V Dao, T. Toriyama, J. Wells, and S. Sugiyama. Silicon piezoresistive six-degree of freedom force-moment micro sensor. *Sensors and Materials*, 15(3):113135, 2003. [cited at p. 98]

[28] HERIBAN David, AGNUS Jol, and GAUTHIER Michal. Micro-manipulation of silicate micro-sized particles for biological applications. In *5th International Workshop on MicroFactories (IWMF06)*, October 2006. [cited at p. 5]

[29] Trinh Chu Duc, Gih-Keong Lau, J. F Creemer, and P. M Sarro. Electrothermal microgripper with large jaw displacement and integrated force sensors. *Journal of Microelectromechanical Systems*, 17(6):1546–1555, December 2008. [cited at p. 69, 98, 99, 103, 104, 106, 112]

[30] Anna Eisinberg, Arianna Menciassi, Paolo Dario, Joerg Seyfried, Ramon Estana, and Heinz Woern. Teleoperated assembly of a micro-lens system by means of a micromanipulation workstation. *Assembly Automation*, 27(2):123–133, 2007. [cited at p. 6, 7, 8, 9, 31, 33]

[31] P. Estevez, S. Khan, P. Lambert, M. Porta, I. Polat, C. Scherer, M. Tichem, U. Staufer, H. Langen, and R. Schmidt. A haptic tele-operated system for microassembly. *Precision Assembly Technologies and Systems*, page 1320, 2010. [cited at p. 2]

[32] Femtotools. FemtoTools: micro force sensors, microgrippers, nanopositioning systems. http://www.femtotools.com/, October 2011. [cited at p. 106]

[33] Michal Gauthier and Stphane Regnier. *Robotic Micro-Assembly*. Wiley-IEEE Press, October 2010. [cited at p. 18]

[34] Jason J. Gorman and Nicholas G. Dagalakis. Force control of linear motor stages for microassembly. *ASME Conference Proceedings*, 2003(37130):615–623, January 2003. [cited at p. 77]

[35] Jie Gu, Won-jong Kim, and Shobhit Verma. Nanoscale motion control with a compact Minimum-Actuator magnetic levitator. *Journal of Dynamic Systems, Measurement, and Control*, 127(3):433–442, 2005. [cited at p. 86]

[36] Hans Nrgaard Hansen, Guido Tosello, Asta Gegeckaite, Mogens Arentoft, and L. Marin. Classification of assembly techniques for micro products. Karlshrue, Germany, 2005. Elsevier Science. [cited at p. 18]

[37] Sandra G. Hart and Lowell E. Staveland. Development of NASA-TLX (Task load index): Results of empirical and theoretical research. In *Advances in Psychology*, volume 52, pages 139–183. Elsevier, 1988. [cited at p. 44]

[38] Hermann A. Haus and James R. Melcher. *Electromagnetic Fields and Energy*. Prentice Hall, September 1989. [cited at p. 137]

[39] Iulian Iordachita, Zhenglong Sun, Marcin Balicki, Jin U. Kang, Soo Jay Phee, James Handa, Peter Gehlbach, and Russell Taylor. A sub-millimetric, 0.25 mN resolution fully integrated fiber-optic force-sensing tool for retinal microsurgery. *International Journal of Computer Assisted Radiology and Surgery*, 4:383–390, April 2009. [cited at p. 5, 98, 101]

[40] L. Jabben. *Mechatronic design of a magnetically suspended rotating platform*. PhD thesis, Delft University of Technology, Delft, The Netherlands, December 2007. [cited at p. 59]

[41] J. W Jansen, C. M.M van Lierop, E. A Lomonova, and A. J.A Vandenput. Magnetically levitated planar actuator with moving magnets. *IEEE Transactions on Industry Applications*, 44(4):1108–1115, August 2008. [cited at p. 78]

[42] L.A. Jones and I.W. Hunter. A perceptual analysis of stiffness. *Experimental Brain Research*, 79(1), January 1990. [cited at p. 40]

[43] Shahzad Khan and Asif Sabanovic. Force feedback pushing scheme for micromanipulation applications. *Journal of Micro-Nano Mechatronics*, 5(1-2):43–55, November 2009. [cited at p. 119]

[44] Byungkyu Kim, Hyunjae Kang, Deok-Ho Kim, and Jong-Oh Park. A flexible microassembly system based on hybrid manipulation scheme for manufacturing photonics components. *The International Journal of Advanced Manufacturing Technology*, 28(3):379–386, March 2006. [cited at p. 76]

[45] D.-H. Kim, B. Kim, and H. Kang. Development of a piezoelectric polymer-based sensorized microgripper for microassembly and micromanipulation. *Microsystem Technologies*, 10(4):275–280, May 2004. [cited at p. 58]

[46] Won-jong Kim, Shobhit Verma, and Huzefa Shakir. Design and precision construction of novel magnetic-levitation-based multi-axis nanoscale positioning systems. *Precision Engineering*, 31(4):337–350, October 2007. [cited at p. 78, 86]

[47] D. Kragic, P. Marayong, M. Li, A. M. Okamura, and G. D. Hager. Human-Machine collaborative systems for microsurgical applications. *The International Journal of Robotics Research*, 24(9):731 –741, 2005. [cited at p. 18]

[48] K. H. E. Kroemer, H. B. Kroemer, and Katrin E. Kroemer-Elbert. *Ergonomics: how to design for ease and efficiency*. Prentice Hall, August 1994. [cited at p. 39]

[49] Rik Lafeber, Gerrit Bosch, Max Murre, Jitze Bassa, Leo Moergestel, and Erik Puik. Characterisation of high accuracy, feedback controlled, adhesive bonding. In Svetan Ratchev, editor, *Precision Assembly Technologies and Systems*, volume 371, pages 144–153. Springer Berlin Heidelberg, Berlin, Heidelberg, 2012. [cited at p. 24]

[50] Y. C Lai and J. Y Yen. Design of a novel 6-DOF planar maglev system. *Journal of Magnetism and Magnetic Materials*, 304(1):e386e390, 2006. [cited at p. 86]

[51] Patrice Lambert, Hans Langen, and Robert Munnig Schmidt. A novel 5 DOF fully parallel robot combining 3T1R motion and grasping. *ASME Conference Proceedings*, 2010(44106):1123–1130, January 2010. [cited at p. 65]

[52] Sangyoon Lee and Gerard Jounghyun Kim. Effects of haptic feedback, stereoscopy, and image resolution on performance and presence in remote navigation. *International Journal of Human-Computer Studies*, 66(10):701–717, October 2008. [cited at p. 32]

[53] Dengfeng Li. *Modeling and control of a high precision 6-DOF Maglev positioning stage with large range of travel*. Florida Institute of Technology, 2008. [cited at p. 78]

[54] Chen Liguo, Sun Lining, Rong Weibin, and Bian Xinqian. Hybrid control of vision and force for MEMS assembly system. In *Robotics and Biomimetics, 2004. ROBIO 2004. IEEE International Conference on*, pages 136–141, 2004. [cited at p. 98]

[55] Xinyu Liu, Keekyoung Kim, Yong Zhang, and Yu Sun. Nanonewton force sensing and control in microrobotic cell manipulation. *The International Journal of Robotics Research*, 28(8):1065 –1076, 2009. [cited at p. 58]

[56] L. J. Love. Force reflecting Micro-Teleoperation with haptic feedback. *ORNL/TM-2002/265*, 2002. [cited at p. 9, 29, 68, 71]

[57] A. Menciassi, A. Eisinberg, G. Scalari, C. Anticoli, M. C Carrozza, and P. Dario. Force feedback-based microinstrument for measuring tissue properties and pulse in microsurgery. In *IEEE International Conference on Robotics and Automation, 2001. Proceedings 2001 ICRA*, volume 1, pages 626– 631 vol.1. IEEE, 2001. [cited at p. 5, 98, 101]

[58] P. Milgram, S. Yin, and J.J. Grodski. An augmented reality based teleoperation interface for unstructured environments. In *Proc. American Nuclear Society 7th Topical Meeting on Robotics and Remote Systems*, 1997. [cited at p. 26]

[59] M. Mitsuishi, N. Sugita, T. Nagao, and Y. Hatamura. A tele-micro machining system with operational environment transmission under a stereo-SEM. In *, 1996 IEEE International Conference on Robotics and Automation, 1996. Proceedings*, volume 3, pages 2194–2201 vol.3. IEEE, April 1996. [cited at p. 98]

[60] J. D Morrow and P. K Khosla. Manipulation task primitives for composing robot skills. In *IEEE International Conference on Robotics and Automation*, page 33543359, 1997. [cited at p. 17, 18]

[61] Alexander Mulder, Pablo Estevez, and Robert Munnig Schmidt. *Design of a 6-DoF Miniature Maglev Positioning Stage for Application in Haptic Micromanipulation*. MSc thesis, July 2011. [cited at p. 22, 38, 75, 82, 88, 90]

[62] Robbert Munnig Schmidt, Georg Schitter, and Jan van Eijk. *The Design of High Performance Mechatronics*. Delft University Press, 1 edition, 2011. [cited at p. 84]

[63] E.A.Y. Murakami, T. Yamada, T. Kondo, and K. Ito. Performance evaluation of bilateral micro-teleoperation systems based on man-machine dynamic characteristics. In *SICE 2002. Proceedings of the 41st SICE Annual Conference*, volume 5, pages 2706–2711 vol.5, 2002. [cited at p. 29, 31]

[64] X. D. Pang, H. Z. Tan, and N. I. Durlach. Manual discrimination of force using active finger motion. *Perception & Psychophysics*, 49(6):531–540, November 1991. [cited at p. 40]

[65] K. E Petersen. Silicon as a mechanical material. *Proceedings of the IEEE*, 70(5):420– 457, May 1982. [cited at p. 103]

[66] M. Porta and M. Tichem. Grasping and interaction force feedback in microassembly. *Precision Assembly Technologies and Systems*, page 199206, 2010. [cited at p. 98]

[67] Martin Probst, Christoph Hrzeler, Ruedi Borer, and Bradley J. Nelson. A microassembly system for the flexible assembly of hybrid robotic mems devices. *International Journal of Optomechatronics*, 3(2):p. 6990, April 2009. [cited at p. 6, 7, 8, 9, 10, 76, 120]

[68] Marwan Radi, Andrea Reiter, Sherif Zaidan, Gunther Reinhart, Verena Nitsch, and Berthold Frber. Telepresence in industrial applications: Implementation issues for assembly tasks. *Presence: Teleoperators and Virtual Environments*, 19(5):415–429, October 2010. [cited at p. 6, 7, 8, 9, 29, 31]

[69] G. Roman, J. Bronson, G. Wiens, J. Jones, and J. Allen. Design of a piezoresistive surface micromachined Three-Axis force transducer for microassembly. *Proceedings of IMECE*, pages 5–11, 2005. [cited at p. 98]

[70] L. B Rosenberg. Virtual fixtures: Perceptual tools for telerobotic manipulation. In *1993 IEEE Virtual Reality Annual International Symposium, 1993.*, page 7682, 1993. [cited at p. 2, 32]

[71] N. Sarkar. Applying microassembly to real-world applications. *Zyvex Corp., Richardson, Tex., Zyvex Application Note*, 9712, 2005. [cited at p. 5]

[72] Stephen D. Senturia. *Microsystem design*. Springer, 2001. [cited at p. 103]

[73] Yantao Shen, Ning Xi, King W.C. Lai, and Wen J. Li. A novel PVDF microforce/force rate sensor for practical applications in micromanipulation. *Sensor Review*, 24(3):274–283, 2004. [cited at p. 6, 7, 9, 98]

[74] Yantao Shen, Ning Xi, and Wen Jung Li. Force-guided assembly of micro mirrors. In *2003 IEEE/RSJ International Conference on Intelligent Robots and Systems, 2003. (IROS 2003). Proceedings*, volume 3, pages 2149– 2154 vol.3. IEEE, October 2003. [cited at p. 5, 58, 98, 101]

[75] A. Sieber, P. Valdastri, K. Houston, C. Eder, O. Tonet, A. Menciassi, and P. Dario. A novel haptic platform for real time bilateral biomanipulation with a MEMS sensor for triaxial force feedback. *Sensors & Actuators: A. Physical*, 142(1):1927, 2008. [cited at p. 5, 6, 7, 9, 19, 58, 98, 101]

[76] Changman Son. Intelligent control planning strategies with neural network/fuzzy coordinator and sensor fusion for robotic part macro/micro-assembly tasks in a partially unknown environment. *International Journal of Machine Tools and Manufacture*, 44(15):1667–1681, December 2004. [cited at p. 22]

[77] B. Stanczyk and M. Buss. Development of a telerobotic system for exploration of hazardous environments. In *Intelligent Robots and Systems, 2004. (IROS 2004). Proceedings. 2004 IEEE/RSJ International Conference on*, volume 3, pages 2532–2537 vol.3, 2004. [cited at p. 2]

[78] B. Tamadazte, N. Le Fort-Piat, S. Dembl, and E. Marchand. Microassembly of complex and solid 3D MEMS by 3D vision-based control. 2009. [cited at p. 18]

[79] Hong Z. Tan, Mandayam A. Srinivasan, Brian Eberman, and Belinda Cheng. Human factors for the design of force-reflecting haptic interfaces. In *Proceedings of the Third (3rd) International Symposium on Haptic Interfaces for Virtual Environment and Teleoperator Systems*, volume 55, pages 353–359, Chicago, IL, 1994. [cited at p. 39, 40]

[80] M. Tavakoli, R V Patel, and M. Moallem. Haptic interaction in robot-assisted endoscopic surgery: a sensorized end-effector. *The International Journal of Medical Robotics and Computer Assisted Surgery*, 1(2):53–63, January 2005. [cited at p. 5, 98, 101]

[81] L. van den Bedem, R. Hendrix, N. Rosielle, M. Steinbuch, and H. Nijmeijer. Design of a minimally invasive surgical teleoperated master-slave system with haptic feedback. In *Mechatronics and Automation, 2009. ICMA 2009. International Conference on*, pages 60–65, 2009. [cited at p. 2]

[82] S. Verma, H. Shakir, and W. J Kim. Novel electromagnetic actuation scheme for multiaxis nanopositioning. *IEEE Transactions on Magnetics*, 42(8):20522062, 2006. [cited at p. 78, 81]

[83] Ashwin P Vijayasai, Ganapathy Sivakumar, Matthew Mulsow, Shelby Lacouture, Alex Holness, and Tim E Dallas. Haptic controlled three-axis MEMS gripper system. *The Review of Scientific Instruments*, 81(10):105114, October 2010. PMID: 21034126. [cited at p. 6, 7, 9]

[84] J. D Wason, J. T Wen, Young-Man Choi, J. J Gorman, and N. G Dagalakis. Vision guided multi-probe assembly of 3D microstructures. In *2010 IEEE/RSJ International Conference on Intelligent Robots and Systems (IROS)*, pages 5603–5609. IEEE, October 2010. [cited at p. 6, 7, 8, 9, 18, 121]

[85] J. Wei, M. Porta, M. Tichem, U. Staufer, and P. M Sarro. A position and force-distribution sensor-array for monitoring the contact condition of objects in micro-handling. In *2010*

IEEE 23rd International Conference on Micro Electro Mechanical Systems (MEMS), pages 623–626. IEEE, January 2010. [cited at p. 104, 107]

[86] Jia Wei, Marcello Porta, Marcel Tichem, Urs Staufer, and P. M. Sarro. Integrated force and position detection sensors for Micro-Handling applications: Part i - principle and 1D position detection. *in submission to JMEMS*, 2011. [cited at p. 103, 104]

[87] Hui Xie, Weibin Rong, and Lining Sun. A flexible experimental system for complex microassembly under microscale force and Vision-Based control. *International Journal of Optomechatronics*, 1(1):81, 2007. [cited at p. 5]

[88] Y. Xie, D. Sun, C. Liu, S.H. Cheng, and Y.H. Liu. A force control based cell injection approach in a bio-robotics system. In *Robotics and Automation, 2009. ICRA'09. IEEE International Conference on*, page 34433448, 2009. [cited at p. 5, 58]

[89] Ho Yu. *Design and control of a compact 6-degree-of-freedom precision positioner with linux-based real-time control*. PhD thesis, TEXAS A&M UNIVERSITY, 2010. [cited at p. 78]

List of Figures

List of Tables

Index

Acknowledgements

This thesis is by far not the result of my sole efforts: through my thesis I had the luck of being accompanied by an amazing team of people, and I must therefore start by acknowledging all those who contributed to it. I doubt that many have the luxury of receiving advice from so many professors, advisors and supervisors through their PhD studies. Rob, Lina, Urs, Just, Marcel, Hans, John and David, it was an honor and a pleasure for me to have access to your knowledge, and to have had the chance of learning from and collaborating with you. Each one of you introduced me to a different discipline, and to a different way to tackle problems.

Accompanying me in this project were Patrice, Ilhan, Shahzad, Marcello and Vega, each one attacking a piece of the problem we set out to solve. Our discussions set the goals of my projects, and thanks to you is that I could find a path toward those goals. A special thanks must go to my master students Alexander, Jesse and Ron. You taught me much more than what I could teach you, and your support was indispensable in tackling the wide variety of challenges that this thesis presented. The support from the whole team of colleagues from BME and PME cannot be overlooked, since they helped me answer the many questions that arose in the last four years.

In an institutional level I must thank the Microned program for providing the fundings for this project. I must also thank the Delft University of Technology, the PME Department and DIMES for providing me the best tools and resources I could have asked for.

But these last four years did not only go by within the University, and the support and company of my friends have made my life in Europe a happy one. My flatmates Friedi and Ivan have become my brothers, and as such I hope will remain. Together we shared the ups and downs of our PhD's and our lives, supporting each other and celebrating each success with a tasty dinner, a fresh beer or even a long run. Together we cultivated an extended family of friends who, by finding our doors always open, flooded our house and lifes with their always welcomed and appreciated presence.

The previous paragraph did not say *Europe* for free. Having a double life between Switzerland and Netherlands would not have been easy without that other group of alpine friends. To them I thank for making me feel at home abroad, or better said making *abroad* become my second home. It would have been also difficult to keep my traveling rhythm without easyjet, and for that I thank Sir Stelios Haji-Ioannou, though I doubt he will come across these aknowledgements.

To my country, Venezuela, I owe my formation as an engineer and as a person. I am sure you will soon overcome the problems you are going through, and I hope I can find my place to support you in that process from where I am now, and even more once I am ready to come back.

Finally I must thank my parents, my brothers, my grandmothers and Barbarita, for it is thanks to my family that I have arrived here, and it is with them and for them that I want to continue forward.

Curriculum Vitae

Education

- **Magister in Electronic Engineering - Mechatronics Option**
  Simon Bolivar University (USB). Caracas, Venezuela – 2005 to 2007
  2-years master program focused on Mechatronics, including control, mechanical design, informatics and electronics. Initiated, guided and developed projects on mobile cooperative robots, localization and mapping, and walking robots, all of which generated publications and continued to be developed in the group.
  GPA 5/5. Outstanding Mention
- **Bachelor in Electronic Engineering**
  Simon Bolivar University (USB). Caracas, Venezuela – 1999 to 2005
  5–years Bachelor program covering varied topics of Electronic Engineering, internships and a 6 months thesis project.
  GPA 4.6 / 5, graduation rank: 1st / 16
- **Introduction to Disaster Risk Management**
  World Bank e–Institute – October 2011
  4-weeks course on the contemporary concepts and practices of DRM.

Work experience

- **PhD Promovendus**
  Mechatronic Systems Design, PME - TUDelft, The Netherlands – 2007 to Present
  Out of my own R&D activities, I managed and coordinated R&D groups composed of several PhD candidates, postdoctoral researchers and master students. I also kept track of the project budget, coordinated and negotiated the specification, pricing and acquisition of equipment, presented the group activities in national and international events and publications, and performed teaching and supervision activities.
- **Founder & Consultant on Electronic Engineering**
  Albatros Ingeniera. Caracas, Venezuela – 2006 to 2007
  Albatros Ingeniera was created by a group of Mechanical, Electronic, Electric, Informatics and Civil Engineers, to provide consultancy on engineering topics. As a founder, I participated in the legal definition of the enterprise, the set-up of the facilities, and the writing of tender applications (including preliminary system-designs).

- **Academic Assistant**
  Electronics Department - Universidad Simón Bolívar, Venezuela – 2005 to 2007
  Within the newborn Mechatronics Section, I participated in the definition of the group development plan, set-up of collaborations, definition of R&D lines, grants applications and PR. I also managed and coordinated R&D groups composed of several master and bachelor students, presented the group activities in various events, and organized group meetings and social activities. In the Electronics Department I was in charge of preparing teaching material, lecturing and project supervision on several topics of mechatronic systems design, digital circuits and programming.
- **R&D Intern at TecO - Context recognition over mobile smart-it platforms – September 2004 to April 2005**
  Karlsruhe, Germany
  Development of software in Matlab and C for context recognition applications on smart-it mobile and distributed platforms. This project constituted my bachelor thesis and was graded with honors.
- **R&D Intern at Geophysics Laboratory, ULA - Low cost seismic measurements**
  Universidad de los Andes, Mrida, Venezuela – 2003
  Acquisition, analysis and backup system for seismometer data using a PC standard sound card and software in LabView. This project won the Latin American Contest on LabView Academic Applications - 2004.
- **Laboratory and classroom assistant**
  Electronics Department - Universidad Simón Bolívar, Venezuela – 1999 to 2005
  Support of laboratory courses on several topics of Electronic Engineering.

Awards and Recognitions

- **2nd Place in the 13th region, ASME Student Design Contest – 2004**
  Electronics and control systems for a mobile robot.
- **1st Place, Latin American Contest on LabView Academic Applications, NI – 2004**
  Acquisition, analysis and backup system for seismometer data.
- **12th Place (over 7000 applicants), Admission Test, Simon Bolivar University – 1999**
- **Silver medal, IV Physics Ibero-American Olympiads – 1999**
  Selected participants from Spain and all Latin-American countries.
  1999
- **Several medals (3 gold, 1 bronze) and other awards in Mathematics, Physics and Chemistry Olympiads, CENAMEC – 1997 to 1999**
  Science Olympiads with more than 50.000 high school initial participants nationwide.

Publications

- Estevez, Pablo, Jesse Bank, Marcello Porta, Jia Wei, P. M. Sarro, Marcel Tichem, and Urs Staufer. **'6 DOF Force and Torque Sensor for Micromanipulation Applications'**. Accepted for publication in Sensors and Actuators A: Physical, 2011.
- Bruinen, Ron, Pablo Estevez, and Robbert Munnig Schmidt. **'Design and analysis of a flexure based 3-DOF micropositioner for haptic teleoperated micromanipulation'**. Delft, The Netherlands, 2011.

- Tolou, Nima, Pablo Estevez, and Just Herder. **'Collinear-Type Statically Balanced Compliant Micro Mechanism (SB-CMM): Experiemental Comparision between Precurved and Straight Beams.'** Washington, USA, 2011.
- Tolou, Nima, Pablo Estevez, and Just Herder. **'Energy efficient MEMS Using Collinear-Type Statically Balanced Compliant Micro Mechanisms (SB-MEMS)'**. Como, Italy, 2011.
- Estevez, Pablo, Marcel Tichem, and Robbert Munnig Schmidt. **'Concept for a teleoperated micromanipulation station with a magnetically levitated stage and piezoresistive force sensing.'**, MicroNano Conference 2010.
- Estevez, P., S. Khan, P. Lambert, M. Porta, I. Polat, C. Scherer, M. Tichem, U. Staufer, H. Langen, and R. Schmidt. **'A Haptic Tele-operated System for Microassembly.'** Precision Assembly Technologies and Systems (2010): 13-20.
- Khan, S., T. de Boer, P. Estevez, H. Langen, and R. Munnig Schmidt. **'Development of Haptic Microgripper for Microassembly Operation.'** Haptics: Generating and Perceiving Tangible Sensations (2010): 309-314.
- Lambert, Patrice, Pablo Estevez, Shahzad Khan, Hans Langen, Robbert Schmidt, Marcello Porta, Marcel Tichem, Urs Staufer, Ilhan Polat, and Carsten Scherer. **'Progress on Haptic Teleoperation for Micro-assembly'**, 2009.
- Estevez, Pablo, Jose Cappelletto, Raul Acua, Fernando Alvarez, and Gerardo Fernandez-Lopez. **'Coordinated Navigation Using Dynamically Varying Velocity Fields.'**. In Proceedings of ICAISC 2008, 2008.
- Cappelletto, Jose, Pablo Estevez, Juan Carlos Grieco, and Gerardo Fernandez-Lopez. **'A CPG with force feedback for a statically stable quadruped gait.'**. In Proc. 10th Int. Conf. Climbing and Walking Robots and the Supporting Technologies for Mobile Machines CLAWAR. Vol. 7, n.d.
- Estevez, Pablo, Juan Hernandez, Jose Cappelletto, and Juan Carlos Grieco. **'Synchronous Local Positioning System Based on Ultrasonic Active Beacons and Feed Forward Neural Networks.'**. In Proceedings of CLAWAR 2007, 2007.
- Cappelletto, J., P. Estevez, W. Medina, L. Fermin, J. Bogado, J. Grieco, and G. Fernandez-Lopez. **'Gait synthesis and modulation for quadruped robot locomotion using a simple feed-forward network.'**. Artificial Intelligence and Soft Computing-ICAISC 2006 (2006): 731-739.
- Cappelletto, J., Pablo Estevez, J. Grieco, G. Fernandez-Lopez, and M. Armada. **'A CPG-Based Model for Gait Synthesis in Legged Robot Locomotion.'**. In Proceedings of CLAWAR 2006. Brussels, BELGIUM, 2006.

Extra-curricular activities and interests

- Fundraising for several charities. Approximately 10k have been raised in 2 years through parties, sport events and direct campaigns, to support water supply systems and risk management activities in the third world (supportinc.blogspot.com).
- Mountain guide and instructor on courses and workshops on mountain sports. Organization of national and international expeditions. OIKOS Mountain Climbing Club, USB, Caracas, 1999-2007.
- Interest on social responsibility, management of social enterprises, development policies and application of technology to development issues.
- Other interests: Biking, Photography, Origami, Juggling, Cooking, Sewing and Needlework.

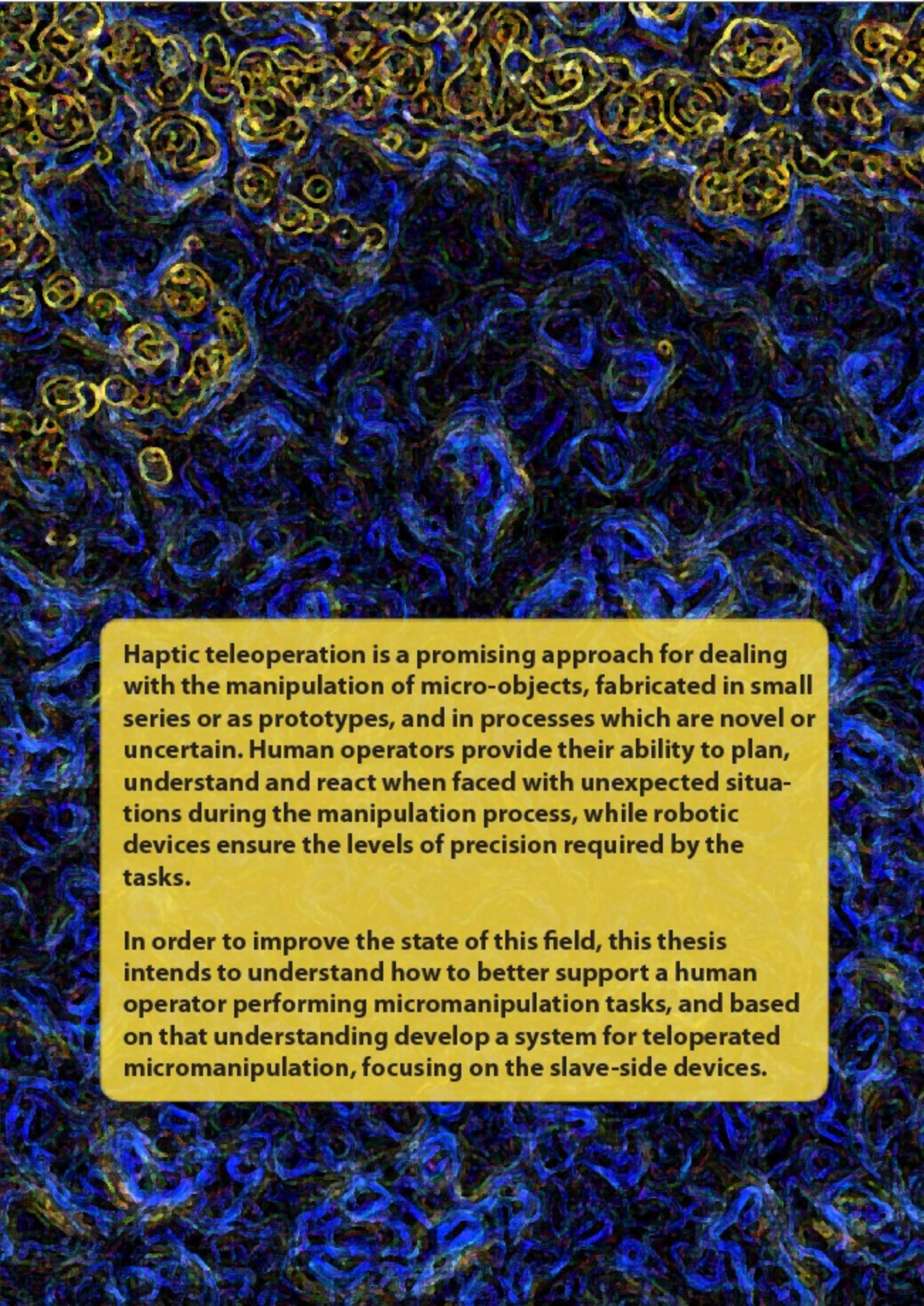

Haptic teleoperation is a promising approach for dealing with the manipulation of micro-objects, fabricated in small series or as prototypes, and in processes which are novel or uncertain. Human operators provide their ability to plan, understand and react when faced with unexpected situations during the manipulation process, while robotic devices ensure the levels of precision required by the tasks.

In order to improve the state of this field, this thesis intends to understand how to better support a human operator performing micromanipulation tasks, and based on that understanding develop a system for teloperated micromanipulation, focusing on the slave-side devices.